

A STUDY ON OPTIMUM LAYOUT OF DRAINAGE GALLERY FOR
CONCRETE DAMS

A THESIS SUBMITTED TO
THE GRADUATE SCHOOL OF NATURAL AND APPLIED SCIENCES
OF
MIDDLE EAST TECHNICAL UNIVERSITY

BY

TAMEEM DAGHESTANI

IN PARTIAL FULFILMENT OF THE REQUIREMENTS
OF
THE DEGREE OF MASTER OF SCIENCE
IN
CIVIL ENGINEERING

JANUARY 2018

Approval of the Thesis:

**A STUDY ON OPTIMUM LAYOUT OF DRAINAGE GALLERY FOR
CONCRETE DAMS**

Submitted by **TAMEEM DAGHESTANI** in partial fulfilment of the requirements for the degree of **Master of Science in Civil Engineering Department, Middle East Technical University** by,

Prof. Dr. Gülbin Dural Ünver
Dean, Graduate School of **Natural and Applied Sciences** _____

Prof. Dr. İsmail Özgür Yaman
Head of Department, **Civil Engineering** _____

Prof. Dr. A. Melih Yanmaz
Supervisor, **Civil Engineering Department, METU** _____

Asst. Prof. Dr. Melih Çalamak
Co-Supervisor, **Civil Engineering Department, TED University** _____

Examining Committee Members:

Prof. Dr. Elçin Kentel
Civil Engineering Dept., METU _____

Prof. Dr. A. Melih Yanmaz
Civil Engineering Dept., METU _____

Assoc. Prof. Dr. Nuri Merzi
Civil Engineering Dept., METU _____

Assoc. Prof. Dr. İsmail Yücel
Civil Engineering Dept., METU _____

Asst. Prof. Dr. Müsteyde Baduna Koçyiğit
Civil Engineering Dept., Gazi University _____

Date: January 30, 2018

I hereby declare that all information in this document has been obtained and presented in accordance with academic rules and ethical conduct. I also declare that, as required by these rules and conduct, I have fully cited and referenced all material and results that are not original to this work.

Name, Last name: Tameem Daghestani

Signature :

ABSTRACT

A STUDY ON OPTIMUM LAYOUT OF DRAINAGE GALLERY FOR CONCRETE DAMS

Daghestani, Tameem

M.S., Civil Engineering Department

Supervisor: Prof. Dr. A. Melih Yanmaz

Co-Supervisor: Asst. Prof. Dr. Melih Çalamak

January 2018, 125 pages

Dams are generally massive structures retaining a large amount of water. Any failure could lead to a disaster. Therefore, keeping the dam within the required safety margins and maintaining those conditions is of the utmost importance. A gravity dam is held in place by its own weight. Uplift pressure reduces the effective weight of the dam, thus reducing its safety. Hence reducing the effect of uplift could have significant results in increasing the safety of the dam. In this study, the optimum location of the drainage gallery was studied by considering the impact of different locations of the gallery, the size and spacing of the drains for various loading conditions on multiple hypothetical cases and a case study. Results show that the presence of a drainage gallery can reduce uplift by over 60% compared to a non-drained case. As the drain diameter increases and/or the spacing between the drains decreases, the location of maximum uplift reduction shifts more towards the upstream face. The optimum horizontal position for the case study is at a distance of 10% of the base width away from the upstream face. The optimum vertical position for the gallery is below or at the level of the

downstream water level. This location combined with the placement of post-tensioning cables on the downstream side, results in the lowest uplift pressure and small cracking on the downstream side.

Keywords: Drainage gallery, Uplift pressure, Gravity Dam, CADAM, SEEP/W.

ÖZ

BETON BARAJ DRENAJ GALERİLERİNİN EN UYGUN YERLEŞİMİ ÜZERİNE BİR ÇALIŞMA

Daghestani, Tameem

Yüksek Lisans, İnşaat Mühendisliği Bölümü

Tez Danışmanı: Prof. Dr. A. Melih Yanmaz

Ortak Tez Danışmanı: Y. Doç. Dr. Melih Çalamak

Ocak 2018, 125 sayfa

Barajlar fazla miktarda su hacimlerinin depolanmasını sağlayan büyük yapılar olup, yıkılmaları afetlere yol açabilir. Bu nedenle barajların yeterli emniyet seviyesinde tutulması ve bunun takip edilmesi çok önemlidir. Bir ağırlık barajının dengesi kendi öz ağırlığınca sağlanır. Baraj altında oluşan alttan kaldırma basınçları barajın etkili ağırlığını azaltmakta ve dolayısıyla emniyetini düşürmektedir. Bu nedenle alttan kaldırma basıncı etkisinin azaltılması baraj emniyetinin artmasında çok önemlidir. Bu çalışmada, drenaj galerisinin pozisyonu ile kullanılan drenlerin çap ve aralığının en uygun drenaj galerisi yerleşimine etkileri çeşitli yükler altında model bir barajda ve bir uygulama örneğinde araştırılmıştır. Sonuçlar etkili bir drenaj galerisiyle alttan kaldırma basınçlarının drenaj sistemi olmayan bir baraja nazaran %60 azaltma sağlanabildiğini göstermiştir. Drenaj galerisi büyük çaplı drenler için memba yüzüne yakın yerleştirilmeli veya dren aralıkları azaltılmalıdır. Galerinin yatay düzlemdeki en uygun konumu memba yüzünden taban genişliğinin %10 mesafesidir. Düşey düzlemdeki en uygun konum ise galerinin mansap su seviyesinde veya daha aşağıda tutulmasıdır. Bu pozisyonla birlikte mansap

yüzünden uygulanan ard-germeli kablolarla alttan kaldırma basınçlarının mansapta ufak çatlamlar olmasına karşın en aza indiği durumdur.

Anahtar kelimeler: Drenaj galerisi, alttan kaldırma basıncı, Ağırlık Barajı, CADAM, SEEP/W

To My Family

ACKNOWLEDGMENTS

The author wishes to express his genuine gratitude and respect to his advisor Prof. Dr. A. Melih Yanmaz for his encouragement, insight, guidance, knowledge, constructive criticism, and patience.

The author also wishes to express his gratefulness and respect to his co-advisor Asst. Prof. Dr. Melih Çalamak for his advice, encouragement, guidance, suggestions, and comments throughout the period of the study.

Their corrections and recommendations were essential in bringing this thesis up to the required standards. This study would not have been possible without their help and advice.

TABLE OF CONTENTS

ABSTRACT.....	v
ÖZ	vii
ACKNOWLEDGMENTS	x
TABLE OF CONTENTS.....	xi
LIST OF TABLES	xiv
LIST OF FIGURES	xvi
LIST OF SYMBOLS AND ABBREVIATIONS	xx
CHAPTERS	
INTRODUCTION.....	1
1.1 General.....	1
1.2 Literature Review	3
UPLIFT DEVELOPMENT BENEATH CONCRETE DAMS.....	9
2.1 Uplift.....	9
2.2 Design Considerations for the Drainage Gallery	10
2.2.1 USACE Guideline	10
2.2.2 USBR Guidelines	14
2.2.3 FERC Guidelines.....	15
THE METHODOLOGY	17
3.1 Stability Analysis.....	17
3.1.1 CADAM	20
3.1.1.1 Analytical Capabilities.....	20

3.1.1.2 Modeling Capabilities	21
3.1.1.3 Output Results.....	23
3.1.1.4 Basic Modelling Information	24
3.1.1.5 Drain Effectiveness Computation	25
3.1.2 Loading Combinations	26
3.2 Seepage Analysis	28
3.2.1 SEEP/W.....	28
PRELIMINARY ANALYSES.....	31
4.1 CADAM Preliminary Analysis	31
4.1.1 Loading Conditions	31
4.1.1.1 Usual Loading Condition.....	31
4.1.1.1.1 Dam Height and Width Variations	31
4.1.1.1.2 Drain Size and Spacing.....	38
4.1.1.1.3 Internal Stresses	42
4.1.1.2 Unusual Loading Case.....	45
4.1.1.3 Extreme Loading Case.....	48
4.1.2 Post-Tension Cables	49
4.1.3 Results and Discussion.....	51
4.1.3.1 Usual Loading Case.....	51
4.1.3.1.1 Dimensional Variations	51
4.1.3.1.2 Drain Size and Spacing.....	56
4.1.3.1.3 Internal Stresses	62
4.1.3.2 Unusual Loading Case	69
4.1.3.2.1 Dimensional Variations	69
4.1.3.2.2 Drain Size and Spacing.....	74

4.1.3.2.3. Internal Stresses	81
4.1.3.3 Extreme Loading Case	88
4.1.3.4 Post Tension Cables	91
4.2 The Analysis of Seepage Beneath the Dam.....	92
4.2.1 Results and Discussion.....	95
4.2.2 Sensitivity Analysis.....	102
CASE STUDY	103
5.1 Introduction.....	103
5.2 The input Data and the computer model.....	104
5.3 The Location of the Drainage Gallery	108
5.4 Water Collection and Removal through Pumping.....	110
5.5 Pumping Schedule	111
CONCLUSIONS	119
REFERENCES	123

LIST OF TABLES

TABLES

Table 4-1 Dam dimensions	32
Table 4-2 Dams names and corresponding dimensions.....	32
Table 4-3 Minimum allowable safety factors (Leclerc et al., 2001).....	34
Table 4-4 Uplift forces of Dam 3 for H_4 and X variations for usual loading case	37
Table 4-5 Uplift forces of Dam 3 with 5 m drain spacing for H_4 variations for usual loading case	39
Table 4-6 Uplift forces of Dam 3 with 5 m drain spacing for X variations for usual loading case	40
Table 4-7 Stresses obtained for usual loading case for Dam 3	44
Table 4-8 Uplift forces of Dam 3 for H_4 and X variations for unusual loading case.....	46
Table 4-9 Post-tension cables crack reduction for 60° angle.....	50
Table 4-10 Uplift forces for Dams 1, 3, and 5 for H_4 variations for usual loading case.....	51
Table 4-11 Uplift forces for Dams 1, 3, and 5 for X variations for usual loading case.....	53
Table 4-12 Uplift forces for Dams 1, 3, and 5 for H_4 variations for unusual loading case.....	70
Table 4-13 Uplift forces for Dams 1, 3, and 5 for X variations for unusual loading case.....	72
Table 4-14 Crack % of base of Dams 1, 3, and 5 for X variations	72
Table 4-15 Cracking of base of Dam 3 for all D and S for H_4 variations.....	79
Table 4-16 Cracking of base of Dam 3 for all D and S for X variations	80
Table 4-17 Location of points considered for the analysis	93

Table 4-18 Seepage rate for Case 2.....	96
Table 4-19 Pore water pressure for Case 2	97
Table 5-1 Porsuk Dam general information (DSİ) and (“Porsuk Dam (Eskisehir, 1972) Structurae,” n.d.)	104
Table 5-2 Porsuk Dam data Beşer, M. R. (2005).....	105
Table 5-3 Porsuk Dam estimated data	107
Table 5-4 Comparison between different X locations	109
Table 5-5 Pump cost.....	113
Table 5-6 Pump calculations	116
Table 5-7 Pumping sessions in a day	117

LIST OF FIGURES

FIGURES

Figure 2-1 Uplift distribution without drains, (Redrawn from US Army Corps of Engineers, 2000)	10
Figure 2-2 USACE uplift distribution for $X \leq 0.05H_1$, (Redrawn from US Army Corps of Engineers, 2000)	11
Figure 2-3 USACE uplift distribution for $X > 0.05H_1$, (Redrawn from US Army Corps of Engineers, 2000)	12
Figure 2-4 USACE uplift distribution $T < X$, (Redrawn from US Army Corps of Engineers, 2000)	13
Figure 2-5 USACE uplift distribution $T > X$, (Redrawn from US Army Corps of Engineers, 2000)	13
Figure 2-6 USBR uplift distribution $T < X$, (Redrawn from US Army Corps of Engineers, 2000)	15
Figure 2-7 FERC uplift distribution $T > X$, (Redrawn from US Army Corps of Engineers, 2000)	16
Figure 3-1 Stability Analysis methodology	19
Figure 3-2 CADAM sign convention, forces and stresses, (Leclerc et al. 2001)	25
Figure 3-3 CADAM sign convention, inertia forces, (Leclerc et al. 2001)	25
Figure 3-4 Drain effectiveness computation, (Leclerc et al. 2001)	26
Figure 4-1 Section geometry for Dam 3	33
Figure 4-2 Dam 3 configuration on CADAM for usual loading case.....	33
Figure 4-3 Uplift pressures & drainage system	35
Figure 4-4 Computation of drain effectiveness	38
Figure 4-5 CADAM report, stresses and uplift.....	42
Figure 4-6 CADAM graphical reports, stresses, uplift	43
Figure 4-7 Dam 3 configuration on CADAM for unusual loading case.....	45

Figure 4-8 CADAM report, stress and uplift, unusual loading case	47
Figure 4-9 CADAM graphical report, unusual loading case	48
Figure 4-10 Dam 1 configuration on CADAM for extreme loading condition ...	48
Figure 4-11 Post-tension cables window	50
Figure 4-12 Post-tension cables for Dam 1	50
Figure 4-13 Uplift force for H_4 variations for Dams 1, 3, and 5.....	52
Figure 4-14 %Reduction of uplift force for H_4 variations for Dams 1, 3, and 5..	52
Figure 4-15 Uplift force for X variations for Dams 1, 3, and 5	53
Figure 4-16 %Reduction of uplift force for X variations for Dams 1, 3, and 5...	54
Figure 4-17 Uplift force for H_4 variations for Dams 3 and 4.....	54
Figure 4-18 Uplift force for X variations for Dams 3 and 4	55
Figure 4-19 Uplift for H_4 variations, $S = 5$ m, all D	57
Figure 4-20 %Reduction of uplift force for H_4 variations, $S = 5$ m, all D.....	57
Figure 4-21 Uplift for X variations, $S = 5$ m, all D.....	58
Figure 4-22 %Reduction of uplift force for X variations, $S = 5$ m, all D	58
Figure 4-23 Uplift for H_4 variations, $D = 0.1$ m, all S	59
Figure 4-24 %Reduction of uplift force for H_4 variations, $D = 0.1$ m, all S.....	59
Figure 4-25 Uplift for X variations, $D = 0.1$ m, all S.....	60
Figure 4-26 %Reduction of uplift force for X variations, $D = 0.1$ m, all S	61
Figure 4-27 %Reduction of uplift force for X variations, $D = 1$ m, all S	62
Figure 4-28 Stresses for H_4 variations for Dam 3	63
Figure 4-29 Stresses for X variations for Dam 3	63
Figure 4-30 Stresses upstream, H_4 variations, $S = 5$ m, all D.....	64
Figure 4-31 Stresses downstream, H_4 variations, $S = 5$ m, all D	65
Figure 4-32 Stresses upstream, X variations, $S = 5$ m, all D	65
Figure 4-33 Stresses downstream, X variations, $S = 5$ m, all D	66
Figure 4-34 Stresses upstream, H_4 variations, $D = 0.25$ m, all S	67
Figure 4-35 Stresses downstream, H_4 variations, $D = 0.25$ m, all S	67
Figure 4-36 Stresses upstream, X variations, $D = 0.25$ m, all S	68
Figure 4-37 Stresses downstream, X variations, $D = 0.25$ m, all S	68
Figure 4-38 Uplift force for H_4 variations for Dams 1, 3, and 5.....	70

Figure 4-39 %Reduction of uplift force for H_4 variations for Dams 1, 3, and 5	71
Figure 4-40 Uplift force for X variations for Dams 1, 3, and 5	73
Figure 4-41 %Reduction of uplift force for X variations for Dams 1, 3, and 5	73
Figure 4-42 Uplift for H_4 variations, $S = 5$ m, all D	74
Figure 4-43 %Reduction of uplift force for H_4 variations, $S = 5$ m, all D	74
Figure 4-44 Uplift for X variations, $S = 5$ m, all D	75
Figure 4-45 %Reduction of uplift force for X variations, $S = 5$ m, all D	75
Figure 4-46 Uplift for H_4 variations, $D = 0.1$ m, all S	76
Figure 4-47 %Reduction of uplift force for H_4 variations, $D = 0.1$ m, all S	76
Figure 4-48 Uplift for X variations, $D = 0.1$ m, all S	77
Figure 4-49 %Reduction of uplift force for X variations, $D = 0.1$ m, all S	77
Figure 4-50 Stresses for H_4 variations for Dam 3	81
Figure 4-51 Stresses for X variations for Dam 3	81
Figure 4-52 Stresses upstream, H_4 variations, $S = 5$ m, all D	83
Figure 4-53 Stresses downstream, H_4 variations, $S = 5$ m, all D	83
Figure 4-54 Stresses upstream, X variations, $S = 5$ m, all D	84
Figure 4-55 Stresses downstream, X variations, $S = 5$ m, all D	84
Figure 4-56 Stresses upstream, H_4 variations, $D = 0.25$ m, all S	85
Figure 4-57 Stresses downstream, H_4 variations, $D = 0.25$ m, all S	86
Figure 4-58 Stresses upstream, X variations, $D = 0.25$ m, all S	86
Figure 4-59 Stresses downstream, X variations, $D = 0.25$ m, all S	87
Figure 4-60 Peak stresses for H_4 variations	88
Figure 4-61 Sustained stresses for X variations	89
Figure 4-62 Crack length, extreme loading case	90
Figure 4-63 %Reduction of cracks vs vertical position of cables	91
Figure 4-64 Cross sectional view of Dam 7	92
Figure 4-65 Comparison of 1 m and 3 m mesh size readings	94
Figure 4-66 Definition of the Dam on SEEP/W	94
Figure 4-67 Drainage details for Case 2 on SEEP/W	95
Figure 4-68 Seepage rates and the velocity field beneath the dam without drains	95

Figure 4-69 Seepage rates and the velocity field beneath the dam for Case 2.....	96
Figure 4-70 Seepage rate for X variations for Case 2.....	97
Figure 4-71 Pore water pressure for X variations for Case 2.....	98
Figure 4-72 Seepage rate for X variations for Case 2 at 0-4%location	99
Figure 4-73 Pore water pressure for X variations for Case 2 at 0-4%location	99
Figure 4-74 Seepage rate comparison for H_4 variations	100
Figure 4-75 Seepage rate comparison for X variations.....	101
Figure 4-76 Pore water pressure for X variations	101
Figure 4-77 Seepage rates of (a) Case 1; (b) Case 2; (c) Case 3.....	102
Figure 5-1 Porsuk Dam (DSI, 2012).....	103
Figure 5-2 Porsuk Dam map (Courtesy of Google Maps).....	104
Figure 5-3 Porsuk Dam cross section (DSI)	106
Figure 5-4 Porsuk Dam cross section (Ural and Ungan 1967)	106
Figure 5-5 Porsuk Dam on CADAM.....	107
Figure 5-6 Porsuk Dam on SEEP/W	107
Figure 5-7 Seepage beneath Porsuk Dam	108
Figure 5-8 The seepage rates passing beneath, and through the drainage gallery of Porsuk Dam	108
Figure 5-9 Sump well details (Kharagpur, 2012).....	111
Figure 5-10 Daily cost for each pumping rate	117
Figure 5-11 Annual cost for each pumping rate.....	118

LIST OF SYMBOLS AND ABBREVIATIONS

A	Cross Sectional Area [m ²]
ANCOLD	Australian National Committee on Large Dams
ASDSO	Association of State Dam Safety Officials
ASTM	American Society for Testing and Materials
B	Gradient matrix
C	Hydraulic conductivity matrix
CADAM	Computer Analysis of Dams
CDF	Cumulative Distribution Function
CDSA	Canadian Dam Safety Association
CRF	Capital Recovery Factor
D/S	Downstream
D	Diameter [m]
<i>dh/dl</i>	Hydraulic head gradient
DSI	General Directorate of State Hydraulic Works
E	Effectiveness
<i>f</i>	Friction factor
F	Elevation where the vertical section on the D/S face ends [m]
FERC	Federal Energy Regulatory Commission
<i>g</i>	Gravitational acceleration [m/s ²]
G	Elevation of the highest point [m]
G	at the location of the gallery
H	Dam height [m]

H	Head boundary condition [m]
H^*	Vertical section at the downstream face [m]
H_1	Upstream water depth [m]
H_2	Downstream water depth [m]
H_3	Intensity at the line of drains [m]
H_4	Elevation of the bottom of the gallery [m]
H_f	Head loss [m]
H_p	Pump head [m]
H_t	Dam height [m]
HPGA	Horizontal Peak Ground Acceleration [m/s^2]
i	unit gradient
K	Efficiency
K	Hydraulic conductivity [m/s]
k_x	Hydraulic conductivity in horizontal direction [m/s]
k_y	Hydraulic conductivity in vertical direction [m/s]
L	Base width [m]
L_1	Base width [m]
L_3	Thickness at point F [m]
L_4	Crest thickness (at point G) [m]
N	Interpolating function vector
OF	Overturning Factor
P	Hydrostatic pressure [kPa]
P	Pressure head [m]
P	Drain efficiency
P_c	Post tension cable (crest) [kN]
P_d	Post tension cable (downstream) [kN]

PDF	Probability Distribution Function
PGA	Peak Ground Acceleration
PSF	Peak Sliding Factor
q	unit flux [m/s]
Q	Discharge [m ³ /s]
Q	Total flux [m ³ /s]
RSF	Residual Sliding Factor
S	Spacing [m]
SEEP/W	Seepage for Windows
SF	Safety Factor
t	Time
t_c	Crest thickness [m]
T	Crack length [m]
T	Length of joint at which the effectiveness is being computed [m]
U/S	Upstream
UF	Uplift Factor
USACE	United States Army Corps of Engineers
USBR	United States Bureau of Reclamation
v	Velocity [m/s]
VPGA	Vertical Peak Ground Acceleration [m/s ²]
W	Base width [m]
X	Distance of center of gallery from the upstream face [m]
z	Distance between drain center and upstream face [m]
γ_w	Specific weight of water [kN/m ³]
θ	Angle of repose
θ	Volumetric water content
τ	Element thickness

CHAPTER 1

INTRODUCTION

1.1 General

Water is retained behind a dam for a number of reasons: power generation, irrigation, drinking water, flood mitigation, recreational purposes, etc. Some water will seep through the foundation and try to make its way towards the downstream side of the dam, thus passing under the dam. This creates an uplift pressure acting upwards and pushing the dam body up and consequently reducing the effective weight of the dam. Gravity dams are held in position by their own weight. Therefore, any reduction of the effective weight will reduce the safety of the dam and could potentially lead to structural failure. Some examples of dam failures (collected from (ASDSO, n.d.)) attributed to the underestimation of the impact of uplift pressure include:

- The Austin (Bayless) Dam (Pennsylvania, USA): this 50 ft. (15.24 m) concrete gravity dam was constructed in 1909 to supply water to the Bayless paper mill. The dam collapsed on September 30th 1911, leading to 78 deaths and an estimated damage of \$70 - \$140 million dollar (estimated by 2010 USD value). The failure was attributed to multiple reasons: crest height modification, concrete did not have enough time to set properly, engineering practice errors, and the failure to consider the full impact of the uplift force (Kline and Fleming 2013 and Rose 2013).
- St. Francis Dam (California, USA): this 205 ft. (62.5 m) curved concrete gravity dam was constructed in 1926 to provide storage reservoir for the

Los Angeles Aqueduct system. The dam collapsed on March 13th 1928, leading to over 450 deaths and an estimated cost of over \$140 million (estimated by 2010 USD value). The failure was attributed to increasing the dam height during construction without modifying the base width thus reducing the factors of safety and structural stability, and the inability of the dam to fully accommodate the full load of the applied uplift force (Rogers and McMahon 1993 and Rogers 2006).

- Malpasset Dam (Fréjus, France): this 218 ft. (66.4 m) arch concrete dam was constructed in 1954 for irrigation and water supply purposes. The dam failed on the 2nd of December 1959, resulting in the death of 421 people. The collapse was attributed to the poor testing of the geological formation at the dam site and the surge in the uplift force as the reservoir was filled to the point that it was strong enough to dislodge the thrust block and lead to the propagation of the cracks created due to the dislodging (Duffaut, 2013).

If the amount of water seeping below the dam and moving towards the downstream side is reduced, uplift pressure can be reduced. This can be achieved by providing an alternate path for the water through the dam body. Due to pressure difference, the water will enter the drains imbedded in the foundation and will make its way towards the drainage gallery located within the dam. This water will then be collected in a sump well to be pumped out of the dam later.

Galleries are openings in a dam that provide access to the interior parts. They along with shafts form a system of connected galleries that allow movement within the dam. Galleries have different purposes depending on their location within the dam. They could be used for drilling and grouting, inspection, storage, or drainage and uplift pressure reduction (the main concern of this study) (USBR, 1976).

There have been numerous studies revolving around the importance of the drainage gallery in reducing the uplift pressure and the relation between the

properties of the drainage system (drain spacing, diameters, location, etc.) and the uplift pressure. Some of these studies are supplied in the next section.

1.2 Literature Review

USBR (1976) and US Army Corps of Engineers (1995) recommend a minimum distance of 5 ft. (1.524 m) between the gallery floor and the foundation level, and between the upstream face of the dam and the upstream wall of the gallery for the placement of mass concrete and to reduce stress concentrations.

According to Hannah and Kennedy (1938) a well-designed dam is provided with drainage and inspection galleries to reduce uplift and monitor the dam body. The gallery should be located between 3 m to 9 m away from the upstream face.

Jansen (1988) state that the gallery must be at least 3 m away from the upstream face and is at a distance of at least 5% of the reservoir head (upstream water level) away from the upstream face. There should be at least a layer of concrete, 1.5 m thick between the upstream face and the gallery and between the floor of the gallery and the foundation level. These recommendations were presented in the aforementioned books and manuals to give a general idea of where the gallery should be located.

The research by Chawla et al. (1990) has shown that the size, location, and spacing of the drains impact the distribution of internal uplift pressure by using an analytical solution based on seepage theory. Different combinations of the ratio of drain spacing, diameter, and distance from upstream face all with respect to the base width of the dam have been considered in order to determine the optimal location of drainage gallery for minimum uplift pressure. The results show that the uplift pressure decreases as the spacing between drains is reduced and the diameter is increased. Furthermore, the location for minimum uplift pressure moves towards the upstream face as the spacing between drains is reduced and the size of the drain diameter is increased. This provides a further

understanding of the relation between uplift pressure and the drain properties and how the uplift pressure can be predicted and its effect mitigated by varying these properties. Also, since ratios are used in this paper, the results can be applied on any dam as long as the conditions are met and the appropriate ratio is used.

El-razek and Elela (2001) attempted to determine the optimum position of the drainage gallery underneath the gravity dam by experimentally determining the position where the maximum reduction in the uplift force occurs. Four different upstream water elevation levels were combined with seven different positions of the drainage gallery beneath the dam with respect to the base width of the dam resulting in 28 possible combinations for the sand model considered that was used to represent a gravity dam. The reduction of uplift pressure at each position is compared with the case of no drainage gallery and the optimum position was determined to be at the center of the dam with an average reduction of 54% showing that a drainage system in a dam can have a very large impact on one of the major forces threatening the safety of the dam if placed at the right location.

Zee et al. (2011) have examined the impact of the size, location, and spacing of the drains and the elevation of the gallery on the drain efficiency by calculating the piezometric head using Laplace equation. The combinations considered were of four drains spacing (2, 2.5, 3, and 3.5 m), three drain diameters (120, 160, and 200 mm), and three distance from upstream face (5, 6, and 7 m). The results indicate that the highest drain efficiency (0.92) is achieved at 2 m drain spacing (smaller spacing), 200 mm drain diameter (larger diameter) and at a distance of 7 m from the upstream face (further distance). In addition, placing the gallery at a lower elevation reduces the uplift pressure further and that the presence of the gallery reduces the accumulation of calcium carbonate in drain wells which reduce their efficiency over time.

Hu and Ma (2016) focused on the variables that lead to a sudden increase in uplift pressure beneath concrete gravity dams. Statistical analyses of measured time series, inversion analyses of seepage fields and field geological

investigation were used to determine the causes of this increase in uplift for a case study. The statistical analysis has shown that the increase in reservoir water level and amount of rainfall and the decrease in temperature during the period under investigation lead to an increase in uplift pressure. However, when high water level alone occurred it did not lead to a significant increase in uplift meaning that the coupled effect of these variables is necessary to generate this increase in uplift. The inverse analysis results indicate that the effectiveness of the water proofing system has a major impact on the seepage flow. The performance of the water proofing system is dependent on the local geology and the condition of the foundation rock affecting the hydraulic conductivity of rock. The image logs obtained during the geological investigations revealed broken rock mass and well developed joint fissures under the dam leading to zones exhibiting tension joints and higher hydraulic conductivity. These results show that the uplift pressure is influenced by the localized foundation configuration and geology and since there is a high spatial and temporal variability in these conditions this makes uplift pressure distribution and behavior difficult to predict. Nonetheless, the application of the analysis methods mentioned in the study allow for a better understanding of uplift and lower the uncertainty during the cause-analysis process.

According to Goodman et al. (1983) the drains have a large influence on the magnitude and distribution of the uplift forces through the cracks located closer to the upstream face and that the location of the drainage gallery that has the largest influence on reducing the uplift forces is approximately between one half and one fifth of the length of the horizontal crack in the dam from its upstream end. In the analytical solution used, the dam has an infinite row of drainage wells passing through the finite crack generated from the heel of the dam and the wells are parallel to the face of the dam and the impervious boundaries considered. It is apparent from the results that the assumption that the head throughout the crack is constant and equal to the reservoir head is not a valid assumption; the drains do indeed reduce the uplift through the crack. In addition, reducing the spacing

between the drains by drilling extra drainage holes reliefs the pressure only slightly. However, much significant reduction is observed if the new drains are forced to discharge at the same rate as the existing drains through pumping, this is not a very feasible option because relying on pumps during a potential flood condition is an unwanted risk.

Amadei et al. (1989) considered an analytical solution to model the internal uplift pressure related to cracks in older concrete gravity dams. Different influences were considered separately to assess their individual impact on drainage effectiveness. Firstly, the effectiveness increases as the ratio of piezometric head to reservoir head decreases, indicating that a lower piezometric head (lower elevation of gallery) or a higher reservoir water level lead to an increase in the efficiency of the drainage system. Secondly, the effectiveness decreases as the lateral width of the crack increases or if the crack occurs closer to the base of the dam. Thirdly, the effectiveness increases as the crack length increase i.e. the crack intercepts the drains. The optimum position for reducing uplift and overturning moments is when the drains are located between one half and one fifth of the crack length and when the drain is located at the longitudinal center line of the crack. Fourthly, the effectiveness increases as the crack aperture decreases, the crack roughness increases, and as the crack degree of separation decreases. These conclusions provide great insight into the relation between drain effectiveness and the properties of a crack at the upstream face

Amadei and Illangasekare (1992) investigated the aforementioned relationship further by using the strength of materials approach to assess the stability of concrete gravity dams with finite cracks generated at their base under usual loading conditions. The results show that the drain effectiveness increases as the crack propagates further into the dam in the horizontal direction (towards the downstream face) and as the lateral width of the crack reduces (parallel the upstream face). Furthermore, as long as the crack intersects the drains it can reduce the magnitude of the minimum allowable compressive stress, provides

more compression at the crack tip and on the edge of the un-cracked part at the upstream side. Finally it reduces the crack uplift force and thus the uplift force coming from the water pressure acting on the un-cracked section of the dam base. This again shows the importance of accounting for the drainage system for cracked dam bases and how that can reduce the maintenance and rehabilitation cost for dams with a cracked base since higher stability is now considered due to the effective drainage system.

These studies have shown that the drainage system has a great impact on reducing uplift. The last three studies show that the system is effective even in the presence of cracks at the upstream face. The effectiveness in reducing uplift is related to the properties of the drainage system including location, drain diameter and spacing. However, these studies focused on the usual loading condition and did not consider the system during unusual or extreme loading conditions. Furthermore, the impact of the drainage system on internal stresses was not considered. Since the extreme loading condition is not addressed, the relation between the location, spacing, and size of drains and the cracks generated at the downstream face due to extreme loading conditions is not considered either. Finally, the relation between the pump schedule and optimal gallery location has not been addressed in any of the aforementioned studies.

The problem is that as the previous studies have shown, increased drain diameter, reduced spacing between drains, and lower placement of gallery have a positive effect on reducing uplift. However, these tend to increase the internal stresses due to the presence of more hollow space in the dam. Consequently, the internal stresses must be measured for each combination and location to determine if the stresses exceed the acceptable range for any combination or location.

Furthermore, the elevation of the top of the sump well (used in this study to remove the accumulated water by pumping) is at the level of the floor of the gallery. This adds further restrictions to the vertical location of the gallery, since the clearance level between the bottom of the gallery and the foundation level

suggested in the literature review should also be considered between the bottom of the sump well and the foundation level as well. Finally, the cracks on the downstream side could be reduced by adding post-tensioning cables, increasing the drain diameter, reducing spacing between drains and by moving the gallery more towards the downstream side. However, this increases the internal stresses and reduces uplift reduction. Therefore, the internal stresses should be checked and the amount of reduction of uplift and crack generation should be studied to determine if the compromise between the two is justifiable.

In this study, the impact of the location of the gallery within the dam (both horizontally and vertically) and the drain size and spacing on the reduction of uplift pressure, development of stresses within the dam and the crack generation and propagation is considered for usual, unusual, and extreme loading conditions. Different dam sizes were used to assess the impact of the dam geometry on the drainage system effectiveness. The investigations were conducted using CADAM and SEEP/W software allowing quick and accurate results. Finally, the results and developed knowledge of the impact of these variables were applied to a case study to compare the real life drainage system properties in the dam and the recommended drainage system properties based on the analysis results. Then, different pumping options were considered for the removal of the water collected in the sump well. The cheapest alternative is taken as the optimum pumping schedule.

CHAPTER 2

UPLIFT DEVELOPMENT BENEATH CONCRETE DAMS

2.1 Uplift

This chapter deals with the definition of uplift and how it is computed based on three different agencies (USACE, USBR, and FERC) as described in US Army Corps of Engineers (2000).

Uplift pressure occurs due to the water seeping from the upstream side to the downstream side of the dam due to pressure difference. This water tries to push the dam up as it passes under it; hence it forms an uplift pressure. This pressure is present in the pores, cracks, joints, between the dam and the foundations, and within the foundation below the base. It is an active force that must be included in the stability and stress analysis to ensure structural safety and adequacy.

When a drainage system is present, the uplift pressure can be reduced up to a certain limit based on the effectiveness of the drainage system. The effectiveness of the drainage system depends on the depth, size, and spacing of the drains, as well as the age and condition of the system, and the foundation characteristics.

Different agencies compute uplift pressure and the drainage effectiveness differently for different scenarios. Figure 2-1 shows the generation of uplift without drainage. This is applicable to all three guidelines. Uplift pressure varies linearly from the upstream side $\gamma_w H_1$ to the downstream pressure head $\gamma_w H_2$, where γ_w is the specific weight of water, H_1 is the upstream water depth, and H_2 is the downstream water depth.

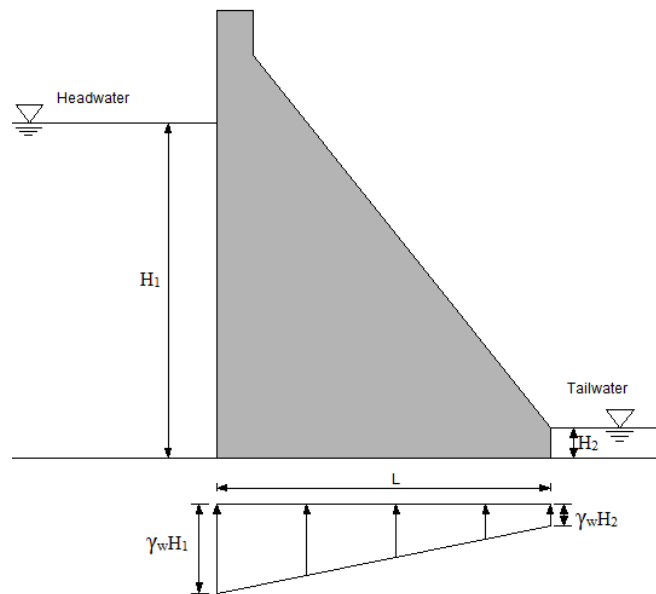


Figure 2-1 Uplift distribution without drains, (Redrawn from US Army Corps of Engineers, 2000)

2.2 Design Considerations for the Drainage Gallery

2.2.1 USACE Guideline

The effectiveness of the drainage system is assumed to vary between 25% and 50%. However, for new dams, a maximum value of 67% can be taken if the foundation testing and flow analysis support this assumption.

Figure 2-2 shows the uplift pressure distribution for a drained dam with the gallery located at a distance of 5% of the reservoir head “ H_1 ” or less away from the upstream face.

Again, the uplift pressure varies linearly from upstream to downstream. However, the pressure below the heel is now $\gamma_w H_3$ (intensity at the line of drains) rather than $\gamma_w H_1$ ($H_3 < H_1$) due to the presence of the gallery. H_3 is computed using Equations (2.1) and (2.2).

$$H_3 = K(H_1 - H_2) + H_2 \quad \text{for } H_4 < H_2 \quad (2.1)$$

$$H_3 = K(H_1 - H_4) + H_4 \quad \text{for } H_4 > H_2 \quad (2.2)$$

where

$$K = 1 - E \quad (\text{in decimal form}) \quad (2.3)$$

where K is the efficiency and E is the effectiveness of the drains. K is computed using Equation (3.1) presented in Chapter 3.

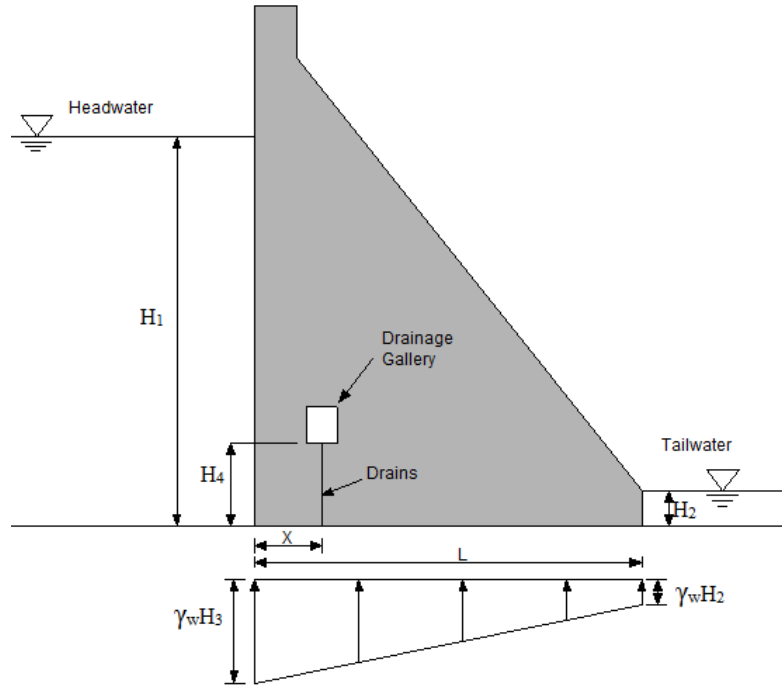


Figure 2-2 USACE uplift distribution for $X \leq 0.05H_1$, (Redrawn from US Army Corps of Engineers, 2000)

Figure 2-3 shows the uplift pressure distribution for a drained dam with the gallery located at a distance farther than 5% of the reservoir head “ H_1 ” away from the upstream face.

H_3 is now computed using Equations (2.4) and (2.5).

$$H_3 = K(H_1 - H_2) \frac{(L - X)}{L} + H_2 \quad \text{for } (H_4 < H_2) \quad (2.4)$$

$$H_3 = K \left[(H_1 - H_2) \frac{(L - X)}{L} + H_2 - H_4 \right] + H_4 \quad \text{for } (H_4 > H_2) \quad (2.5)$$

This indicates that as the gallery moves further away from the upstream face the reduction of uplift pressure becomes less effective leading to a larger pressure below the heel of the dam.

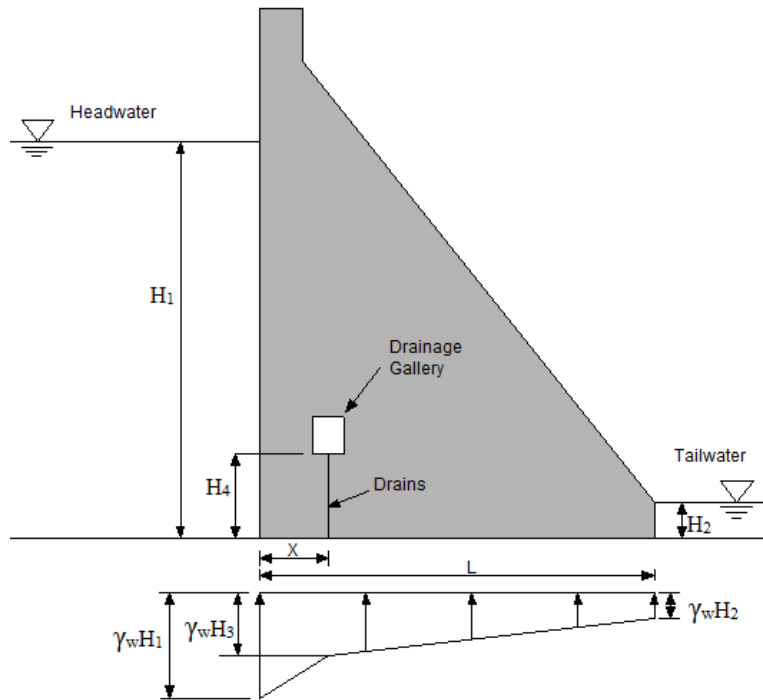


Figure 2-3 USACE uplift distribution for $X > 0.05H_1$, (Redrawn from US Army Corps of Engineers, 2000)

Figure 2-4 shows the uplift distribution in the case of a base crack (zero compression zone) when the crack length “T” does not extend beyond the location of the gallery “X”. The gallery is still considered to be functional and can reduce the uplift pressure.

H_3 is computed using the Equations (2.6) and (2.7).

$$H_3 = K \left[(H_1 - H_2) \frac{L - X}{L - T} \right] + H_2 \quad \text{for } (H_4 < H_2) \quad (2.6)$$

$$H_3 = K \left[(H_1 - H_2) \frac{L - X}{L - T} + H_2 - H_4 \right] + H_4 \quad \text{for } (H_4 > H_2) \quad (2.7)$$

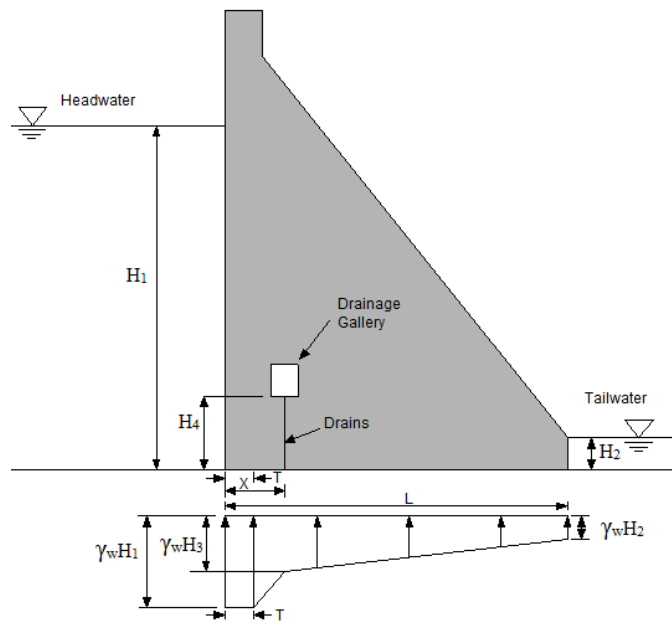


Figure 2-4 USACE uplift distribution $T < X$, (Redrawn from US Army Corps of Engineers, 2000)

For the case when the crack length “T” extends beyond the location of the gallery “X” the gallery is considered to be completely ineffective in reducing the uplift pressure as shown in Figure 2-5.

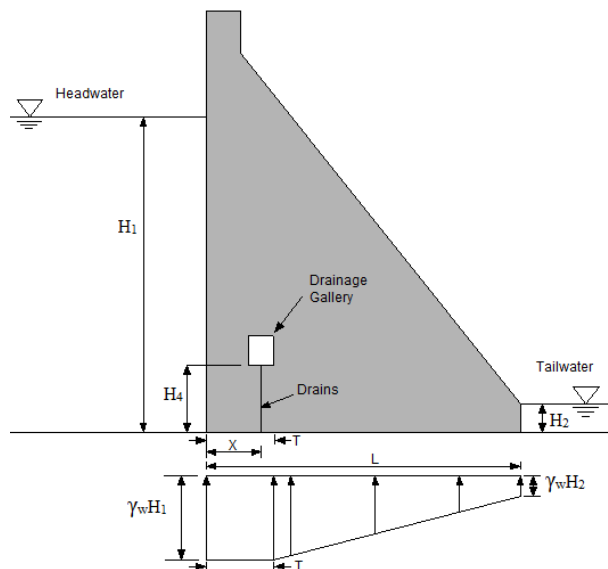


Figure 2-5 USACE uplift distribution $T > X$, (Redrawn from US Army Corps of Engineers, 2000)

2.2.2 USBR Guidelines

For the case where there is no cracking, the uplift distribution is similar to that of USACE (see Figure 2-3). H_3 is computed using Equations (2.8) and (2.9).

$$H_3 = K(H_1 - H_2) + H_2 \quad (\text{for } H_4 < H_2) \quad (2.8)$$

$$H_3 = K(H_1 - H_4) + H_4 \quad (\text{for } H_4 > H_2) \quad (2.9)$$

H_4 is the elevation of the drainage gallery measured from the bottom of the gallery, and K is the efficiency of the drains.

Uplift profiles gathered from existing dams estimated that H_3 is equivalent to the downstream pressure “ $\gamma_w H_2$ ” plus one-third of the difference between the upstream water pressure “ $\gamma_w H_1$ ” and the downstream water pressure. Using Equation (2.8), $K = 1/3$ and the efficiency $E = 2/3 = 0.67$.

Comparing Equations (2.4) and (2.8) for $H_4 < H_2$ and $T=0$ show one extra variable in Equation (2.4) $((L-X)/L)$ which is less than one. This indicates that the pressure values obtained from the USBR equation are more conservative than those of the USACE equation for the same drain effectiveness.

USBR considers the drains to be fully nonfunctional for any crack length (see Figure 2-6). This assumption is very conservative, since the drains might reduce the pressure even more effectively than before (the cracks relieve the pressure and leave more spaces). Therefore, the drain effectiveness must be well verified after crack formation before any conclusions about structural stability and safety or modifications to the structure take place. For the case when the crack extends beyond the position of the gallery the uplift distribution is similar to that defined by USACE (see Figure 2-5). H_3 is computed using Equations (2.10) and (2.11).

$$H_3 = \frac{L - X}{L - T}(H_1 - H_2) + H_2 \quad (\text{for } H_4 < H_2) \quad (2.10)$$

$$H_3 = \frac{L - X}{L - T}(H_1 - H_2) + H_4 \quad (\text{for } H_4 > H_2) \quad (2.11)$$

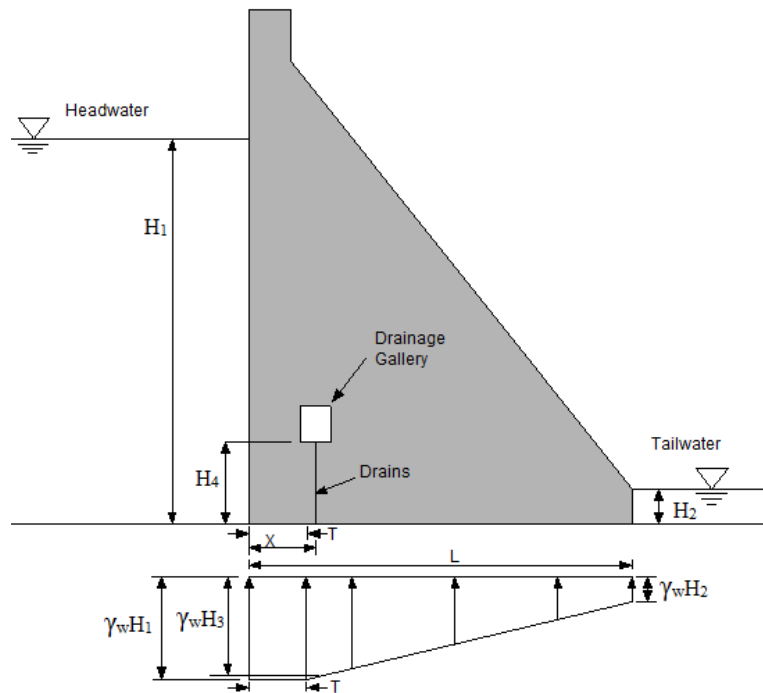


Figure 2-6 USBR uplift distribution $T < X$, (Redrawn from US Army Corps of Engineers, 2000)

2.2.3 FERC Guidelines

The FERC (Federal Energy Regulatory Commission) assumes an uplift pressure distribution similar to that defined by USACE (see Figure 2-3). Thus, H_3 is computed using either Equation (2.4) or (2.5). Though, it does not consider the case where the gallery is less than 5% of the reservoir head away from the upstream (see Figure 2-2). For the case when the crack length does not reach the gallery, the application presented in Figure 2-4 is applicable and H_3 is computed using either Equation (2.6) or (2.7). However, FERC considers the drains to be effective for the case when the crack length extends beyond the gallery if the piezometric readings support this assumption as shown in Figure 2-7. In this case, H_3 is computed using either Equation (2.1) or (2.2).

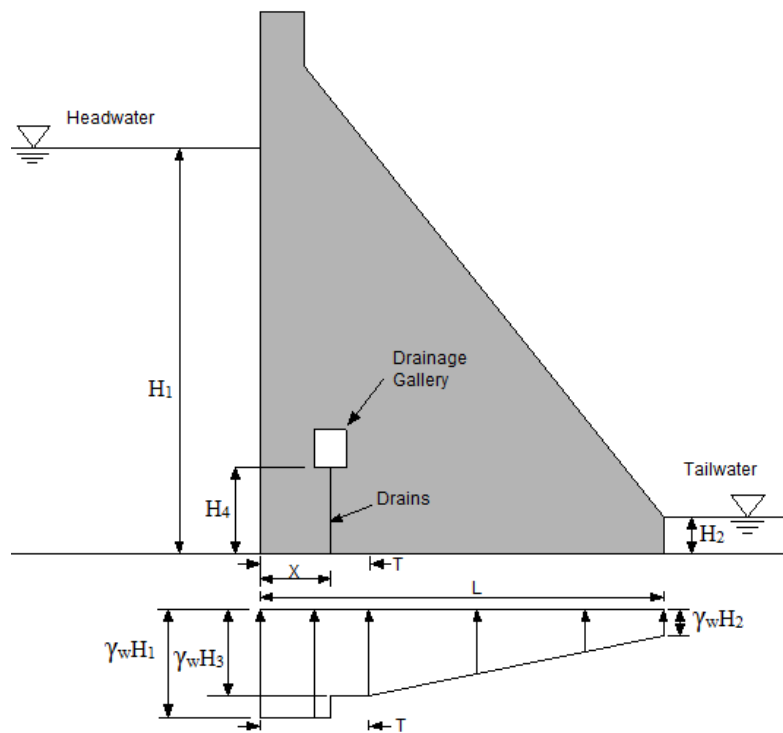


Figure 2-7 FERC uplift distribution $T > X$, (Redrawn from US Army Corps of Engineers, 2000)

CHAPTER 3

THE METHODOLOGY

3.1 Stability Analysis

The goal of the stability analysis is to determine the impact of the properties of the drainage system: horizontal location, vertical location, drain diameter, and drain spacing on the uplift generated beneath the dam. The internal stresses are expected to increase due to the presence of the drainage system (more hollow space), that is why the stresses have to be measured at each step to make sure they are within a tolerable range. Furthermore, multiple hypothetical dams were used to study the impact of the height and base width changes on uplift. Finally, the analysis was considered for usual, unusual, and extreme loading conditions to provide a more comprehensive analysis.

Figure 3-1 represents the methodology used in the stability analysis. First, a dam model is defined (step 1). This includes the dam geometry, the water level, ice load, silt accumulation, etc. The analysis that follows is carried out for each of the loading conditions defined (step 2). Once a dam is defined and the loading condition is selected, the analysis is carried out for the case without a drainage system (steps 3 and 4). If cracks are observed on the downstream side, post-tensioning cables could be added to reduce the generation and propagation of these cracks (step 5). Then, the uplift force calculated is recorded and the stresses and safety factors are checked to make sure the dam is stable (step 6). Next, a drainage system is added for a specified combination of drain diameter and spacing between drains (step 7). After running the analysis (step 8), cracks on the

downstream side are checked again and post-tensioning cables are added if needed (step 9). Otherwise, the new uplift force and stresses and safety factors are recorded (step 10). Once every vertical location of the drainage gallery “H₄” for a fixed horizontal location “X” is tested (step 11), the horizontal location is fixed and the vertical location becomes the variable term and the analysis is carried out again (step 12).

By changing the dam geometry in step 1, the impact of the geometry on uplift force is studied. By considering the different loading combinations in step 2, the dam is subjected to different forces (e.g. flooding, earthquake) allowing stresses to increase and cracks to generate. This gives a better view of how the properties of the drainage system can affect stresses and cracks. More information about the components of each loading combination is presented in section 3.1.2. Running the analysis in steps 8 through 12 for different combinations of drain diameter and spacing defined in step 7, provides insight into how these two properties influence uplift, internal stresses, and cracks generated. The impact of the vertical location of the gallery in step 11 and the horizontal location in step 12 are considered separately by varying the location of one of them and fixing the other. Finally, the results of both cases (with a drainage gallery and without a drainage gallery) are compared to see the effect of these properties and to determine the optimum location where maximum uplift reduction occurs.

The stability analysis was carried out on CADAM, a program capable of defining all the properties mentioned above as input variables and generating the required output at each step in a quick and accurate manner.

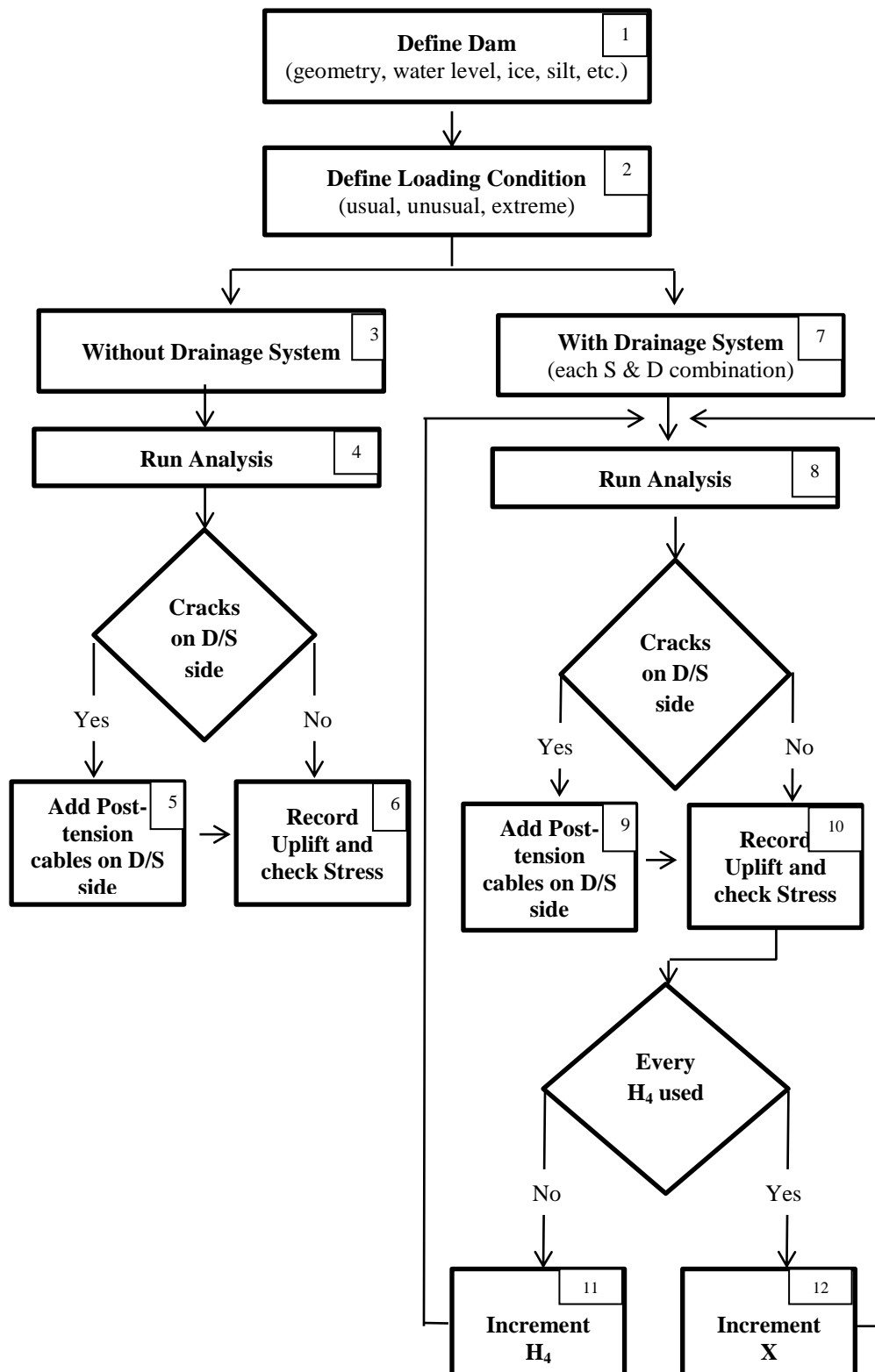


Figure 3-1 Stability Analysis methodology

3.1.1 CADAM

CADAM (Computer **A**nalysis of **D**ams) was developed by Leclerc M., Légar P., and Tenawi R. at the Department of Civil, Geological, and Mining Engineering in École Polytechnique de Montréal in 1991 in the context of the industrial chair of Structural Safety on Existing Concrete Dams, with funding from NSERC (Natural Sciences and Engineering Research Council), Hydro Québec, and Alcan. The program was developed for concrete gravity dams for the purpose of learning the principles of structural stability evaluation and to support research and development of structural behavior and safety of concrete gravity dams. CADAM is based on the gravity method (rigid body equilibrium and beam theory). It is capable of performing stability analysis on hydrostatic and seismic load combinations. The various modeling options included allow the user to see the structural behavior of the gravity dam such as geometry, uplift pressure and drainage, crack initiation and propagation, etc. under different loading combinations. The material provided in this section is gathered from (Leclerc et al. 2001), (Leclerc et al. 2002), and (Leclerc et al. 2003).

The user can choose between the various dam safety guidelines imbedded in the program, such as CDSA, USACE, FERC, and USBR. The version used for the purpose of this study is 1.4.7 (2001).

3.1.1.1 Analytical Capabilities

CADAM has the following capabilities:

- **Static Analysis:** this analysis can be performed for normal operating levels, flood levels, and crest overtopping.
- **Seismic Analysis:** this can be performed using either pseudo-static or pseudo-dynamic methods based on the simplified response spectra analysis described by Chopra for gravity dams.
- **Post-Seismic Analysis:** the specified cohesion is not applied over the length of crack induced by the seismic event. The post-seismic uplift

pressure could either be built up to its full value in seismic cracks or it could return to its initial value if the seismic cracks are closed after the earthquake.

- Probabilistic Safety Analysis (Monte-Carlo Simulations): CADAM can perform this analysis to predict the probability of failure of dam-foundation-reservoir system as a function of the uncertainties in loading and strength parameters that are considered as random variables with specified probability density functions. Static and seismic analysis can also be considered as a part of this analysis.
- Incremental Load Analysis: CADAM can automatically perform sensitivity analysis by computing and plotting the evolution of typical performance indicator for example, the sliding safety factor as a function of a progressive application in the applied loading, say, reservoir elevation.

3.1.1.2 Modeling Capabilities

The analysis can be carried out for a single 2D monolith of a gravity dam-foundation-reservoir system subdivided into lift joints. The following need to be defined in order to carry out an analysis:

- Section Geometry: the overall dimension of the section geometry, inclined upstream and downstream faces, and embedding in the foundation (passive rock wedge) can be defined.
- Masses: concentrated masses can be located anywhere inside or outside the cross section to add or subtract vertical forces in static analysis and inertia forces in seismic analysis.
- Materials: properties, such as tensile, compressive and shear strengths (peak and residual) of lift joints, base joint, and rock joint (passive rock wedge) can be defined.
- Lift joints: the elevation, inclination, and material properties of lift joint can be assigned.

- Pre-cracked lift joints: cracks in joint(s) can be assigned upstream or downstream as initial conditions.
- Reservoir, ice load, floating debris and silt: water density, normal operating and flood head water and tail water elevations, ice loads floating debris and silt pressure (equivalent fluid, frictional material at rest, active or passive) can be defined.
- Drainage system: the drain location and effectiveness can be defined. The stress computation can be performed using linearization of effective stress as defined by the following guidelines (CDSA, FERC, USACE, and USBR) or superposition of total stresses with uplift pressures as defined by (FERC).
- Post-tension cable: definition of forces induced by straight or inclined post-tension cables installed along the crest or the downstream face.
- Applied forces: horizontal and vertical forces can be placed anywhere.
- Pseudo-static analysis: the horizontal and vertical peak ground accelerations and the sustained accelerations can be specified. Westergaard added mass represents the hydrodynamic effects of the reservoir. Water compressibility effect, inclination of the upstream face, limiting the variation of hydrodynamic pressures over a certain depth of the reservoir can also be accounted for. The hydrodynamic pressures for silt are approximated from Westergaard formulation for a liquid of higher mass density than water.
- Pseudo-dynamic analysis: peak ground and spectral acceleration data, dam and foundation stiffness and damping properties, reservoir bottom damping properties and velocity of an impulsive pressure wave in water model summation rules can be specified to perform this analysis using the simplified method proposed by Chopra.
- Cracking options: tensile strength for crack initiation and propagation, dynamic amplification factor for the tensile strength, the incidence of

cracking on static uplift pressure distributions (drain effectiveness), the effect of cracking on the transient evolution of uplift pressure during earthquakes (full pressure, no change from static values, zero pressures in seismic cracks), the evolution of uplift pressure in the post-seismic conditions (return to initial uplift pressures or build-up full uplift pressures in seismically induced cracks) can be specified.

- Load combination: user defined multiplication factors of basic load conditions to form the load combinations. The five load combinations supported by CADAM are normal operating, flood, seismic 1, seismic 2, and post-seismic.
- Probabilistic Analysis: estimation of the probability of failure of a dam-foundation-reservoir system using the Monte-Carlo simulation, as a function of uncertainties (Probability Density Function) in loading and strength parameters that are taken as random variables.
- Incremental Analysis: automatic computation of the evolution of safety factors and other performance indicators as a function of a stepping increment applied to a single load condition specified by the user.

3.1.1.3 Output Results

CADAM can present the outputs in three different formats:

- CADAM Reports
 - Input parameters
 - Loads
 - Load combinations
 - Stability drawings
- MS Excel reports
 - Input parameters
 - Loads
 - Load combinations

- Graphical plots
 - Joint cracking, stresses and resultants
 - Probabilistic analyses results (CDF, PDF)
 - Incremental analyses results (SF vs. Load)

where CDF, PDF, and SF represent Cumulative Distribution Function, Probability Distribution Function, and Safety Factor, respectively.

3.1.1.4 Basic Modelling Information

CADAM can work in either international system (SI) units or imperial units as defined by the user. The analysis is performed on a 2D monolith of unit thickness (1 m). Therefore, all forces should be defined in kN/m. The gravity method is used for the analysis of hydrostatic loads and seismic loads. It is based on the rigid body equilibrium to determine the internal forces acting on the potential failure plane (joints and concrete-rock interface) and on beam theory to compute stresses. The evaluation of the structural stability of the dam against sliding, overturning and uplifting is performed considering two analyses: a stress analysis to determine eventual crack length and compressive stresses and a stability analysis to determine the safety margins against sliding along joints, and the position of the resultant of all forces acting on the joint.

The origin of the global axis is located at the heel of the dam, and a local one-dimensional coordinate system with the heel of the dam taken as the origin is considered for each joint and lift joint. Figure 3-2 (a) shows the positive direction considered for forces and momentum. Figure 3-2 (b) shows the positive directions considered for stresses.

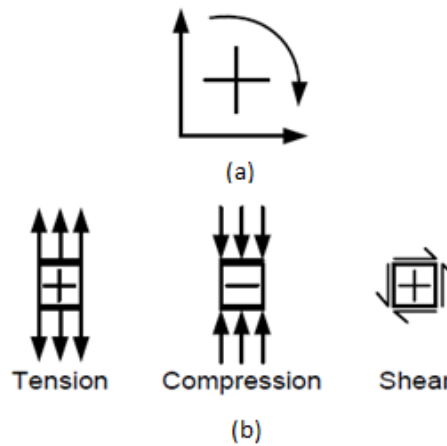


Figure 3-2 CADAM sign convention, forces and stresses, (Leclerc et al. 2001)

The inertia force caused by an earthquake (HPGA, VPGA) acts in the opposite direction to the applied base acceleration according to d'Alembert principle as shown in Figure 3-3.

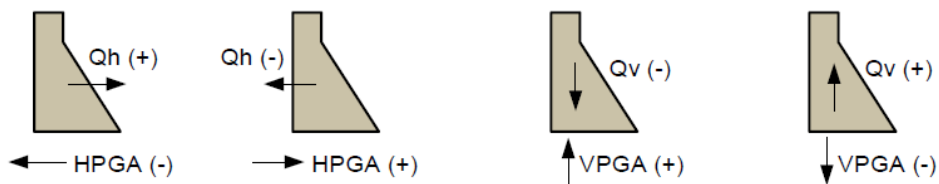


Figure 3-3 CADAM sign convention, inertia forces, (Leclerc et al. 2001)

3.1.1.5 Drain Effectiveness Computation

The drain effectiveness is computed based on the simplified seepage analysis of ANCOLD and Ransford. Figure 3-4 (a) presents the variables needed to compute the drain effectiveness used in Equation (3.1). Figure 3-4 (b) illustrates that K is the efficiency of the drain as was presented in Equation (2.3) of Chapter 2.

$$K = \frac{\frac{1}{2\pi} \ln \left(\frac{\sinh 2\pi \frac{z}{s}}{\sinh 2\pi \frac{d}{s}} \right) - \frac{z}{s}}{\frac{1}{2\pi} \ln \left(\frac{\sinh 2\pi \frac{z}{s}}{\sinh 2\pi \frac{d}{s}} \right) - \frac{z^2}{s \cdot T}} \quad (3.1)$$

where z is the distance between the center line of the drains and the upstream face of the dam, s is the spacing between the drain centers, T is the length of the joint at which the efficiency is being computed.

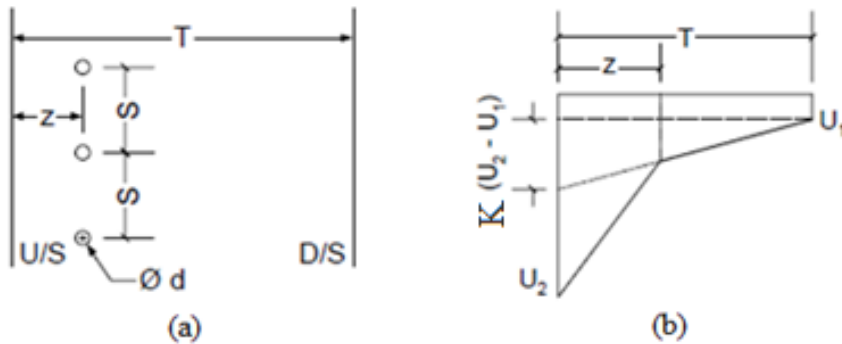


Figure 3-4 Drain effectiveness computation, (Leclerc et al. 2001)

3.1.2 Loading Combinations

A dam has to prove its stability and safety under various loading conditions that can occur at any point in the service life of the dam. The probability of occurrence of extreme events is rather low, and so the probability of the occurrence of multiple extreme events simultaneously is almost negligible. Therefore, the appropriate loads must be selected for each combination. These loads are generally selected based on logical reasoning, for example the ice load cannot be considered for an unusual loading combination if over crest flooding is considered since these two have the opposite meaning (Yanmaz 2013). The three possible loading combinations of the forces acting on a dam are as follows:

- Usual Loading
 - Dead load
 - Hydrostatic forces for reservoir at normal operating level
 - Uplift force
 - Sediment load
 - Ice load
 - Temperature stresses for normal temperature during that period of the year.
- Unusual Loading
 - Hydrostatic forces for reservoir at maximum (full reservoir) operating level
 - Uplift force
 - Sediment load
 - Temperature stresses produced by minimum temperature at full level
- Extreme Loading (usual loading + earthquake forces)
 - Dead load
 - Hydrostatic forces for reservoir at normal operating level
 - Uplift force
 - Sediment load
 - Ice load
 - Temperature stresses for normal temperature during that period of the year.
 - Earthquake forces

3.2 Seepage Analysis

The impact of the location of the gallery and the diameter of the drains was studied further by estimating the amount of seepage passing beneath the dam and entering the gallery. As the seepage entering the gallery increases, the pore water pressure decreases, and the uplift force decreases. Furthermore, the amount of water entering the gallery that will eventually be collected in the sump well will determine the size of the well required, and will affect the power of the pump needed and thus the cost of the pumping operation as presented in Chapter 5. This analysis was carried out on SEEP/W.

3.2.1 SEEP/W

SEEP/W is a product of GeoSlope Int. Ltd. which was established in 1977 and has since then become one of the pioneers of developing state-of-the-art software for geotechnical and geo-environmental modeling (“GEO-SLOPE > About,” 2017) GeoStudio 2012 is released by GeoSlope Int. Ltd. and has different packages used for different needs and purposes. In this study it was used to compute the seepage rate below the dam and seepage rate entering the gallery from the foundation.

SEEP/W package for groundwater seepage analysis was used in this study to determine the seepage rate under the dam. SEEP/W calculates the quantity of flow based on Darcy’s law provided in Equation (3.2) (GEO-SLOPE International, 2010).

$$Q = -KA \frac{dh}{dl} \quad (3.2)$$

where, K is the hydraulic conductivity, A is the cross sectional area of flow, dh/dl is the hydraulic head gradient.

When two-dimensional seepage analysis is considered, Equation (3.2) is redefined as the differential equation presented in Equation (3.3).

$$\frac{\partial}{\partial x} \left(k_x \frac{\partial H}{\partial x} \right) + \frac{\partial}{\partial y} \left(k_y \frac{\partial H}{\partial y} \right) + Q = \frac{\partial \theta}{\partial t} \quad (3.3)$$

where H is the total head, Q is the applied boundary flux; k_x and k_y are the hydraulic conductivity in the horizontal and vertical directions, respectively, θ is the volumetric water content, and t is the time. Equation (3.3) shows that the rate of change of flow at a point in time in the horizontal and vertical directions, in addition to the external flux applied, is equivalent to the change in storage of the soil system i.e. the rate of change of volumetric water content with respect to time (GEO-SLOPE International, 2010).

SEEP/W is a tool which uses a numerical model i.e. it can mathematically simulate the real physical process of water flow through a medium. It uses finite element method to solve the governing equation of the flow through porous medium by dividing the problem into small elements of a predefined size. By applying Galerkin method to Equation (3.3), the finite element form of the two-dimensional seepage equation is as shown in Equation (3.4).

$$\begin{aligned} \tau \int_A ([B]^T [C] [B] dA \{H\} + \tau \int_A (\lambda \langle N \rangle^T \langle N \rangle) dA \{H\}, t \\ = q \tau \int_L (\langle N \rangle^T) dL \end{aligned} \quad (3.4)$$

where B is the gradient matrix, C is the matrix of hydraulic conductivity, N is the interpolating function vector, H is the nodal head vector, τ is the element thickness, λ is a storage term, q is the unit flux, A and L indicate summation over area of element and edge of element, respectively (GEO-SLOPE International, 2010).

The user is able to define the following for the analysis:

- Define the time dependency of the problem i.e. steady state or transient.
- Sketch axes, polylines, lines, arrows, circles, arches, etc. to define the overall shape and domain of the problem.

- Domain: regions, lines, points (included in analysis).
- Materials:
 - Saturated soil model: saturated conductivity, anisotropy, saturated volumetric water content, etc. are needed
 - Unsaturated soil model: conductivity function (Van Genuchten), anisotropy, saturated volumetric water content function (can be estimated from literature for selected material and saturated water content) are needed.
 - Interface material: impermeable layers.
- Boundary Conditions: Head (H), Total Flux (Q), Unit Flux (q), Unit Gradient (i), and Pressure Head (P).
- Flux section at any point.
- Mesh properties: can apply a constant mesh size for all or various mesh sizes for different regions, lines, or points.

After the analysis is completed the following can be viewed

- Contours (Total Head, Pore Water Pressure, Pressure Head, etc.), Flow Paths, Vectors, Isolines, Phreatic Surface.
- Result information (Total Head, Pore Water Pressure, Pressure Head, etc.) at any point.
- Object information (Boundary conditions, material properties, etc.) for any region, line, or point.
- Reports of input data in HTML format.
- Graphs (pore pressure, water flow, material properties, convergence, etc.) can be generated for a region or a defined line, and exported as an image or data to MS. Excel.

CHAPTER 4

PRELIMINARY ANALYSES

4.1 CADAM Preliminary Analysis

This section presents the cases and variables considered and the analyses conducted using CADAM.

4.1.1 Loading Conditions

The three loading conditions mentioned in Chapter 3 are used in the analyses.

4.1.1.1 Usual Loading Condition

The impact of the variables on optimal location is investigated in this section.

4.1.1.1.1 Dam Height and Width Variations

In order to assess the impact of the dam height and width, six hypothetical cases having three alternative heights “H” were considered: 50 m, 100 m and 200 m, whereas the base width “W” was taken as 80% and 90% of the corresponding dam height. Table 4-1 shows the dimensions taken for each of the dams considered. In practice, the angle between the downstream side and the horizontal should be less than 45° . The angles shown in Table 4-1 were calculated to make sure that the hypothetical dams have realistic dimensions and could exist in reality. Table 4-2 provides the names and the corresponding dimensions for each dam used.

Table 4-1 Dam dimensions

H	H*	t _c	80% Width		90% Width	
			W (m)	Angle (°)	W (m)	Angle (°)
50	5.375	4.767	40	38.292	45	42.037
100	10.75	7.142	80	39.226	90	42.873
200	21.5	11.892	160	39.684	180	43.283

In Table 4-1, H* (vertical section at the downstream face) and t_c (crest thickness) are calculated using Equations (4.1) and (4.2), which were proposed by Yanmaz (2013) and are represented in CADAM as difference between heights G and F and L₄, respectively (refer to Figure 4-1).

$$H^* = 0.1075H_t \quad (4.1)$$

$$t_c = 0.0475H_t + 2.392 \quad (4.2)$$

where

H_t is the height of the dam in m.

Table 4-2 Dams names and corresponding dimensions

Dam Name	Dimensions (m x m)
	Height x Base width
Dam 1	50 x 40
Dam 2	50 x 45
Dam 3	100 x 80
Dam 4	100 x 90
Dam 5	200 x 160
Dam 6	200 x 180

For each dam dimensional configuration, the upstream (U/S) water level was taken as 75% of the dam height to represent normal operating conditions. The downstream (D/S) water level was taken as 2% of the dam height.

Figure 4-1 shows the section geometry for Dam 3, and Figure 4-2 shows the CADAM sketch for the same dam configuration.

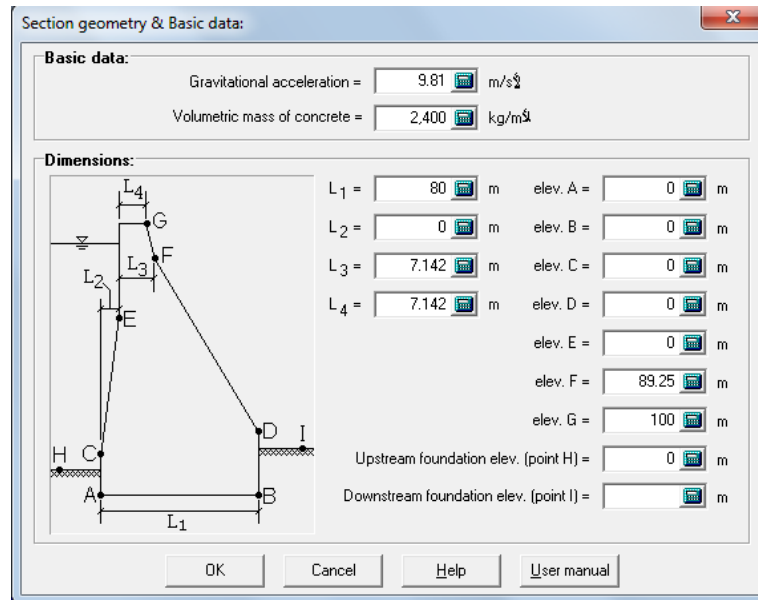


Figure 4-1 Section geometry for Dam 3

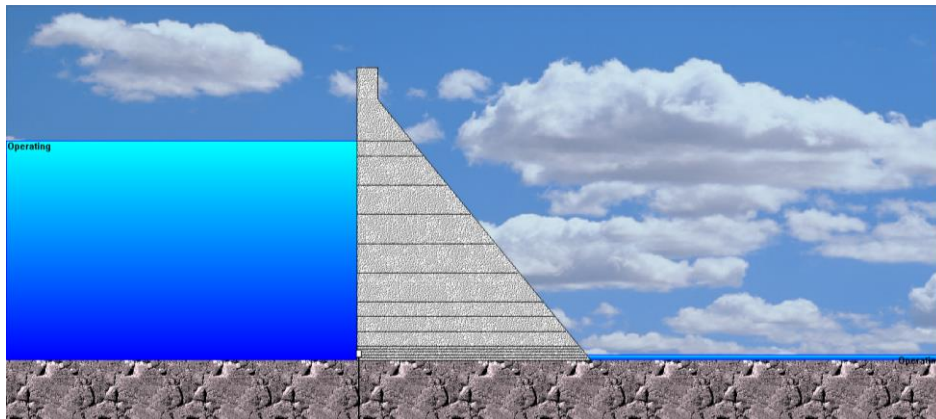


Figure 4-2 Dam 3 configuration on CADAM for usual loading case

First, the uplift force was determined for the non-drained case. Then, a drainage gallery was added with the USACE uplift pressure guideline presented in section 2.2.1 (no drain effectiveness when cracking is beyond drain line). The standard drain spacing was taken as 3 m and the drain diameter was taken as 0.25 m and is

used throughout this study unless otherwise mentioned. These were selected based on the drain diameter and spacing used in existing gravity dams (Zee et al., 2011). The compressive strength was taken as 30 MPa and the tensile strength as 3 MPa (Concrete Society n.d.).

The load combinations (multiplication factors) were taken as 1 for each case which included the dead load, hydrostatic loads at the upstream and the downstream sides and uplift pressures. The safety factors were taken as those set as standard by the program for each case and are shown in Table 4-3.

Table 4-3 Minimum allowable safety factors (Leclerc et al., 2001)

	Usual	Flood	Extreme
Peak Sliding Factor (PSF)	3.0	2.0	1.3
Residual Sliding Factor (RSF)	1.5	1.3	1.0
Overturning Factor (OF)	2.0	1.5	1.1
Uplifting Factor (UF)	1.2	1.1	1.1

The impact of the location of the gallery on the uplift pressure was considered in two steps as stated in Chapter 3. The first was the variation of the vertical location of the gallery (labeled as H_4) for a fixed horizontal location (labeled as X). The second was the variation of the horizontal location for a fixed vertical location. Figure 4-3 shows the definition of the horizontal and vertical positions of the gallery on CADAM.

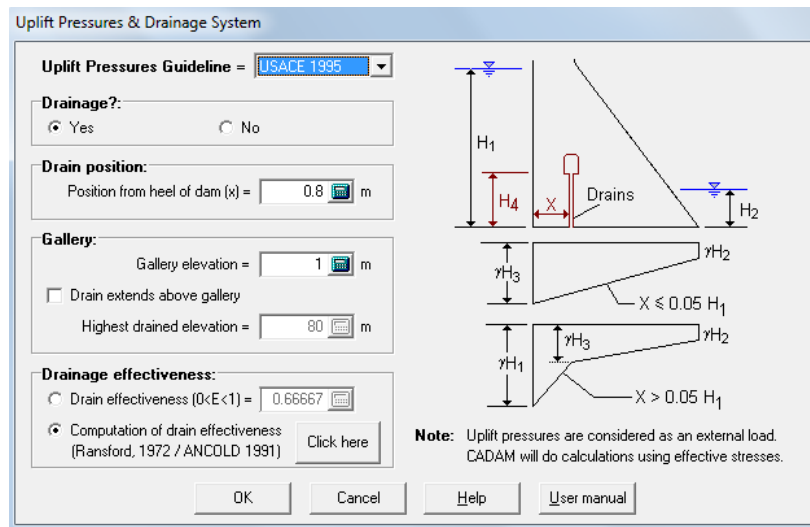


Figure 4-3 Uplift pressures & drainage system

The variable term (between H_4 and X) was moved between 0, 1, 2, 3, 4, 5, 10, 15, 20, 30, 40, 50, 60, 70, 80, 90, and 100% of the corresponding dimension “%location” i.e. dam height for H_4 and base width for X . The non-variable term was set as 1% of the corresponding dimension. For example, for the 100 m x 80 m dam (Dam 3) the H_4 variations are considered with X set at 0.8 m (1% of 80 m) while H_4 is set to 1 m (1% of 100 m) for X variations. The higher %locations are not very realistic, but are considered to examine more possibilities and have a wider range. Table 4-4 shows the uplift force values and the percent reduction for Dam 3 for various H_4 and X locations considered for the usual loading case. In Table 4-4, percent reduction corresponds to the percentage of reduction of the uplift between the case without drainage and any of the drainage location cases. Uplift is in kN per unit width. E represents the drain effectiveness. The effectiveness of the drain is automatically computed by CADAM based on Ransford and ANCOLD and is presented in the output reports. The effectiveness is constant for H_4 variations since the vertical position of the gallery is not a variable in Equation (3.1). The effectiveness varies for X variations since the horizontal position of the gallery is one of the variables needed in Equation (3.1). Even though the effectiveness of the drainage system increases as the gallery

moves towards the downstream side, the percent reduction of uplift decreases. This occurs due to the fact that as the gallery moves more towards the downstream side there is less water entering the gallery and so the amount of uplift reduction decreases.

Table 4-4 Uplift forces of Dam 3 for H₄ and X variations for usual loading case

H ₄				X					
%location	Location (m)	Uplift (kN/m)	%reduction in the uplift	E	%location	Location (m)	Uplift (kN/m)	%reduction in the uplift	E
w/o	-	30214.80			w/o	-	30214.80		
Drainage	0	14164.46	53.1	0.560	Drainage	0	30214.80	0.0	0
0	1	14164.46	53.1	0.560	0	0.8	14164.46	53.1	0.560
1	2	14164.46	53.1	0.560	1	1.6	9853.54	67.4	0.711
2	3	14384.32	52.4	0.560	2	2.4	7735.13	74.4	0.785
3	4	14604.19	51.7	0.560	3	3.2	6499.00	78.5	0.828
4	5	14824.06	50.9	0.560	4	4	6916.70	77.1	0.856
5	10	15923.40	47.3	0.560	5	8	6534.21	78.4	0.919
10	15	17022.74	43.7	0.560	10	12	7300.81	75.8	0.941
15	20	18122.08	40.0	0.560	15	16	8387.49	72.2	0.952
20	30	20320.75	32.7	0.560	20	24	10897.37	63.9	0.963
30	40	22519.43	25.5	0.560	30	32	13580.87	55.1	0.968
40	50	24718.11	18.2	0.560	40	40	16335.32	45.9	0.969
50	60	26916.78	10.9	0.560	50	48	19125.51	36.7	0.968
60	70	29115.46	3.6	0.560	60	56	21935.90	27.4	0.963
70	75	30214.80	0.0	0.560	70	64	24757.97	18.1	0.952
75					80	72	27583.62	8.7	0.919
					100	80	30214.80	0.0	0

4.1.1.1.2 Drain Size and Spacing

To test the impact of the drain size and spacing, Dam 3 configuration was used. The various diameter “D” sizes considered are: 0.1 m, 0.25 m, 0.5 m, 0.75 m and 1 m. The spacing “S” values considered are: 1 m, 2 m, 3 m, 4 m, and 5 m. These values were taken based on the works of Chawla et al. (1990) and Yanmaz (2013). Larger drain diameters were not considered, since they would be uneconomical and unrealistic. Each drain size was coupled with each of the spacing values to create 25 possible scenarios. Then, each scenario was tested using the same procedure as before i.e. H_4 is varied for constant X and vice versa. Figure 4-4 shows the input parameters needed to compute the drain effectiveness that is presented in the final report.

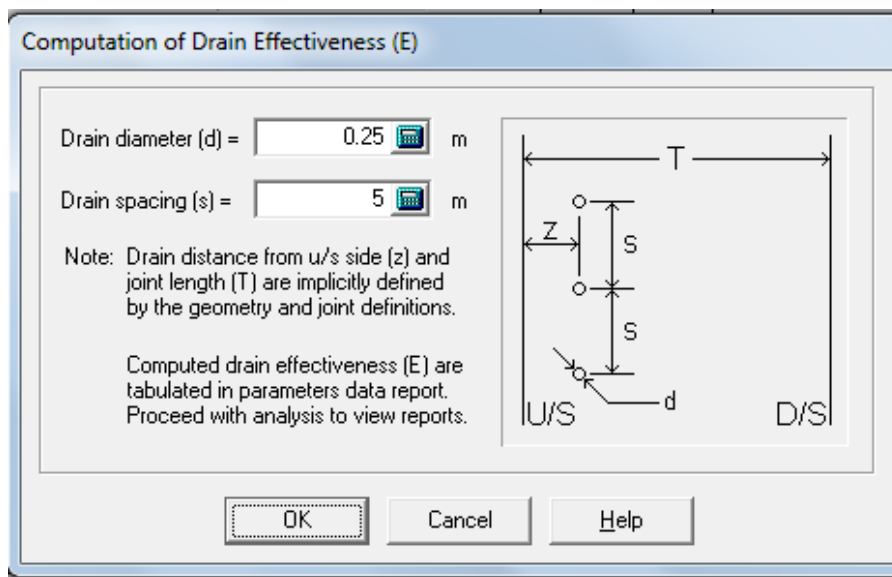


Figure 4-4 Computation of drain effectiveness

Tables 4-5 and 4-6 shows the uplift force and the percent reduction for the H_4 and X variations, respectively for Dam 3 for the 5 m drain spacing for all 5 drain diameters considered.

Table 4-5 Uplift forces of Dam 3 with 5 m drain spacing for H₄ variations for usual loading case

Drain diameter		0.1 m		0.25 m		0.5 m		0.75 m		1 m	
Efficiency		0.275		0.368		0.496		0.624		0.766	
% location (H ₄)	Location (m) (H _d)	Uplift (kN/m)	% reduction	Uplift (kN/m)	% reduction	Uplift (kN/m)	% reduction	Uplift (kN/m)	% reduction	Uplift (kN/m)	% reduction
w/o	-	30214.80		30214.80		30214.80		30214.80		30214.80	
0	0	22336.30	26.1	19661.54	34.9	15997.40	47.1	12336.69	59.2	8281.30	72.6
1	1	22336.30	26.1	19661.54	34.9	15997.40	47.1	12336.69	59.2	8281.30	72.6
2	2	22336.30	26.1	19661.54	34.9	15997.40	47.1	12336.69	59.2	8281.30	72.6
3	3	22444.23	25.7	19806.10	34.4	16192.16	46.4	12581.59	58.4	8581.76	71.6
4	4	22552.15	25.4	19950.67	34.0	16386.92	45.8	12826.50	57.5	8882.22	70.6
5	5	22660.07	25.0	20095.23	33.5	16581.67	45.1	13071.40	56.7	9182.68	69.6
10	10	23199.70	23.2	20818.06	31.1	17555.47	41.9	14295.93	52.7	10684.97	64.6
15	15	23739.32	21.4	21540.88	28.7	18529.26	38.7	15520.46	48.6	12187.27	59.7
20	20	24278.94	19.6	22263.71	26.3	19503.06	35.4	16744.99	44.6	13689.56	54.7
30	30	25358.19	16.1	23709.36	21.5	21450.65	29.0	19194.05	36.5	16694.15	44.7
40	40	26437.44	12.5	25155.02	16.7	23398.24	22.6	21643.10	28.4	19698.74	34.8
50	50	27516.68	8.9	26600.67	12.0	25345.83	16.1	24092.16	20.3	22703.33	24.9
60	60	28595.93	5.4	28046.32	7.2	27293.42	9.7	26541.22	12.2	25707.92	14.9
70	70	29675.18	1.8	29491.97	2.4	29241.01	3.2	28990.27	4.0	28712.51	5.0
75	75	30214.80	0.0	30214.80	0.0	30214.80	0.0	30214.80	0.0	30214.80	0.0

Table 4-6 Uplift forces of Dam 3 with 5 m drain spacing for X variations for usual loading case

Drain diameter		0.1 m			0.25 m		
%location (X)	Location (m) (X)	Uplift (kN/m)	%reduction in the uplift	E	Uplift (kN/m)	%reduction in the uplift	E
w/o Drainage	-	30214.80			30214.80		
0	0	30214.80	0.0	0	30214.80	0.0	0
1	0.8	22336.30	26.1	0.275	19661.54	34.9	0.368
2	1.6	18255.19	39.6	0.418	15370.40	49.1	0.518
3	2.4	15487.64	48.7	0.514	12657.76	58.1	0.613
4	3.2	13528.77	55.2	0.583	10848.63	64.1	0.676
5	4	12985.61	57.0	0.633	10600.49	64.9	0.721
10	8	10472.12	65.3	0.766	8810.58	70.8	0.830
15	12	10189.51	66.3	0.822	8937.35	70.4	0.874
20	16	10662.30	64.7	0.853	9662.42	68.0	0.897
30	24	12486.81	58.7	0.884	11778.69	61.0	0.919
40	32	14796.03	51.0	0.897	14251.66	52.8	0.929
50	40	17312.73	42.7	0.901	16874.18	44.2	0.931
60	48	19935.62	34.0	0.897	19572.70	35.2	0.929
70	56	22617.09	25.1	0.884	22313.61	26.1	0.919
80	64	25326.67	16.2	0.853	25076.71	17.0	0.897
90	72	28021.17	7.3	0.766	27836.55	7.9	0.830
100	80	30214.80	0.0	0	30214.80	0.0	0

Table 4-6 Uplift forces of Dam 3 with 5 m drain spacing for X variations for usual loading case (cont.)

0.5 m			0.75 m			1 m		
Uplift (kN)	%reduction in the uplift	E	Uplift (kN/m)	%reduction in the uplift	E	Uplift (kN/m)	%reduction in the uplift	E
30214.80	0.0	0	30214.80	0.0	0	30214.80	0.0	0
30214.80	47.1	0.496	30214.80	8.7	0.624	30214.80	72.6	0.766
15997.40	60.1	0.634	27590.63	69.3	0.731	8281.30	77.8	0.821
12043	68.0	0.718	9274.95	75.7	0.798	6703.14	82.3	0.868
9659.40	73.0	0.770	7357.32	79.5	0.839	5358.32	84.9	0.896
8159.41	72.5	0.805	6192.14	77.9	0.865	4548.16	82.3	0.914
8297.20	75.7	0.887	6666.42	78.8	0.924	5337.22	81.3	0.953
7349.80	73.9	0.917	6390.93	76.2	0.945	5651.23	77.9	0.966
7877.05	70.98	0.933	7200.71	72.5	0.956	6689.21	73.8	0.973
8832.37	62.9	0.948	8310.65	64.1	0.966	7920.03	65.0	0.979
11202.20	54.3	0.954	10845.00	55.2	0.970	10580.11	55.8	0.982
13812.04	45.3	0.956	13541.25	46.0	0.971	13341.21	46.6	0.982
16520.84	36.2	0.954	16303.54	36.8	0.970	16143.21	37.2	0.982
19279.63	27.0	0.948	19099.10	27.5	0.966	18965.74	27.9	0.979
22066.54	17.7	0.933	21913.46	18.1	0.956	21799.93	18.4	0.973
24869.19	9.4	0.887	24738.76	8.8	0.924	24641.11	9.0	0.953
27374.24	0.0	0	27567.70	0.0	0	27485.51	0.0	0
30214.80			30214.80			30214.80		

No cracking occurred in any of the dams for the usual loading case.

4.1.1.1.3 Internal Stresses

The stresses developed at the upstream and downstream faces of the dam are shown in Figure 4-5 for Dam 3. Each level represents one of the joints located in the dam. These joints were placed according to the vertical locations of the gallery H₄ mentioned before. Figure 4-5 is provided only for illustration, the numerical values for each elevation were used to create Table 4-7.

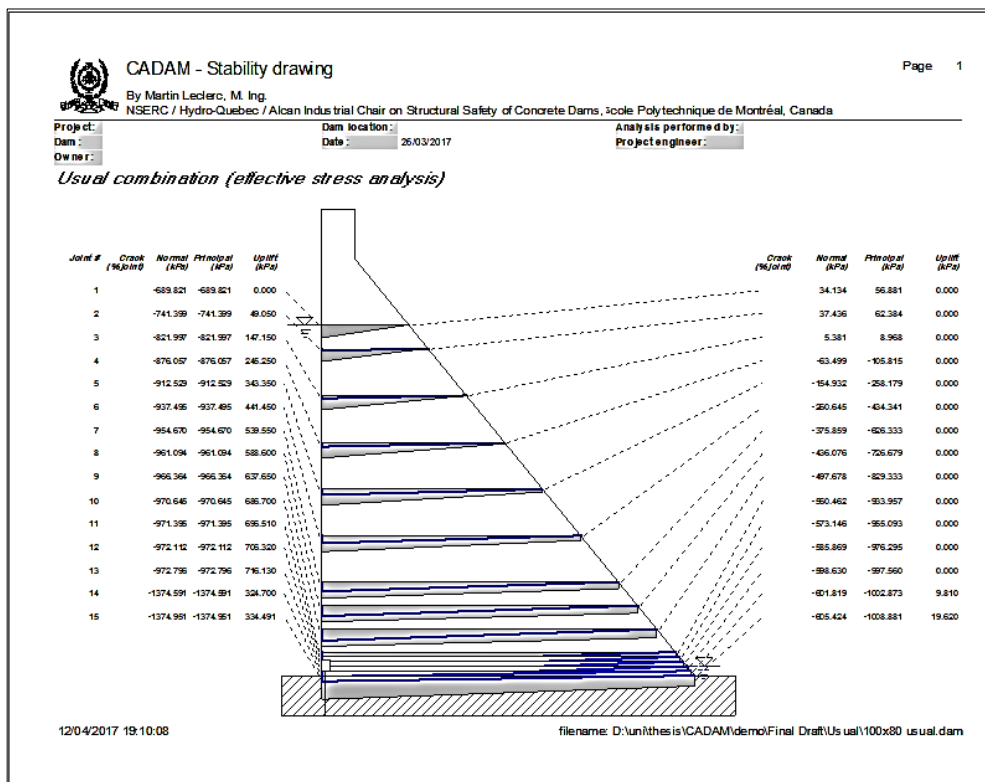


Figure 4-5 CADAM report, stresses and uplift

Figure 4-6 shows a sample of the graphical report. The internal stresses at the location of the gallery can be obtained from this graph. However, since the variation between the upstream and downstream stresses is taken as linear, linear interpolation can be used to produce quick and accurate readings.

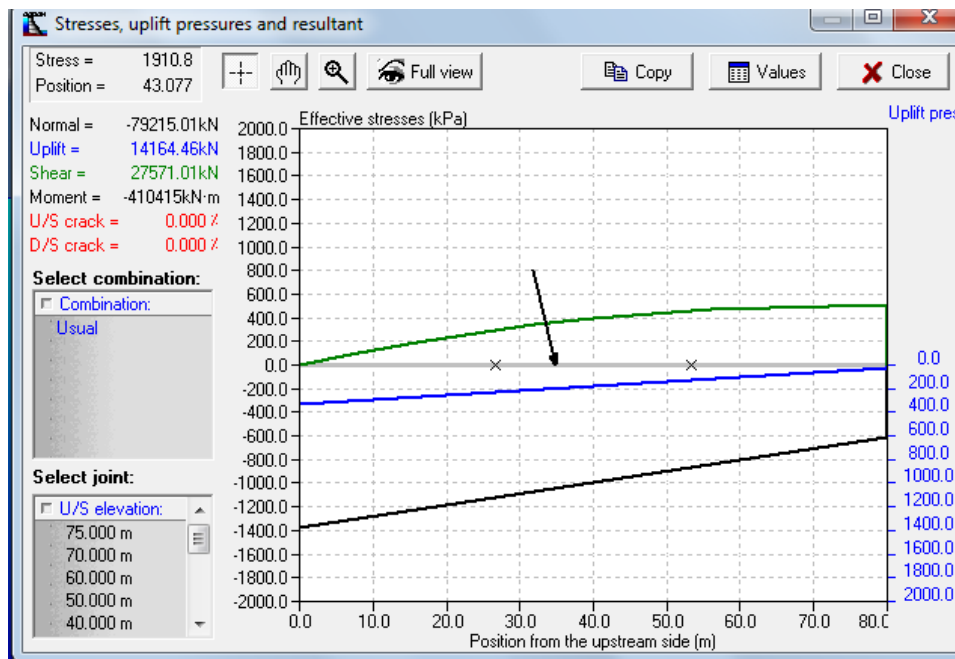


Figure 4-6 CADAM graphical reports, stresses, uplift

The stresses were determined for each of the cases considered (various dimensional configurations, various drain spacing and diameter, etc.) Table 4-7 shows the upstream, downstream, and internal stresses of Dam 3 for various H_4 and X locations considered for the usual loading case. According to the sign convention, the negative values represent compression, while the positive values represent tension. The stresses remained below the allowable compressive stress in concrete of 3750 kN/m^2 (Table 5-2) showing that these locations are safe and do not lead to excessive stresses in the concrete.

Table 4-7 Stresses obtained for usual loading case for Dam 3

H ₄				X					
%location	Location (m)	Stress at U/S face (kPa)	Stress at D/S face (kPa)	Internal stress (kPa)	%location	Location (m)	Stress at U/S face (kPa)	Stress at D/S face (kPa)	Internal stress (kPa)
w/o	-	-973.693	-605.424	-970.010	w/o	-	-973.693	-605.424	-973.351
Drainage	0	-1374.951	-605.424	-1367.256	Drainage	0	-973.351	-601.819	-1366.784
0	1	-1374.591	-601.819	-1366.784	1	0.8	-1374.591	-601.819	-1464.560
1	2	-1374.018	-598.630	-1366.103	2	1.6	-1482.352	-601.819	-1507.011
2	3	-1367.818	-585.869	-1359.752	3	2.4	-1535.304	-601.819	-1527.230
3	4	-1361.586	-573.146	-1353.366	4	3.2	-1566.203	-601.819	-1480.836
4	5	-1355.322	-560.462	-1346.946	5	4	-1526.038	-631.223	-1419.692
5	10	-1323.469	-497.678	-1314.273	10	8	-1504.895	-661.556	-1341.763
10	15	-1290.631	-436.076	-1280.541	15	12	-1458.451	-688.465	-1267.000
15	20	-1256.643	-375.859	-1245.577	20	16	-1407.597	-711.783	-1138.383
20	30	-1184.361	-260.645	-1171.049	30	24	-1308.371	-747.523	-1037.247
30	40	-1104.321	-154.932	-1088.280	40	32	-1219.388	-768.681	-957.338
40	50	-1012.834	-63.499	-993.451	50	40	-1143.231	-775.238	-890.690
50	60	-899.696	3.325	-876.407	60	48	-1080.787	-767.190	-828.835
60	70	-766.704	36.519	-738.590	70	56	-1032.438	-744.543	-763.131
70	75	-689.821	34.134	-658.973	80	64	-998.38	-707.318	-655.632
75					90	72	-978.72	-655.632	-601.819
					100	80	-973.351	-601.819	

4.1.1.2 Unusual Loading Case

For this case, a flood water level was added above the water's usual operation level (75%) to reach the top level of the dam as shown in Figure 4-7 for Dam 3. The same dimensional configurations, H_4 and X variations, drain spacing and diameters were considered.

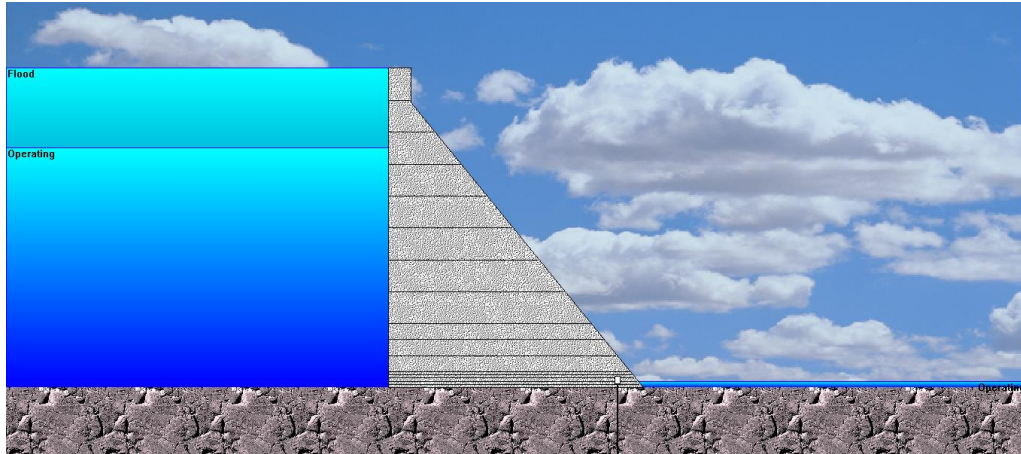


Figure 4-7 Dam 3 configuration on CADAM for unusual loading case

Table 4-8 shows the uplift force values and the percent reduction for Dam 3 for the various H_4 and X locations considered for the unusual loading case for 3 m drain spacing and 0.25 m drain diameter.

Table 4-8 Uplift forces of Dam 3 for H₄ and X variations for unusual loading case

H ₄				X					
%location w/o Drainage	Location (m)	Uplift (kN/m)	%reduction in the uplift	E	%location w/o Drainage	Location (m)	Uplift (kN/m)	%reduction in the uplift	E
0	-	39240.00	56.0	0.560	0	-	39240.00	0.0	0
1	0	17253.23	55.5	0.560	1	0	39240.00	55.5	0.560
2	1	17473.1	54.9	0.560	2	0.8	17473.10	70.4	0.711
3	2	17692.96	54.4	0.560	3	1.6	11626.78	77.7	0.785
4	3	17912.83	53.8	0.560	4	2.4	8753.87	82.0	0.828
5	4	18132.7	53.2	0.560	5	3.2	7077.47	84.8	0.856
10	5	18352.57	50.4	0.560	10	4	5981.00	81.8	0.919
15	10	19451.91	47.6	0.560	15	8	7161.27	79.1	0.941
20	15	20551.24	44.8	0.560	20	12	8220.25	75.2	0.952
30	20	21650.58	39.2	0.560	30	16	9713.33	66.5	0.963
40	30	23849.26	33.6	0.560	40	24	13155.79	57.1	0.968
50	40	26047.94	28.0	0.560	50	32	16833.56	47.5	0.969
60	50	28246.61	22.4	0.560	60	40	20607.27	37.7	0.968
70	60	30445.29	16.8	0.560	70	48	24428.96	27.9	0.963
80	70	32643.97	11.2	0.560	80	56	28277.07	18.1	0.952
90	80	34842.65	5.6	0.560	90	64	32138.65	8.3	0.919
100	90	37041.32	0.0	0.560	100	72	35996.08	0.0	0
	100	39240.00		0.560		80	39240.00		

Figures 4-8 and 4-9 show the stress and uplift results, respectively for the non-drained case for Dam 3 configuration. Both Figures show that the base of the dam is cracked by 42.3% of the base width from the upstream face. This is the maximum cracking case since there is no drainage considered. The presence of the gallery reduces uplift pressure and the crack propagation as a result. Figure 4-8 is provided only for illustration.

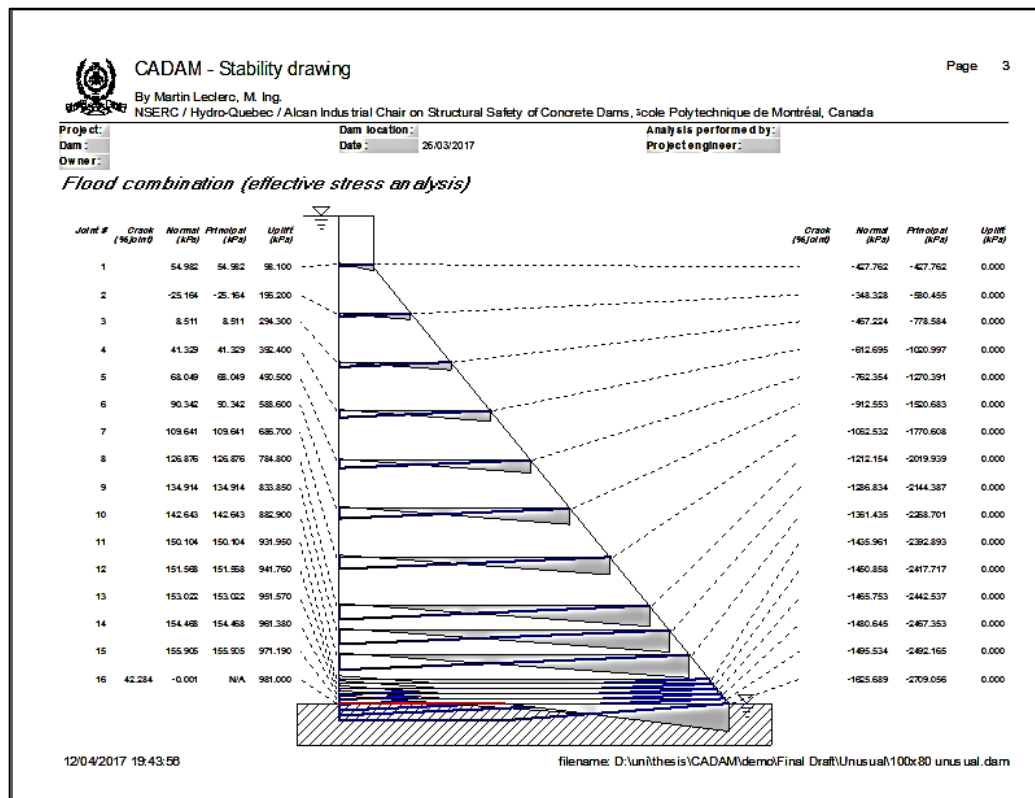


Figure 4-8 CADAM report, stress and uplift, unusual loading case

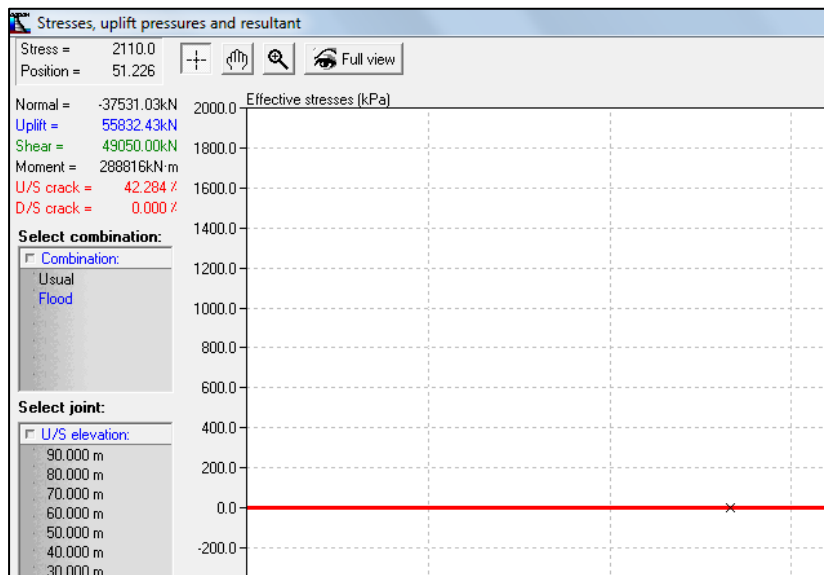


Figure 4-9 CADAM graphical report, unusual loading case

4.1.1.3 Extreme Loading Case

Only Dam 1 as shown in Figure 4-10 was considered for this loading condition since it is very similar to the case study dam (Porsuk Dam). This allows the results of crack generation and post-tension cables to be directly implemented in the case study. The peak ground acceleration values used were the same as those used in the case study, 0.30 g and 0.20 g corresponding to the horizontal and vertical peak ground accelerations, respectively (see Table 5-2).

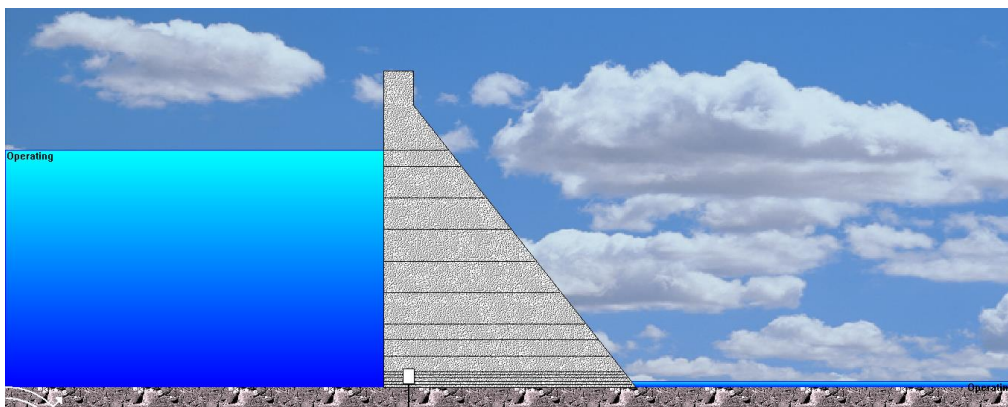


Figure 4-10 Dam 1 configuration on CADAM for extreme loading condition

4.1.2 Post-Tension Cables

Post-tension cables were considered as an added feature to reduce the crack generated at the downstream face of the dam.

Placing a post-tension cable in a dam is a form of pre-stressing. Pre-stressing is a process in which a known stress is applied to the structure prior to the full impact of the live load or the structures full load. This pre-stressing is used to counteract the stresses that will be induced by the full or live load. Therefore, the range of acceptable stresses applied on the structure increase, making it more resilient to applied loads (Prestressing Manual, 2011).

Seven wire strands (ASTM A 416/A 416 M) with a diameter of 15.24 mm (0.6 inch) having a minimum breaking strength of 260.7 kN were used (ArcelorMittal, 2010). The cables were stressed to 60% of minimum breaking strength i.e. 156.42 kN. Four different inclination angles were considered (45°, 60°, 75°, and 90°). The elevation of the cables from the downstream face was considered between 1 m and 10 m with 1 m increment. These angles and distances were selected to provide a realistic range of application of post-tension cables.

Dam 1 was used again since it is the only dam **in this study** with extreme load combination (earthquake load). The gallery was placed at an elevation of 0.5 m and 4 m away from the upstream face. The drain diameter was set as 0.25 m with 3 m spacing between centers. Figure 4-11 shows the properties of post-tension cables. The added cables are presented in Figure 4-12 (cables are near the toe of the dam). Table 4-9 presents the amount of crack generated at the toe of the dam (downstream side) as a percentage of the base width and the amount of reduction of crack length between the cases without cables and each vertical position.

The post-tensioning from the crest “P_c” led to an increase in the crack propagation downstream. Therefore, only the post-tensioning from the downstream side “P_d” was considered.

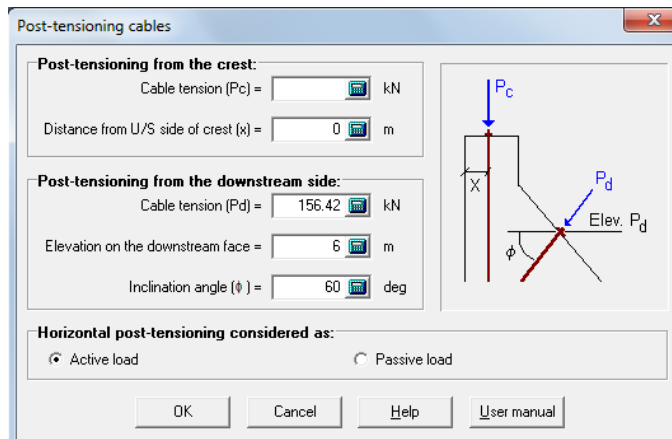


Figure 4-11 Post-tension cables window

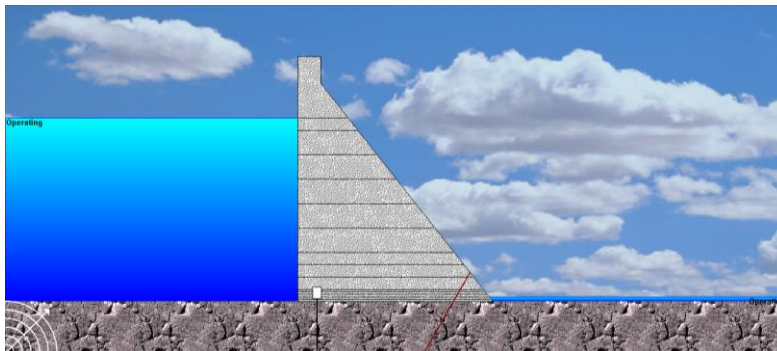


Figure 4-12 Post-tension cables for Dam 1

Table 4-9 Post-tension cables crack reduction for 60° angle

Vertical Position of Post-Tension Cable from D/S (m)	ϕ	60°
	Crack (%)	Crack Reduction (%)
Without Cables	19.681	
1	18.63	5.34
2	18.682	5.08
3	18.733	4.82
4	18.784	4.56
5	18.836	4.29
6	18.887	4.03
7	18.939	3.77
8	18.99	3.51
9	19.042	3.25
10	19.093	2.99

4.1.3 Results and Discussion

This section presents the results of the above-mentioned analyses for all loading cases and the corresponding discussions.

4.1.3.1 Usual Loading Case

The impact of the variables on uplift and stresses for the usual loading case is examined here.

4.1.3.1.1 Dimensional Variations

Table 4-10 shows the uplift force and percent reduction for Dams 1, 3, and 5 for each of the H_4 percent locations considered. These three dams were comparable since they each have a base width of 80% of the dam height. Figures 4-13 and 4-14 are the graphical representations of the same data for the uplift force and the percent reduction, respectively.

Table 4-10 Uplift forces for Dams 1, 3, and 5 for H_4 variations for usual loading case

	Dam 1 (50 m x 40 m)		Dam 3 (100 m x 80 m)		Dam 5 (200 m x 160 m)	
%location	Uplift (kN/m)	%reduction in the uplift	Uplift (kN/m)	%reduction in the uplift	Uplift (kN/m)	%reduction in the uplift
w/o Drainage	7553.70		30214.80		120859.20	
0	4522.47	40.1	14164.46	53.1	39175.55	67.6
1	4522.47	40.1	14164.46	53.1	39175.55	67.6
2	4522.47	40.1	14164.46	53.1	39175.55	67.6
3	4564.00	39.6	14384.32	52.4	40294.50	66.7
4	4605.52	39.0	14604.19	51.7	41413.45	65.7
5	4647.04	38.5	14824.06	50.9	42532.41	64.8
10	4854.66	35.7	15923.40	47.3	48127.18	60.2
15	5062.28	33.0	17022.74	43.7	53721.95	55.6
20	5269.90	30.2	18122.08	40.0	59316.72	50.9
30	5685.14	24.7	20320.75	32.7	70506.26	41.7
40	6100.37	19.2	22519.43	25.5	81695.80	32.4
50	6515.61	13.7	24718.11	18.2	92885.35	23.1
60	6930.85	8.2	26916.78	10.9	104074.89	13.9
70	7346.08	2.7	29115.46	3.6	115264.43	4.6
75	7553.70	0.0	30214.80	0.0	120859.20	0.0

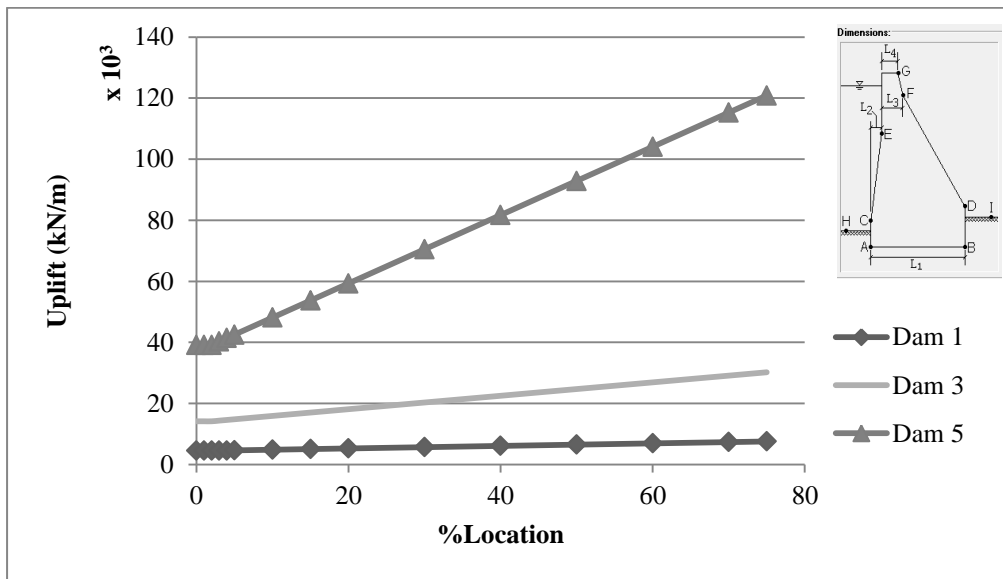


Figure 4-13 Uplift force for H_4 variations for Dams 1, 3, and 5

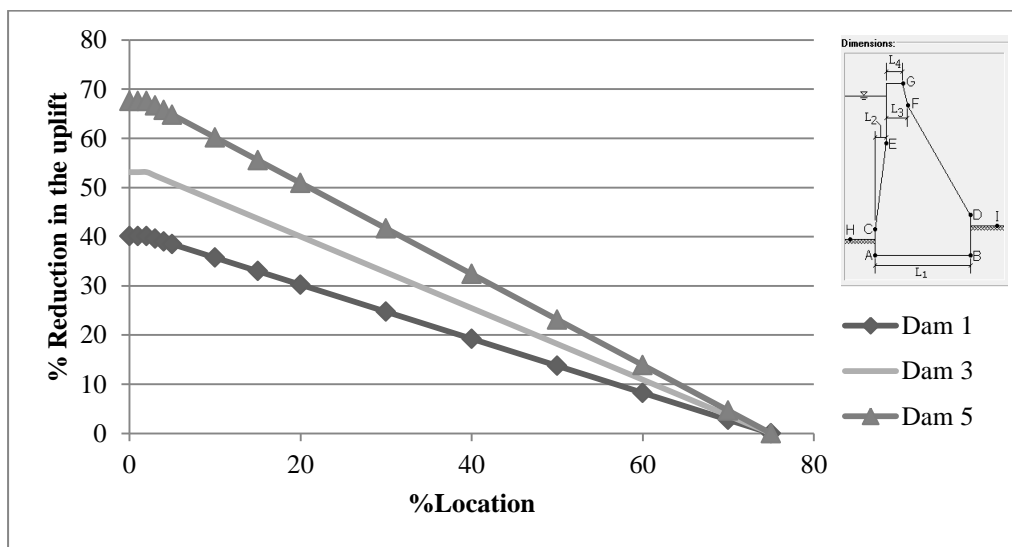


Figure 4-14 %Reduction of uplift force for H_4 variations for Dams 1, 3, and 5

Table 4-11 shows the uplift force and percent reduction for the various heights considered for a base width of 80% of dam height for each of the X percent locations considered. Figures 4-15 and 4-16 are the graphical representations of the same data for the uplift force and the percent reduction, respectively.

Table 4-11 Uplift forces for Dams 1, 3, and 5 for X variations for usual loading case

%location	Dam 1 (50 m x 40 m)		Dam 3 (100 m x 80 m)		Dam 5 (200 m x 160 m)	
	Uplift (kN/m)	%reduction in the uplift	Uplift (kN/m)	%reduction in the uplift	Uplift (kN/m)	%reduction in the uplift
w/o Drainage	7553.70		30214.80		120859.20	
0	7553.70	0.0	30214.80	0.0	120859.20	0.0
1	4522.47	40.1	14164.46	53.1	39175.55	67.6
2	3559.04	52.9	9853.54	67.4	25661.66	78.8
3	2921.13	61.3	7735.13	74.4	20096.95	83.4
4	2493.87	67.0	6499.00	78.5	17065.33	85.9
5	2461.49	67.4	6916.70	77.1	20443.96	83.1
10	2079.48	72.5	6534.21	78.4	22114.99	81.7
15	2143.91	71.6	7300.81	75.8	26421.44	78.1
20	2344.39	69.0	8387.49	72.2	31425.25	74.0
30	2894.93	61.7	10897.37	63.9	42148.44	65.1
40	3524.89	53.3	13580.87	55.1	53235.19	56.0
50	4187.96	44.6	16335.32	45.9	64468.96	46.7
60	4867.83	35.6	19125.51	36.7	75776.53	37.3
70	5557.08	26.4	21935.90	27.4	87126.02	27.9
80	6251.37	17.2	24757.97	18.1	98500.71	18.5
90	6945.45	8.1	27583.62	8.7	109887.62	9.1
100	7553.70	0.0	30214.80	0.0	120859.20	0.0

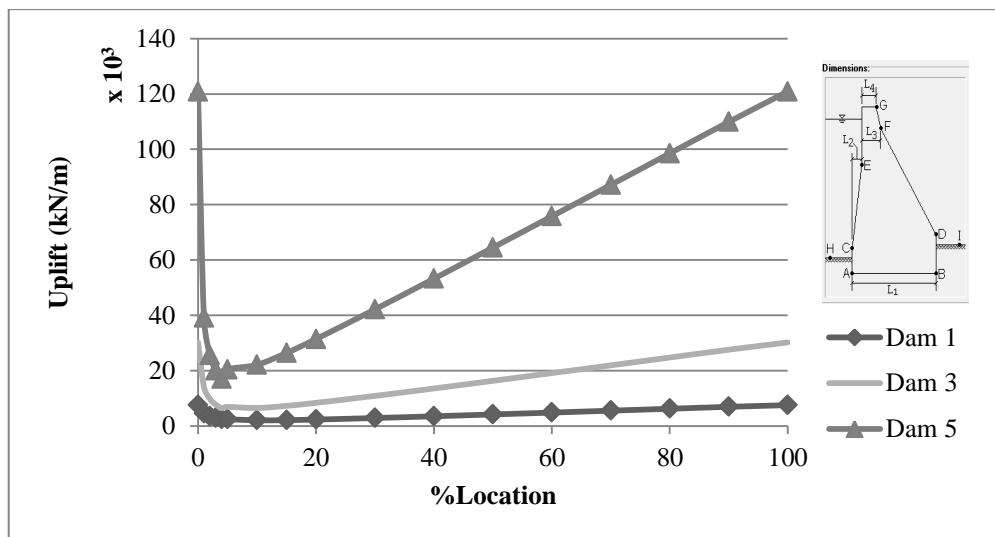


Figure 4-15 Uplift force for X variations for Dams 1, 3, and 5

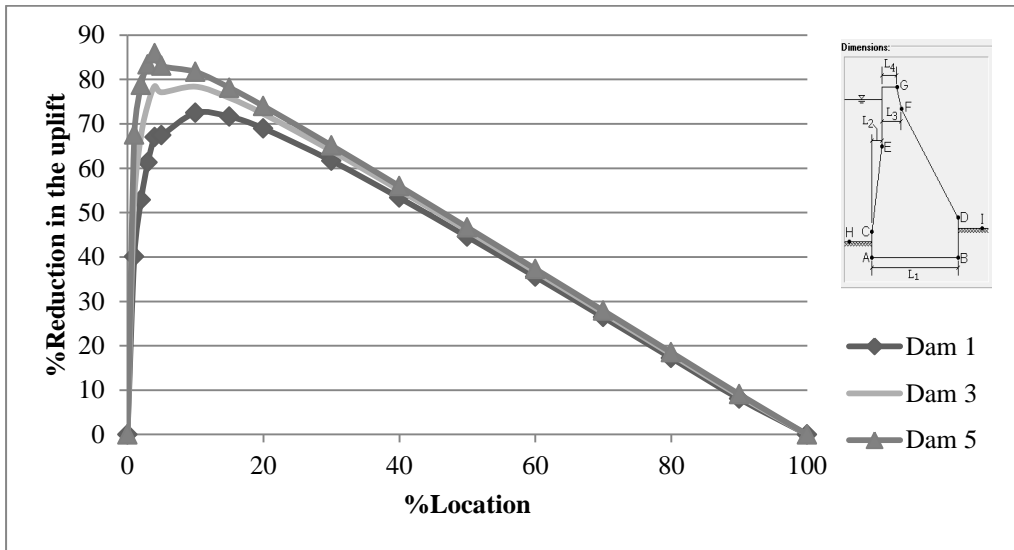


Figure 4-16 %Reduction of uplift force for X variations for Dams 1, 3, and 5

Figure 4-17 and 4-18 show the variation of uplift with respect to the percent location of H_4 and X variations, respectively, for Dams 3 and 4. This is done to compare two dams having the same height but a different base width.

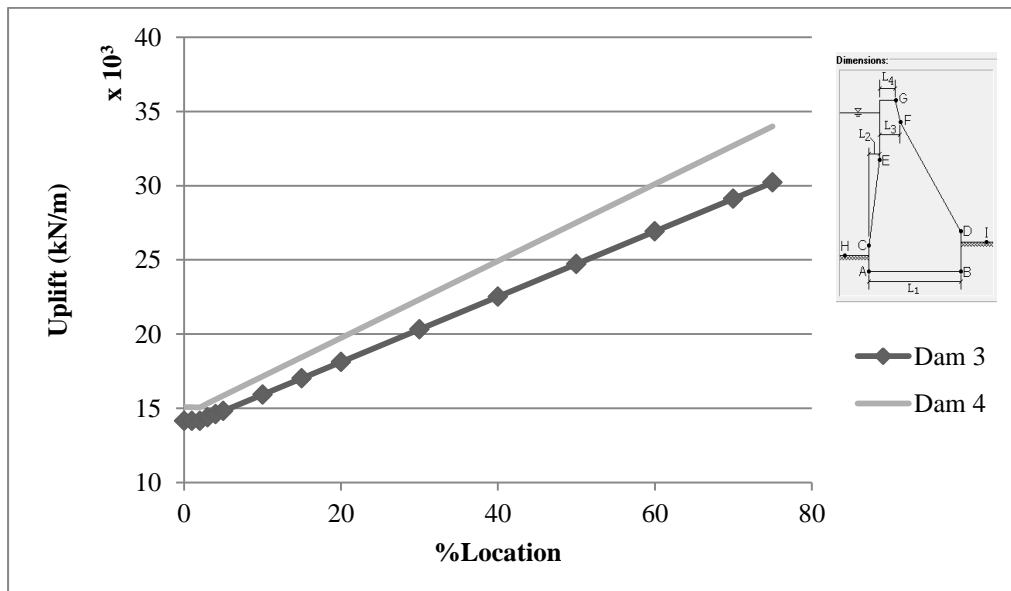


Figure 4-17 Uplift force for H_4 variations for Dams 3 and 4

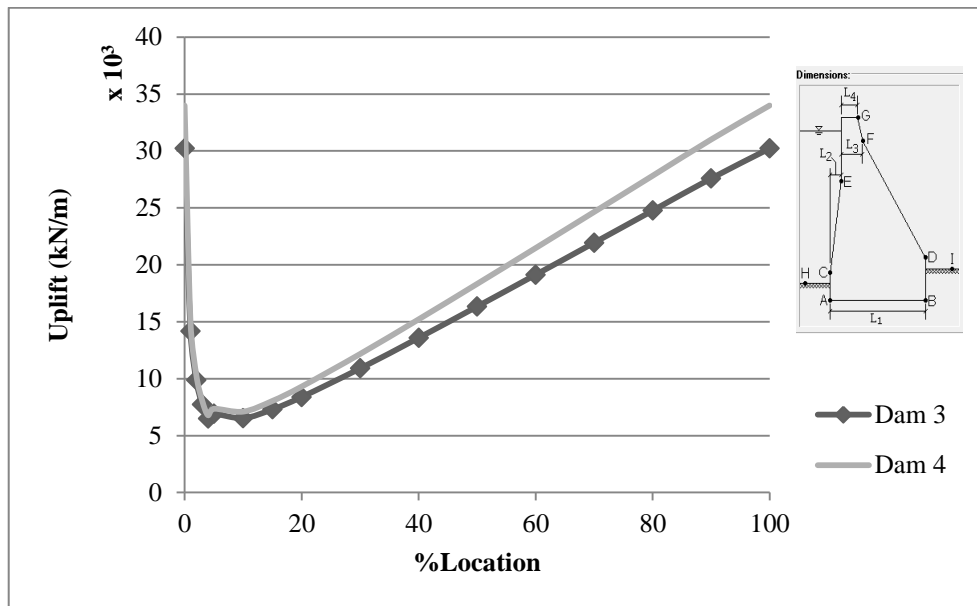


Figure 4-18 Uplift force for X variations for Dams 3 and 4

The following discussions can be made based on the aforementioned results:

- The presence of a drainage gallery can significantly reduce uplift by at least 60% as opposed to a case without a drainage gallery.
- The dam can retain more water as the height of the dam and the width of the base increase. The presence of more water on the upstream side increases the uplift pressure generated at the base and the percent reduction of uplift increases as well.
- The effectiveness of the drainage system decreases (less uplift reduction) as the gallery is moved farther away from the base (increase H_4).
- The uplift and the percent reduction remain the same until the gallery is at a location higher than 2% of the dam height. This is because of the fact that the water level downstream is at 2% of the dam height. Therefore, if the downstream water level is at an elevation Y, then the uplift force will be the same until the gallery goes above elevation Y. As long as the gallery remains at the level or below the level of the downstream water

elevation, the maximum uplift reduction can be achieved for any H_4 location. This is also apparent from Equations (2.1, 2.4, 2.6, 2.8, and 2.10) presented in Chapter 2 for $H_4 < H_2$. As long as H_4 is less than H_2 , the governing term is H_2 which is a constant, resulting in a constant H_3 for any $H_4 < H_2$.

- For the X variations, the location of maximum uplift reduction shifts more towards the upstream side as the height of the dam increases. But, as the base width of the dam increases, the location of maximum reduction remains at the same location.
- The graphs generated for H_4 variations (Figures 4-13, 4-14, and 4-17) show linear change due to the fact that the effectiveness calculation does not depend on the vertical location of the gallery i.e. the effectiveness is constant as the gallery is moved vertically through the dam.
- As shown in Tables 4-10 and 4-11 and the percent reduction graphs, percent reduction of 0% is attained at the last location. This occurs when the gallery is placed at a very high level or very far downstream, leading to an ineffective gallery that has no impact on the uplift force.

4.1.3.1.2 Drain Size and Spacing

Figures 4-19 and 4-20 show the variation of uplift and percent reduction, respectively, with respect to percent location for H_4 variations for the 5 m spacing for all diameters.

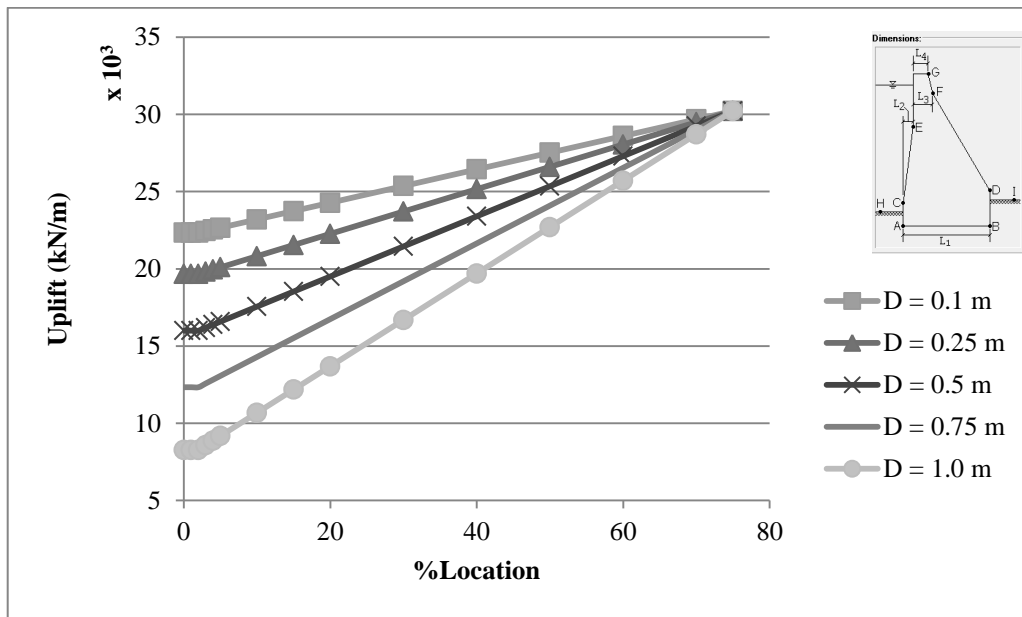


Figure 4-19 Uplift for H_4 variations, $S = 5$ m, all D

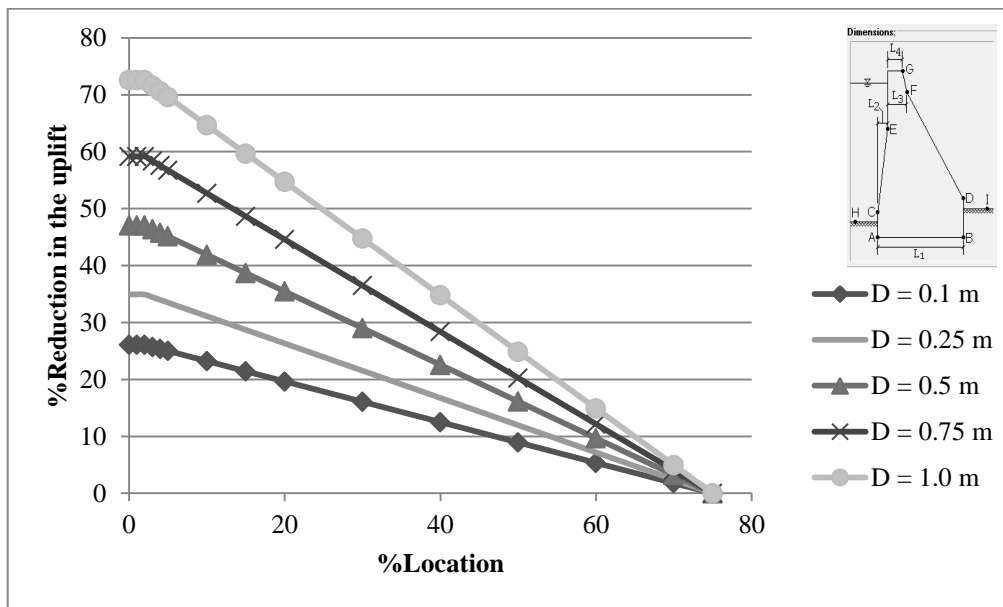


Figure 4-20 %Reduction of uplift force for H_4 variations, $S = 5$ m, all D

Figures 4-21 and 4-22 show the variation of uplift and percent reduction with respect to percent location, respectively for X variations for 5 m spacing for all diameters.

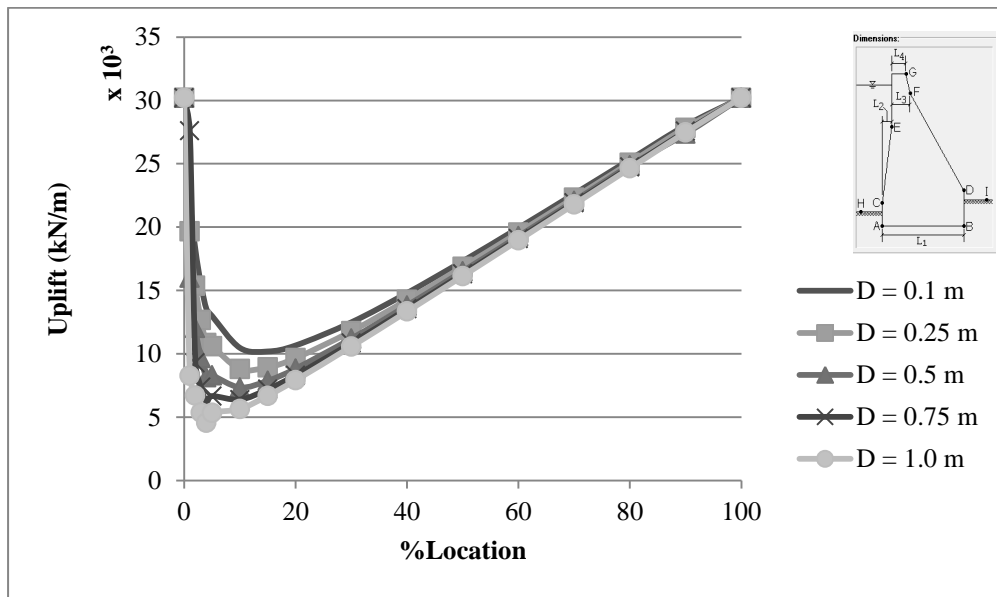


Figure 4-21 Uplift for X variations, S = 5 m, all D

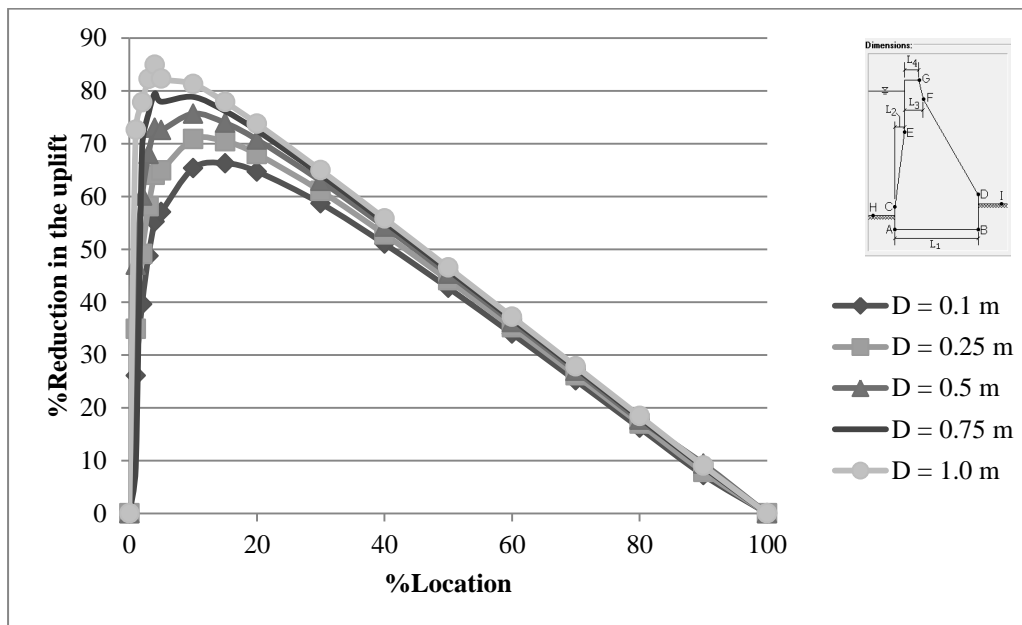


Figure 4-22 %Reduction of uplift force for X variations, S = 5 m, all D

The results indicate that as the drain diameter increase the uplift decreases and the percent reduction increases. In addition, as the diameter increases the minimum

uplift and maximum percent reduction (peak) shifts more towards the upstream side. This is consistent with the results of Chawla et al. (1990).

Figures 4-23 and 4-24 show the variation of uplift and percent reduction with respect to percent location, respectively, for H_4 variations for all S for 0.1 m drain diameter.

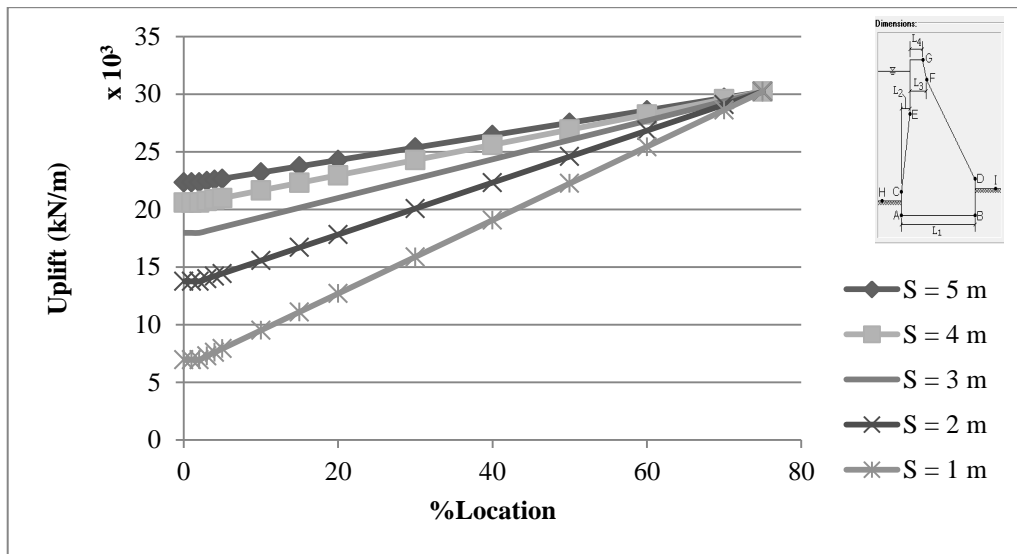


Figure 4-23 Uplift for H_4 variations, $D = 0.1$ m, all S

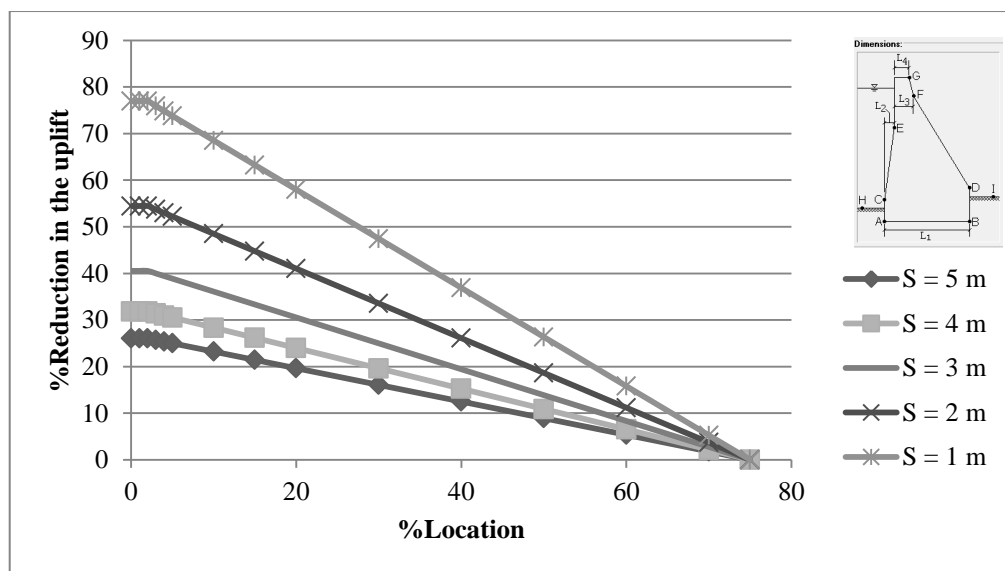


Figure 4-24 %Reduction of uplift force for H_4 variations, $D = 0.1$ m, all S

The results show that smaller spaces between the drains (more drains per unit area) lead to reduced uplift (higher percent reduction). Again, the drainage effectiveness does not depend on vertical variations.

Figures 4-25 and 4-26 show the variation of uplift and percent reduction with respect to percent location, respectively, for X variations for all spacing for 0.1 m drain diameter.

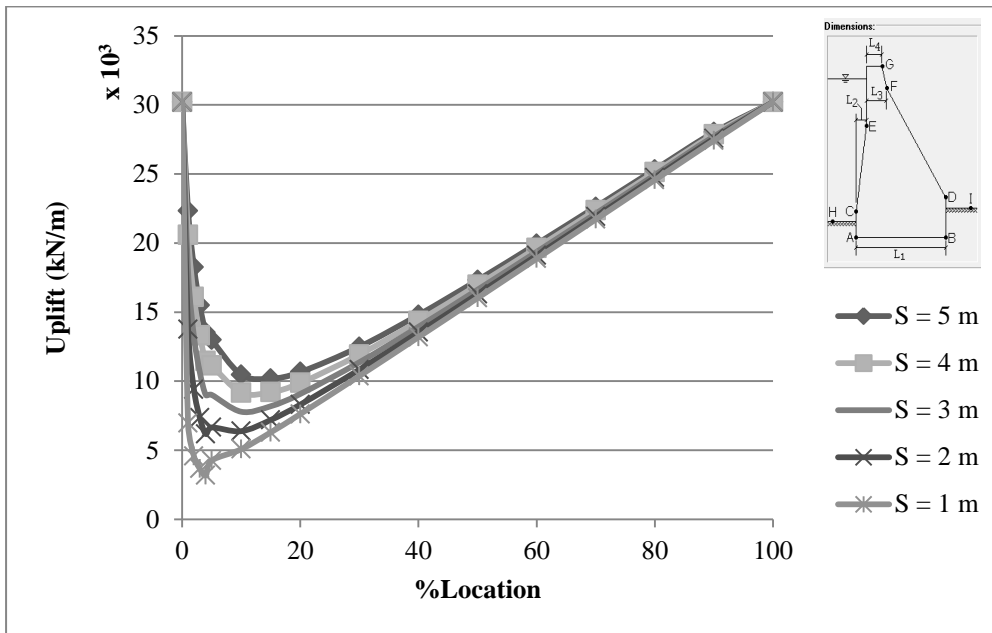


Figure 4-25 Uplift for X variations, D = 0.1 m, all S

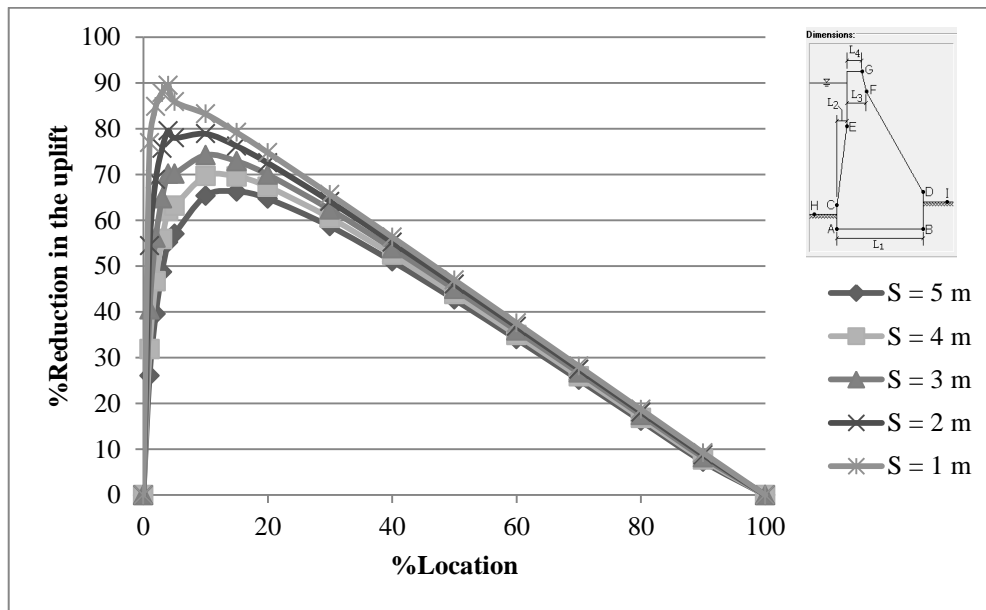


Figure 4-26 %Reduction of uplift force for X variations, D = 0.1 m, all S

The results show that as the spacing increases the optimum point for maximum uplift reduction moves more towards the downstream similar to the results presented by Chawla et al. (1990).

Figure 4-27 represents the percent reduction for all S for the 1 m drain diameter. Only the large spaces considered i.e. 5 m and 4 m are present since the other smaller spaces combined with a large diameter i.e. 1 m lead to negative uplift in the results. This means that the effectiveness of the drainage system “E” is larger than one due to the use of larger drains with smaller spacing; leading to a negative efficiency “K” and negative uplift computation (refer to Chapter 2). In practice, this means that the drains are so large that the pressure difference causing the water to enter the drains decreases to such a point that no water enters the drains at all, making the drainage system redundant. Even though the largest possible diameter (1 m) and smallest possible spacing (4 m) in this case can reduce the uplift up to 90% it is not feasible to consider this alternative. Large diameters and increased number of drains per unit area may increase the cost and lead to higher stresses as shown in the next section.

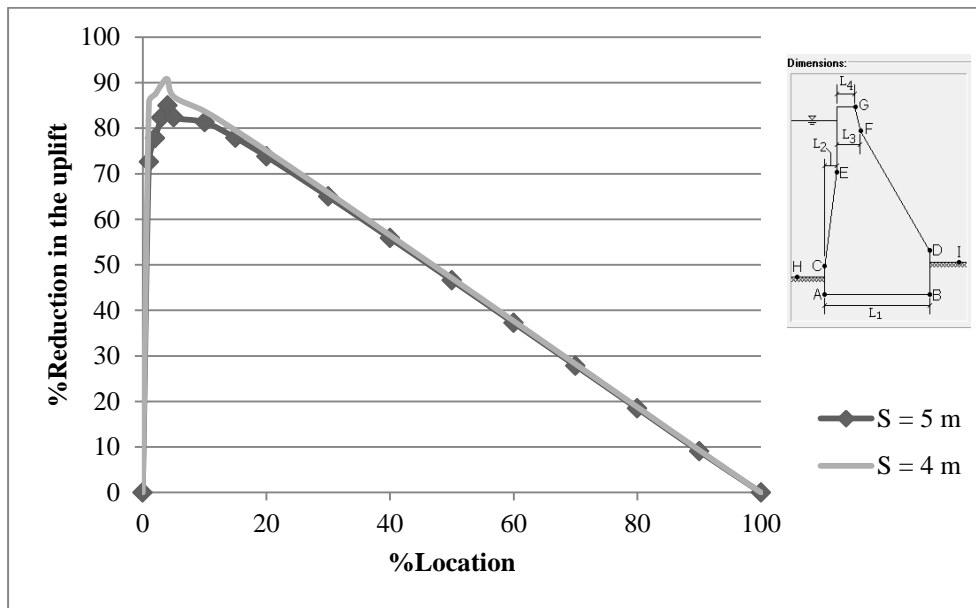


Figure 4-27 %Reduction of uplift force for X variations, D = 1m, all S

Figure 4-19 through Figure 4-27 show that as the gallery is moved away from the base of the dam (H_4 variation) or away from the upstream face (X variation), the effectiveness of the drainage system decreases until a point at which the drainage system becomes ineffective. At this point (last H_4 or X location considered) the uplift force for any diameter or spacing scenario is the same as that achieved in the non-drained case, leading to a 0% percent reduction in the uplift.

4.1.3.1.3 Internal Stresses

Figures 4-28 and 4-29 show the H_4 and X variation of internal stresses, respectively, for Dam 3.

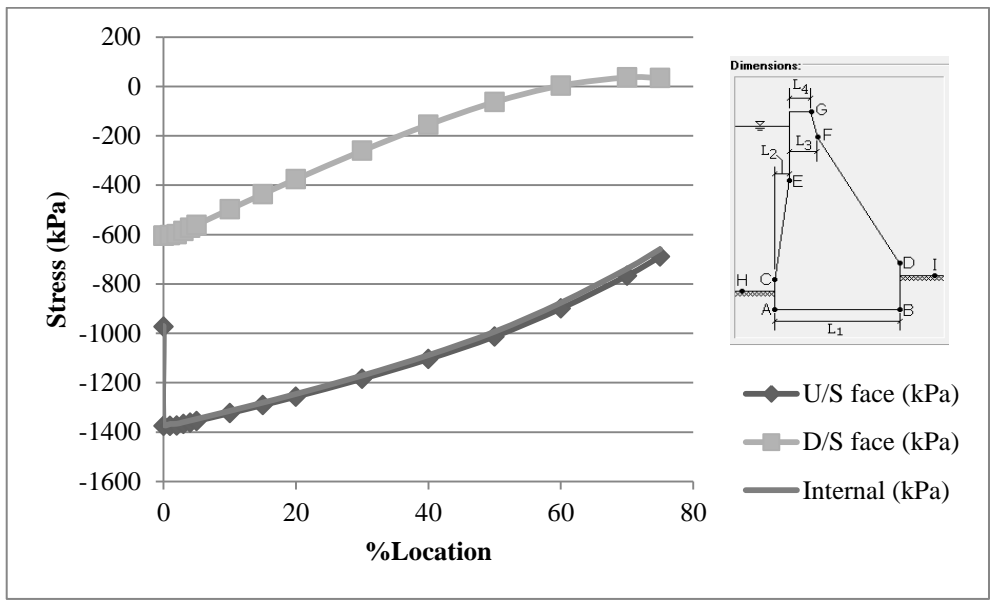


Figure 4-28 Stresses for H_4 variations for Dam 3

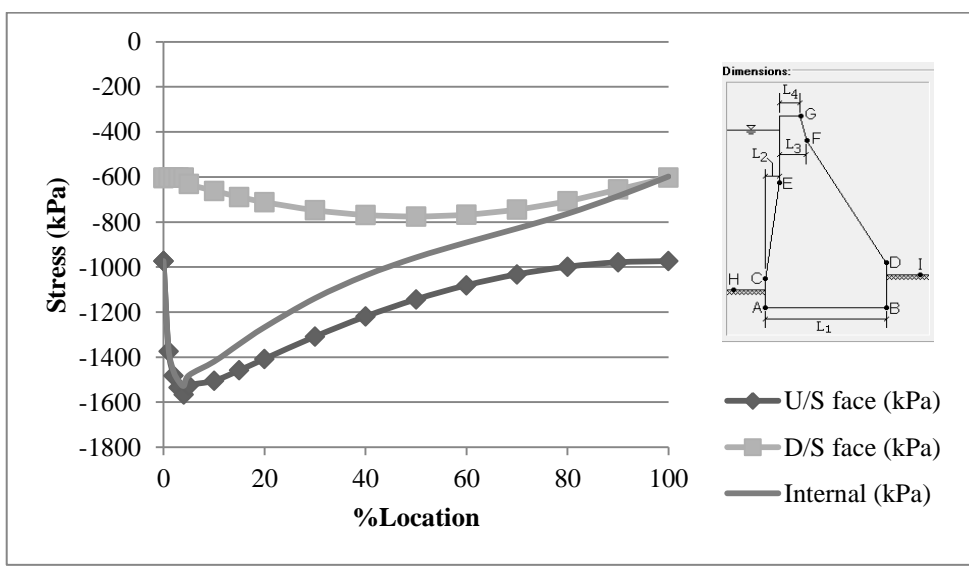


Figure 4-29 Stresses for X variations for Dam 3

The presence of a gallery increases the stress at the upstream side because the gallery is practically a hollow space that reduces the amount of concrete resisting the stresses. The internal stresses are very close to the upstream stresses in Figure

4-28 since the gallery is only 1% of the base width away from the heel of the dam for the H_4 variations. The stress upstream and downstream at the level of the gallery decrease as the gallery is moved vertically away from the base because the impact of the hollow space (gallery) is less profound as it moves away from the base where the most pressure is applied.

As the gallery moves in the downstream direction (X variations), the stress upstream increases till the gallery is at a distance of 4% of the base width away from the heel of the dam. The stress downstream remains constant until the gallery is moved more than 4% away from the heel, and then increase to a maximum at a distance of 50% of the base width from dam heel. This behavior was observed for all six dams considered in the analysis. The internal stresses corresponding to the location of the gallery vary from the stress upstream when the gallery is at the dam heel to the stress downstream when the gallery is at the dam toe.

Figures 4-30 and 4-31 correspond to the stresses upstream and downstream, respectively, for H_4 variations, 5 m spacing, and all diameters case. Figures 4-32 and 4-33 correspond to the stresses upstream and downstream, respectively, for X variations, 5 m spacing, and all diameters.

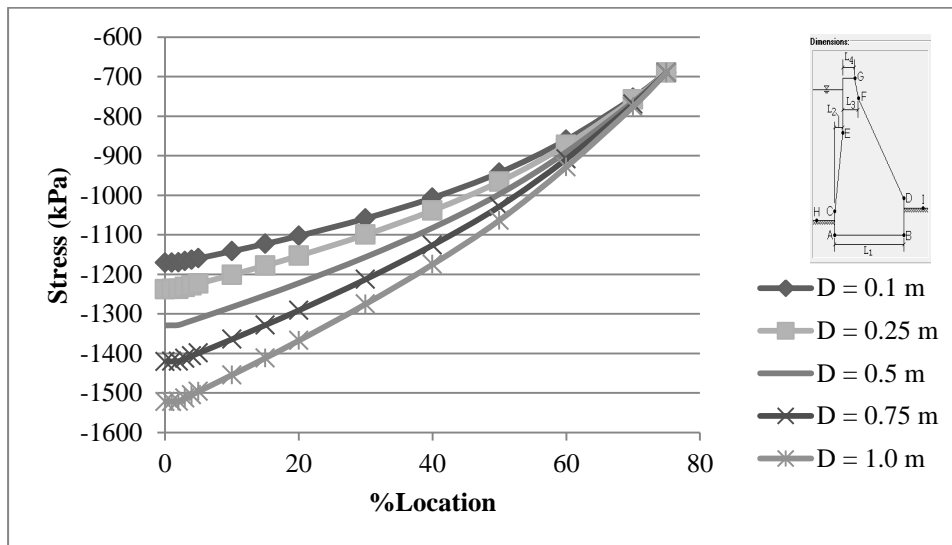


Figure 4-30 Stresses upstream, H_4 variations, $S = 5$ m, all D

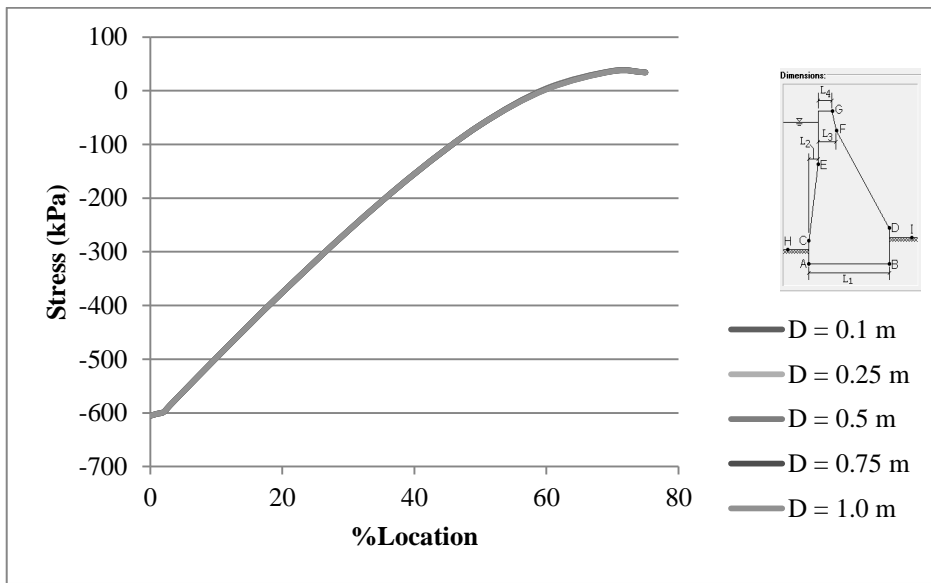


Figure 4-31 Stresses downstream, H_4 variations, $S = 5$ m, all D

As the diameter increases the stresses upstream also increase, due to increased hollow spaces leading to lower concrete area. However, the stresses downstream are not affected by the drain diameter size for H_4 variations. Therefore, the stresses measured for all diameters are all the same showing one curve on top of the other in Figure 4-31.

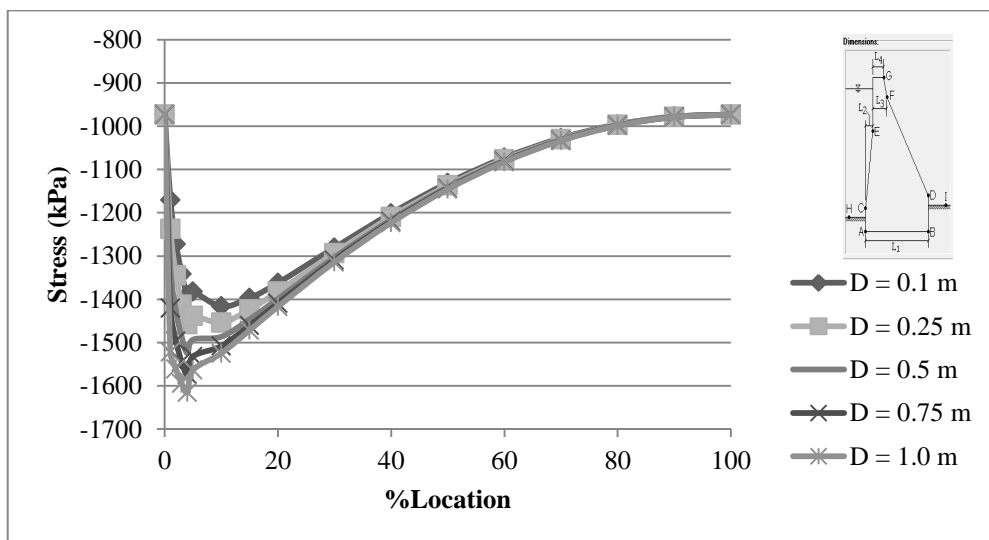


Figure 4-32 Stresses upstream, X variations, $S = 5$ m, all D

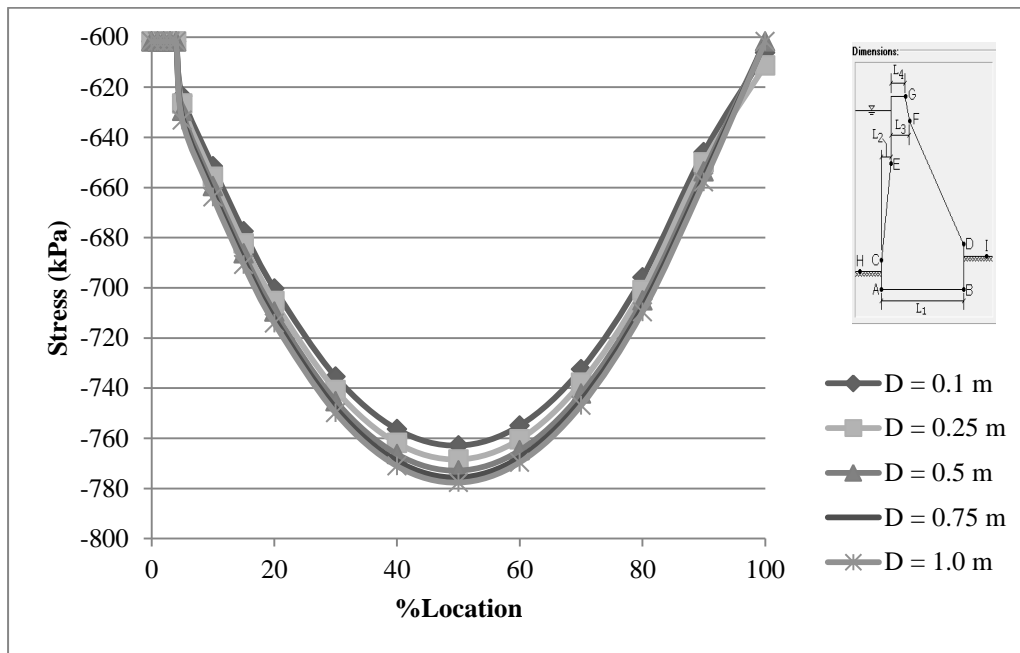


Figure 4-33 Stresses downstream, X variations, S = 5 m, all D

Similarly, larger diameters generate more stresses both upstream and downstream due to reduced concrete area.

The internal stresses exhibit very similar results to those of the upstream stresses for H_4 variations (Figures 4-30) since the gallery is very close to the upstream face. The internal stresses show a similar behavior to that of Figure 4-32 for X variations but with lower stresses as the gallery moves more towards the downstream side.

Figures 4-34 and 4-35 correspond to the stresses upstream and downstream, respectively, for H_4 variations, 0.25 m diameter, and all spacing case. The stresses downstream are not affected by the various spacing considered for various H_4 positions. That is why the curve for each case is identical to the other as shown in Figure 4-35. Figures 4-36 and 4-37 correspond to the stresses upstream and downstream, respectively, for X variations, 0.25 m diameter, and all spacing.

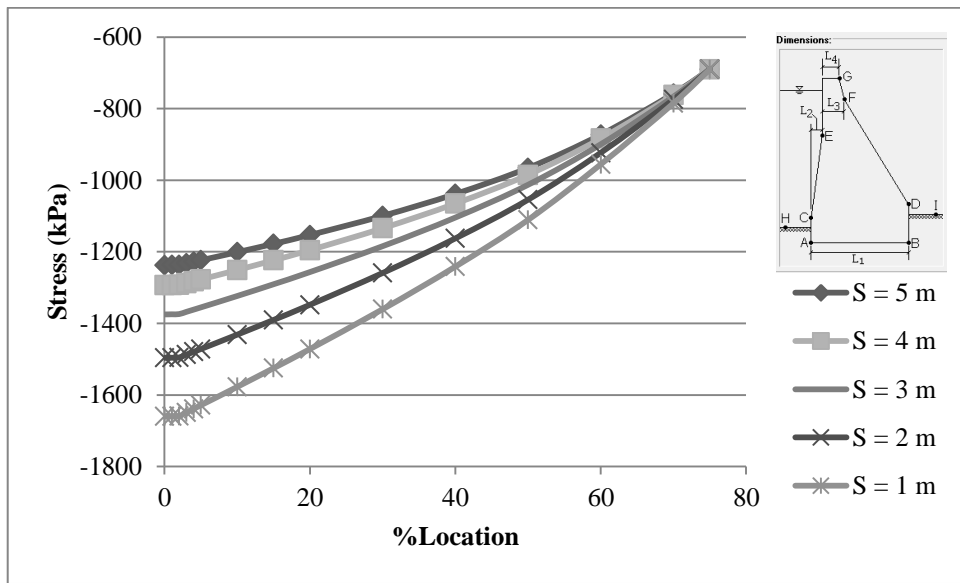


Figure 4-34 Stresses upstream, H_4 variations, $D = 0.25$ m, all S

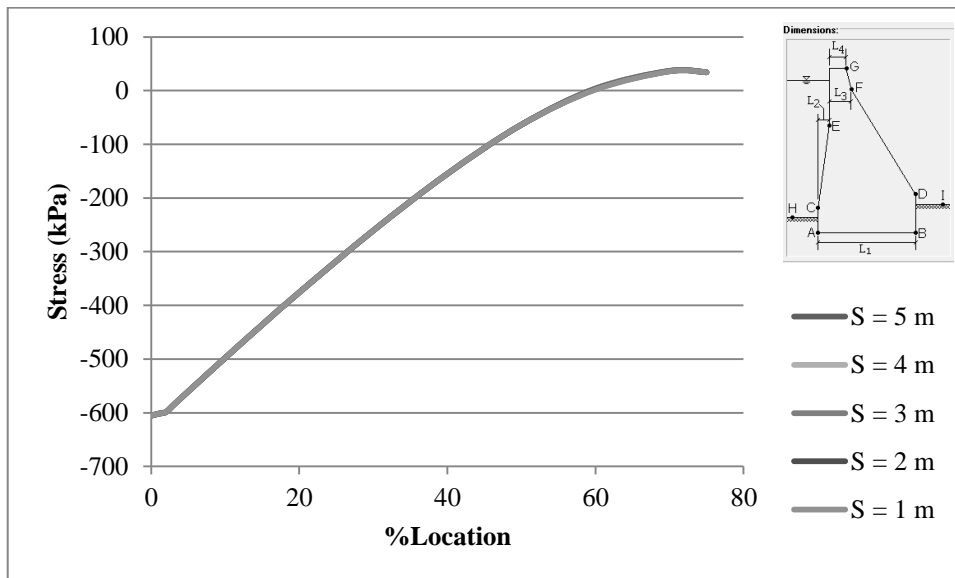


Figure 4-35 Stresses downstream, H_4 variations, $D = 0.25$ m, all S

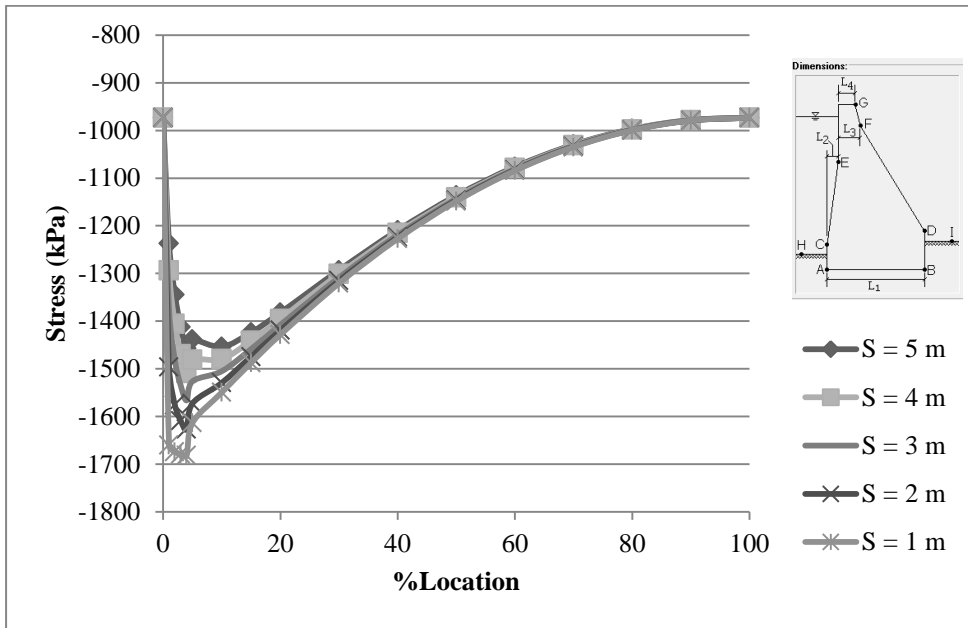


Figure 4-36 Stresses upstream, X variations, $D = 0.25$ m, all S

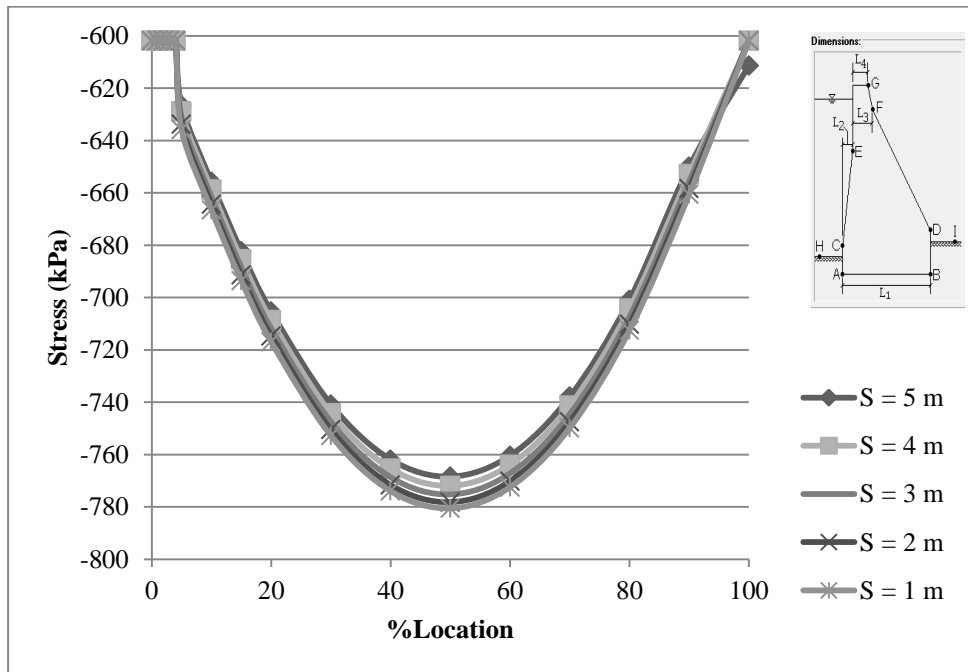


Figure 4-37 Stresses downstream, X variations, $D = 0.25$ m, all S

Both H_4 and X variations show that the stresses at both upstream and downstream faces increase as the spacing between the drains decrease, due to more drains per unit area decreasing the area of concrete.

The stresses in Figure 4-28 through Figure 4-37 were all less than the allowable compressive stress in concrete (3750 kN/m^2) presented in Table 5-2. This shows that all the considered combinations are realistic and appropriate and will not lead to excessive stresses in the dam.

4.1.3.2 Unusual Loading Case

The impact of the variables on uplift and stresses for the unusual loading case is examined here.

4.1.3.2.1 Dimensional Variations

Table 4-12 shows the uplift force and percent reduction for Dams 1, 3, and 5 for each of the H_4 percent locations considered. Figures 4-38 and 4-39 are the graphical representations of the uplift force and the percent reduction, respectively. In Table 4-12, the shaded areas represent the vertical locations of the gallery that lead to a crack in the base.

A base crack occurs for the none drainage case corresponding to 18.2% of base width for dam 1, 42.3% of base width for Dam 3, and 59.1% of the base width for Dam 5. The base cracks immediately with the percentages mentioned above for Dams 3 and 5 when the gallery reaches 80% or more of the height of the dam.

Table 4-12 Uplift forces for Dams 1, 3, and 5 for H_4 variations for unusual loading case

%location	Dam 1 (50 m x 40 m)		Dam 3 (100 m x 80 m)		Dam 5 (200 m x 160 m)	
	Uplift (kN/m)	%reduction in the uplift	Uplift (kN/m)	%reduction in the uplift	Uplift (kN/m)	%reduction in the uplift
w/o Drainage	9810.00		39240.00		156960.00	
0	5657.63	42.3	17253.23	56.0	45064.58	71.3
1	5699.16	41.9	17473.10	55.5	46183.54	70.6
2	5740.68	41.5	17692.96	54.9	47302.49	69.9
3	5782.21	41.1	17912.83	54.4	48421.45	69.2
4	5823.73	40.6	18132.70	53.8	49540.40	68.4
5	5865.25	40.2	18352.57	53.2	50659.35	67.7
10	6072.87	38.1	19451.91	50.4	56254.12	64.2
15	6280.49	36.0	20551.24	47.6	61848.91	60.6
20	6488.11	33.9	21650.58	44.8	67443.67	57.0
30	6903.34	29.6	23849.26	39.2	78633.21	49.9
40	7318.58	25.4	26047.94	33.6	89822.75	42.8
50	7733.82	21.2	28246.61	28.0	101012.29	35.6
60	8149.05	16.9	30445.29	22.4	112201.83	28.5
70	8564.29	12.7	32643.97	16.8	123391.37	21.4
80	8979.53	8.5	34842.65	11.2	134580.92	14.3
90	9394.76	4.2	37041.32	5.6	145770.46	7.1
100	9810.00	0.0	39240.00	0.0	156960.00	0.0

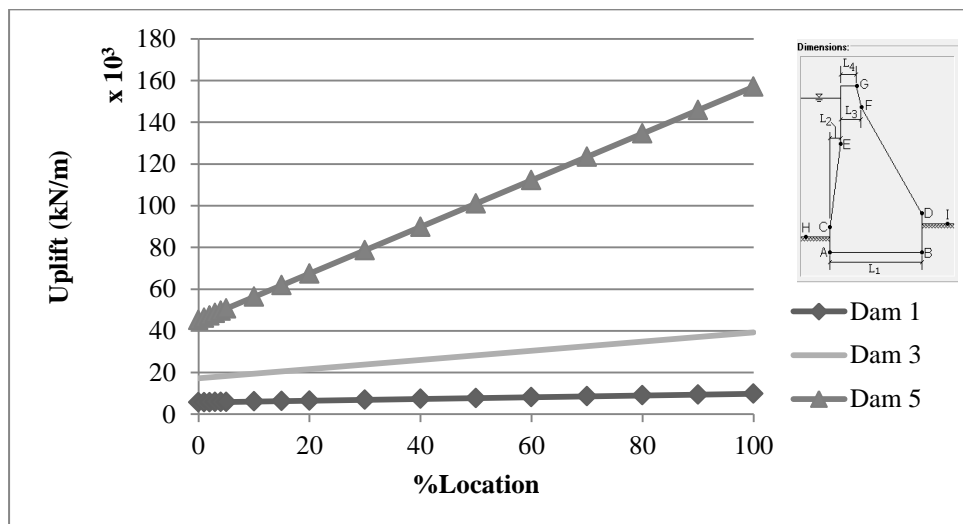


Figure 4-38 Uplift force for H_4 variations for Dams 1, 3, and 5

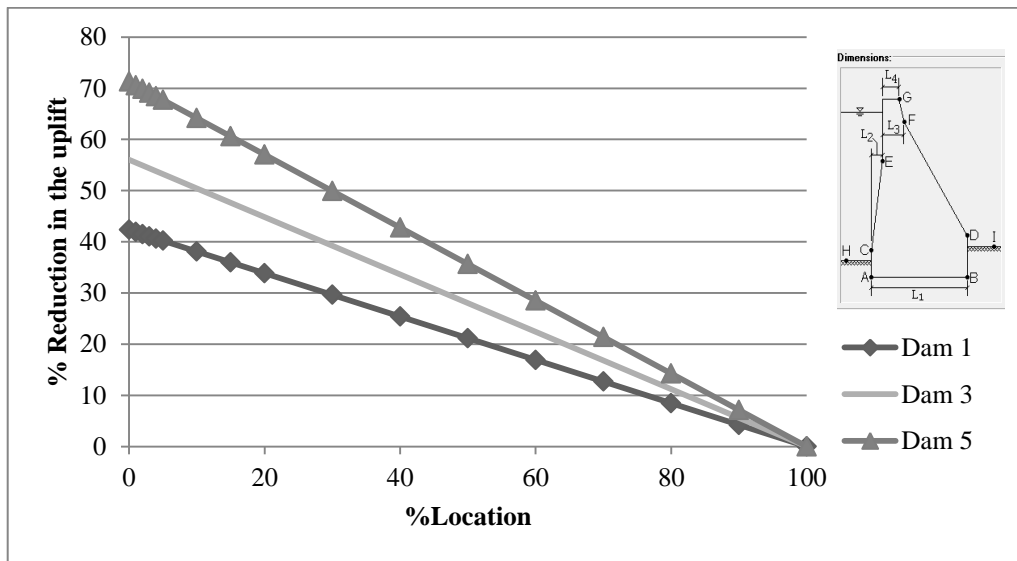


Figure 4-39 %Reduction of uplift force for H_4 variations for Dams 1, 3, and 5

Table 4-13 shows the uplift force and percent reduction for the various heights considered for a base width of 80% of dam height for each of the X percent locations considered. Figures 4-40 and 4-41 are the graphical representations of the same data for the uplift force and the percent reduction, respectively. Results show that once the gallery is moved 60% or more towards the downstream direction for H_4 at 1% of dam height the base starts to crack by the values shown in Table 4-14.

Table 4-13 Uplift forces for Dams 1, 3, and 5 for X variations for unusual loading case

%location	Dam 1 (50 m x 40 m)		Dam 3 (100 m x 80 m)		Dam 5 (200 m x 160 m)	
	Uplift (kN/m)	%reduction in the uplift	Uplift (kN/m)	%reduction in the uplift	Uplift (kN/m)	%reduction in the uplift
w/o Drainage	9810.0		39240.0		156960.0	
0	9810.0	0.0	39240.0	0.0	156960.0	0.0
1	5699.16	41.905	17473.10	55.471	46183.54	70.576
2	4392.58	55.223	11626.78	70.370	27856.48	82.252
3	3527.48	64.042	8753.87	77.691	20309.82	87.061
4	2948.04	69.949	7077.47	81.964	16198.46	89.680
5	2540.66	74.101	5981.00	84.758	13613.09	91.327
10	2394.39	75.592	7161.27	81.750	23196.92	85.221
15	2486.51	74.653	8220.25	79.051	29115.17	81.451
20	2763.16	71.833	9713.33	75.246	35979.15	77.078
30	3519.29	64.125	13155.79	66.474	50677.36	67.713
40	4383.06	55.320	16833.56	57.101	65868.29	58.035
50	5291.61	46.059	20607.27	47.484	81258.04	48.230
60	6222.70	36.568	24428.96	37.745	96746.84	38.362
70	7166.08	26.951	28277.07	27.938	112290.49	28.459
80	8115.19	17.276	32138.65	18.097	127863.34	18.538
90	9060.11	7.644	35996.08	8.267	140501.42	10.486
100	9810.0	0.0	39240.0	0.0	156960.0	0.0

Table 4-14 Crack % of base of Dams 1, 3, and 5 for X variations

X (%)	Crack % of base from U/S face		
	Dam 1	Dam 3	Dam 5
w/o Drainage	18.23%	42.28%	59.11%
0	18.23%	42.28%	59.11%
1-50			
60		2.45%	13.76%
70		20.03%	33.67%
80		32.58%	47.91%
90		40.01%	56.41%
100		42.28%	59.11%

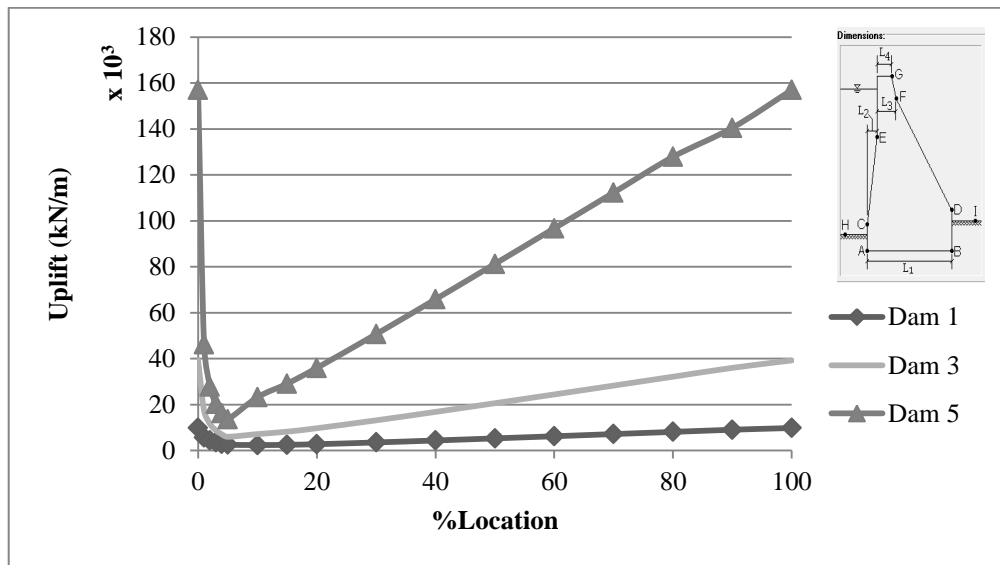


Figure 4-40 Uplift force for X variations for Dams 1, 3, and 5

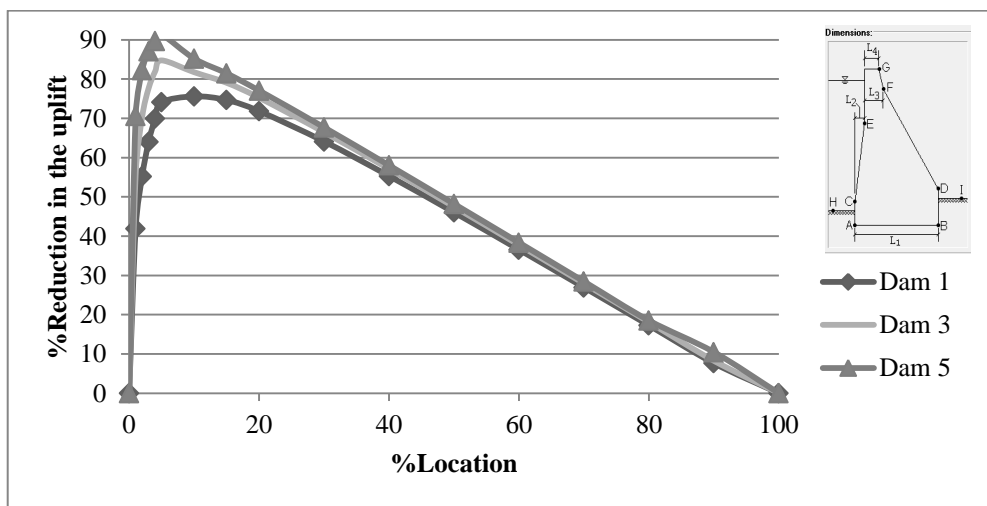


Figure 4-41 %Reduction of uplift force for X variations for Dams 1, 3, and 5

No cracking occurs for any of the height \times 90% base width dams (Dams 2, 4, and, 6). The larger base width increases the safety of the dam, leading to smaller cracks if any at all. Figures 4-38 through 4-41 provide the same conclusions as Figures 4-13 through 4-16 for the usual loading case. However, due to the presence of more water on the upstream side, the uplift force and the percent reduction for the unusual case are higher.

4.1.3.2.2 Drain Size and Spacing

Figures 4-42 and 4-43 show the variation of uplift and percent reduction with respect to percent location, respectively, for H_4 variations for the 5 m spacing for all diameters.

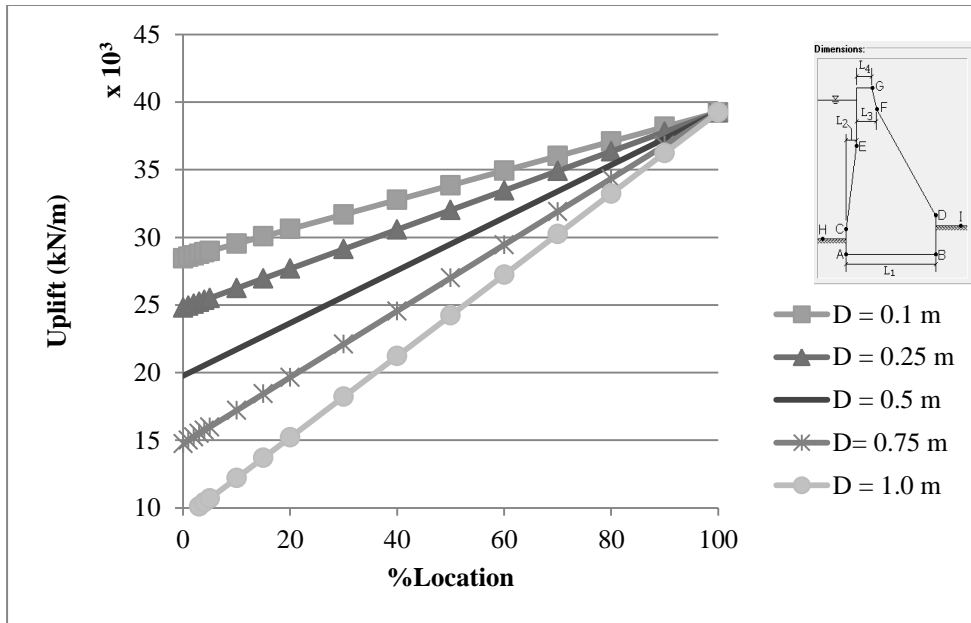


Figure 4-42 Uplift for H_4 variations, $S = 5$ m, all D

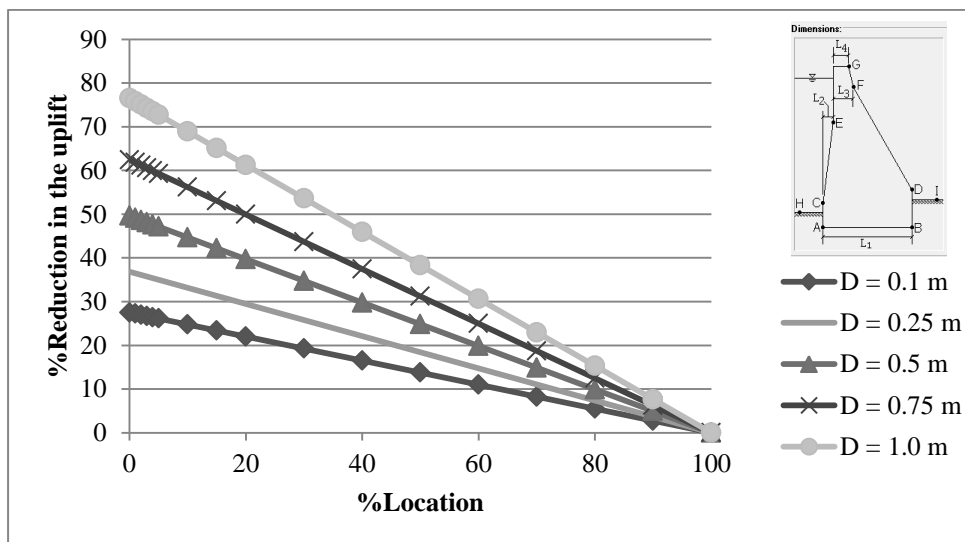


Figure 4-43 %Reduction of uplift force for H_4 variations, $S = 5$ m, all D

Figures 4-44 and 4-45 show the variation of uplift and percent reduction with respect to percent location, respectively, for X variations for 5 m spacing for all diameters.

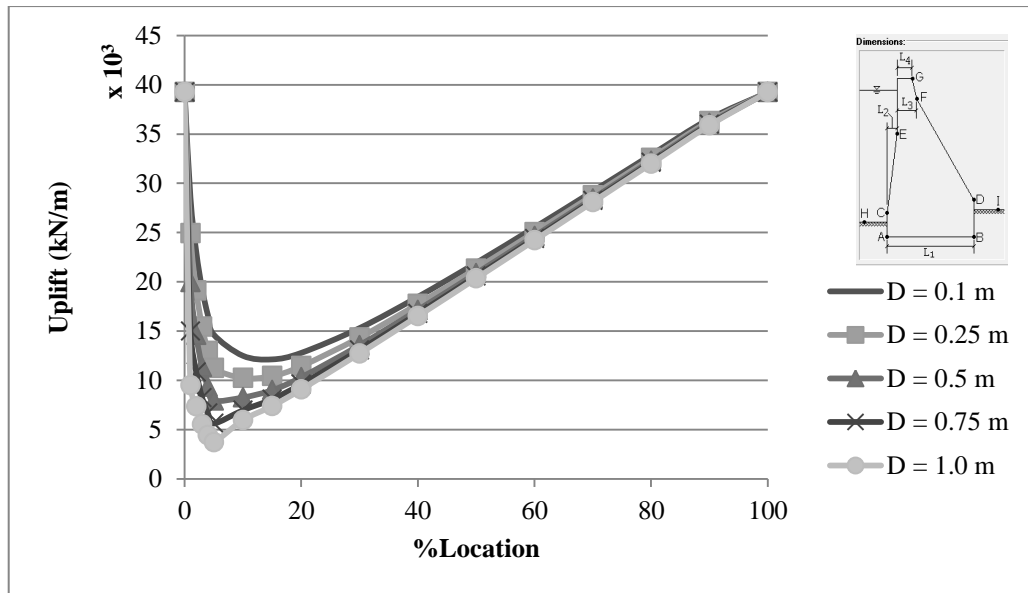


Figure 4-44 Uplift for X variations, S = 5 m, all D

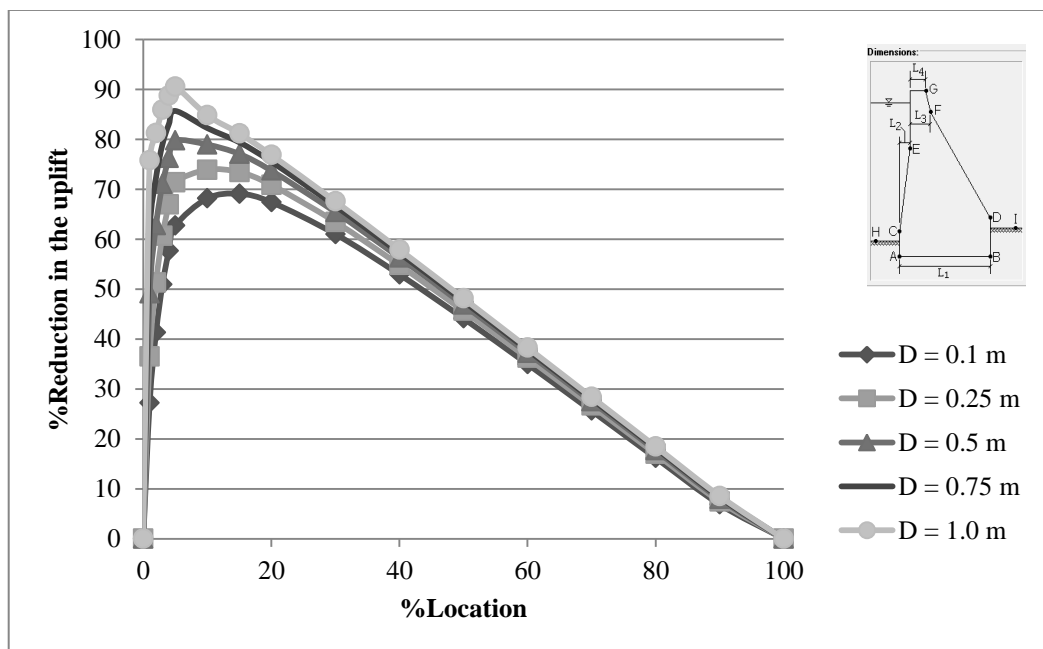


Figure 4-45 %Reduction of uplift force for X variations, S = 5 m, all D

Figures 4-46 and 4-47 show the variation of uplift and percent reduction with respect to percent location, respectively, for H_4 variations for all S for 0.1 m drain diameter.

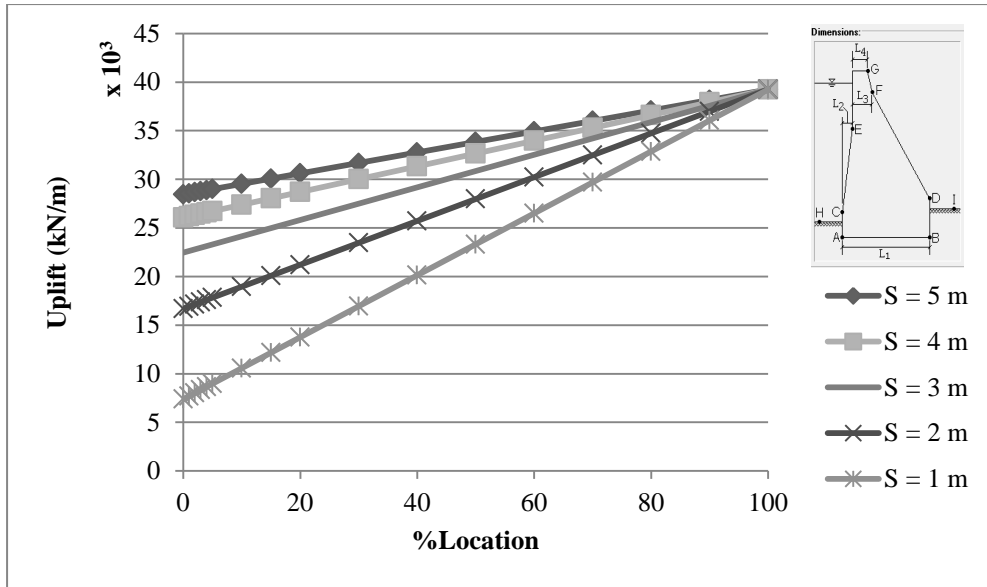


Figure 4-46 Uplift for H_4 variations, $D = 0.1$ m, all S

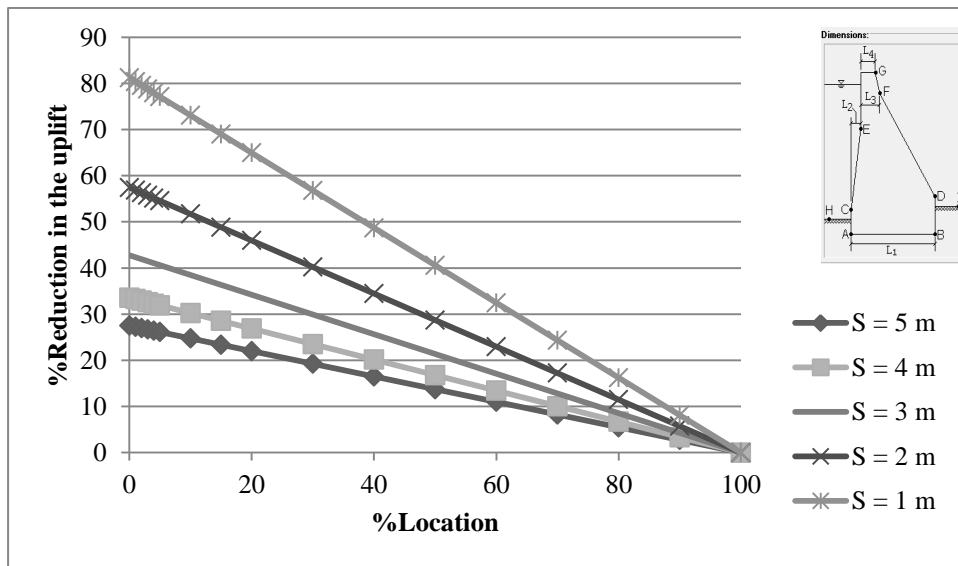


Figure 4-47 %Reduction of uplift force for H_4 variations, $D = 0.1$ m, all S

Figures 4-48 and 4-49 show the variation of uplift and percent reduction with respect to percent location, respectively, for X variations for all spacing for 0.1 m drain diameter.

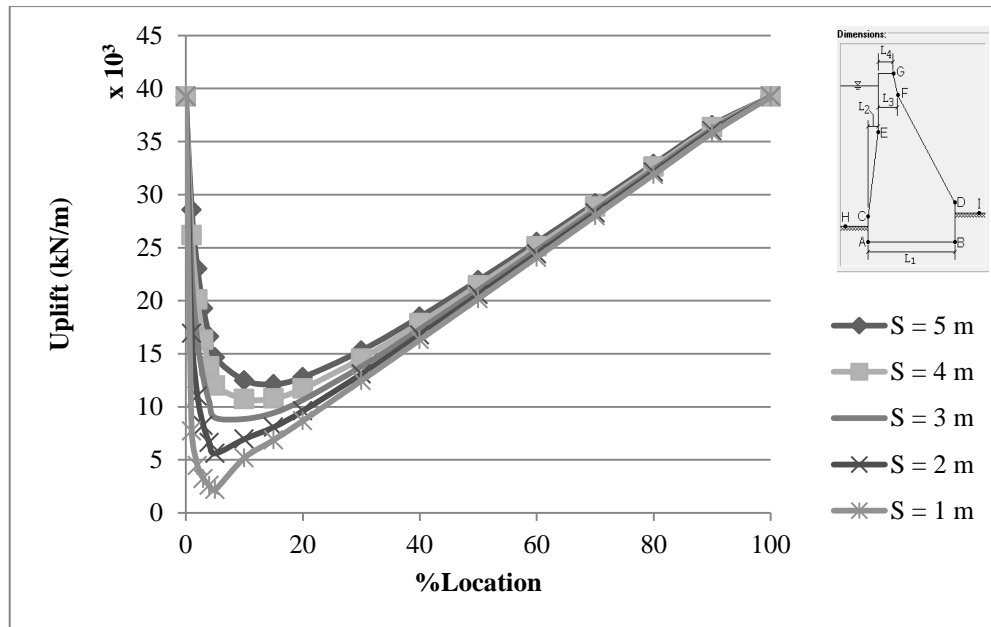


Figure 4-48 Uplift for X variations, D = 0.1 m, all S

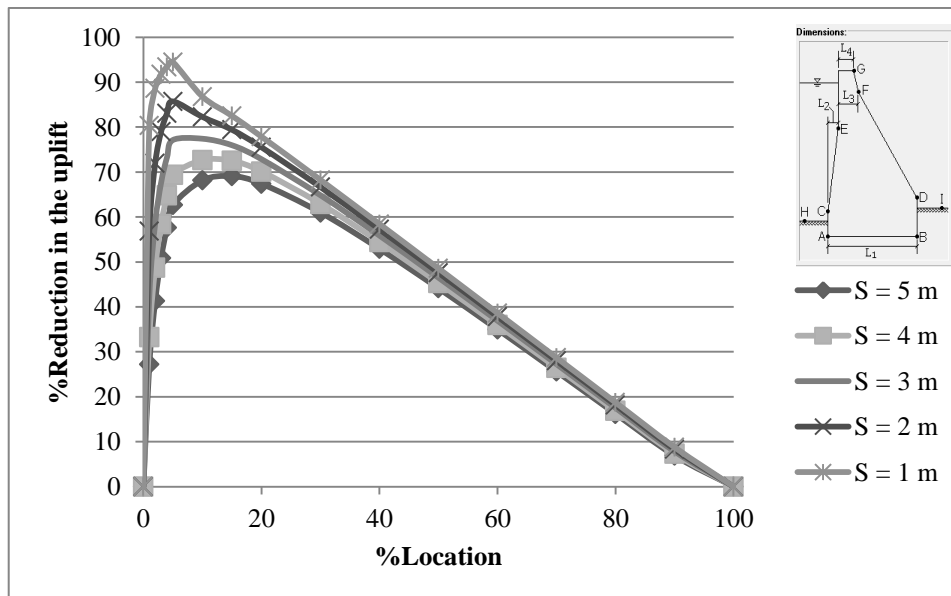


Figure 4-49 %Reduction of uplift force for X variations, D = 0.1 m, all S

The same convergence behavior discussed for Figures 4-19 through 4-27 is observed in Figures 4-42 through 4-49 which is caused by the ineffectiveness of the drainage system. A comparison between Figures 4-19 through 4-26 for the usual loading condition and Figures 4-42 through 4-49 for the unusual loading condition show that the behavior for varying the drain diameter and spacing is the same for both loading conditions i.e. larger diameter and smaller spacing reduce uplift further and shift the optimal location for uplift reduction towards the upstream side. Once more, the amount of uplift generated and the amount of reduction for the unusual case are higher due to the presence of more water on the upstream side.

Tables 4-15 and 4-16 show the cracking percentage for all the spacing and diameter combinations considered for Dam 3 for H_4 and X variations, respectively. The “X” in Table 4-15 indicated a crack at the upstream face of 42.284%, which once initiates remains the same even at higher elevations. Furthermore, smaller spacing and larger diameter led to the crack initiation at a higher level (see Table 4-15) or become smaller at the same level (see Table 4-16).

Table 4-15 Cracking of base of Dam 3 for all D and S for H_4 variations

H_4 (m)	1S/0.1D	1S/0.25D	2S/0.1D	2S/0.25D	2S/0.5D	3S/0.1D	3S/0.25D	3S/0.5D	3S/0.75D
0-40									
50									
60									
70						X			
80			X	X		X	X	X	
90	X	X	X	X	X	X	X	X	X
100	X	X	X	X	X	X	X	X	X

H_4 (m)	4S/0.1D	4S/0.25D	4S/0.5D	4S/0.75D	4S/1D	5S/0.1D	5S/0.25D	5S/0.5D	5S/0.75D	5S/1D
0-40										
50						X				
60						X	X			
70						X	X	X		
80	X	X	X	X		X	X	X	X	X
90	X	X	X	X	X	X	X	X	X	X
100	X	X	X	X	X	X	X	X	X	X

where

1S/0.1D	S = 1 m and D = 0.1 m
---------	-----------------------

Table 4-16 Cracking of base of Dam 3 for all D and S for X variations

X (m)	1S/0.1D	1S/0.25D	2S/0.1D	2S/0.25D	2S/0.5D	3S/0.1D	3S/0.25D	3S/0.5D	3S/0.75D
0	42.3%	42.3%	42.3%	42.3%	42.3%	42.3%	42.3%	42.3%	42.3%
0.8-40									
48	1.5%	1.2%	2.4%	1.8%	1.3%	3.3%	2.5%	1.8%	1.4%
56	19.4%	19.2%	20.0%	19.6%	19.3%	20.6%	20.0%	19.6%	19.3%
64	32.2%	32.1%	32.5%	32.3%	32.2%	32.9%	32.6%	32.3%	32.2%
72	39.9%	39.8%	40.0%	39.9%	39.8%	40.1%	40.0%	39.9%	39.8%
80	42.3%	42.3%	42.3%	42.3%	42.3%	42.3%	42.3%	42.3%	42.3%

4S/0.1D	4S/0.25D	4S/0.5D	4S/0.75D	4S/1D	5S/0.1D	5S/0.25D	5S/0.5D	5S/0.75D	5S/1D
42.3%	42.3%	42.3%	42.3%	42.3%	42.3%	42.3%	42.3%	42.3%	42.3%
4.3%	3.2%	2.4%	1.8%	1.4%	5.3%	4.0%	3.0%	2.4%	1.9%
21.2%	20.5%	20.0%	19.6%	19.4%	21.9%	21.0%	20.4%	20.0%	19.7%
33.2%	32.9%	37.5%	32.4%	32.2%	33.6%	33.1%	32.8%	32.5%	32.4%
40.3%	40.1%	40.0%	39.9%	39.9%	40.4%	40.2%	40.1%	40.0%	39.9%
42.3%	42.3%	42.3%	42.3%	42.3%	42.3%	42.3%	42.3%	42.3%	42.3%

where

1S/0.1D	S = 1 m and D = 0.1 m
---------	-----------------------

4.1.3.2.3. Internal Stresses

Figures 4-50 and 4-51 show the H_4 and X variation of stresses, respectively, for Dam 3.

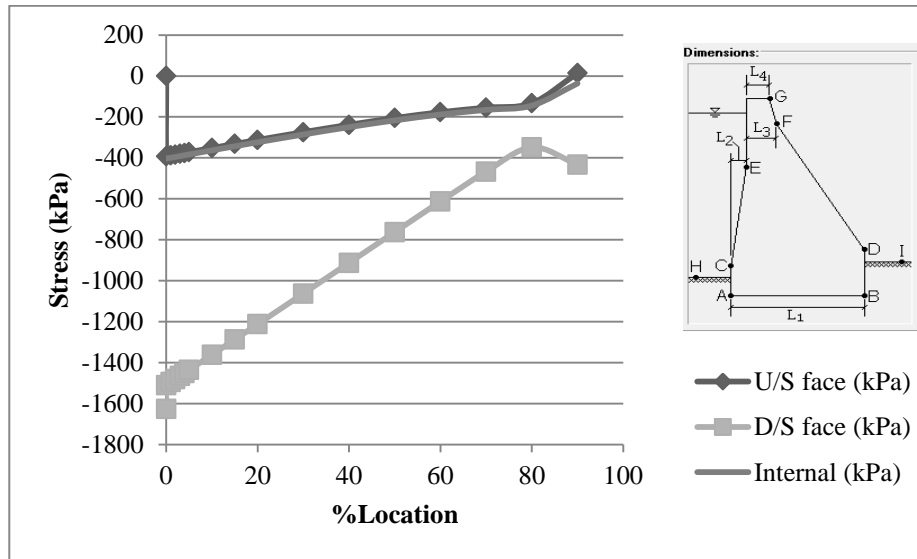


Figure 4-50 Stresses for H_4 variations for Dam 3

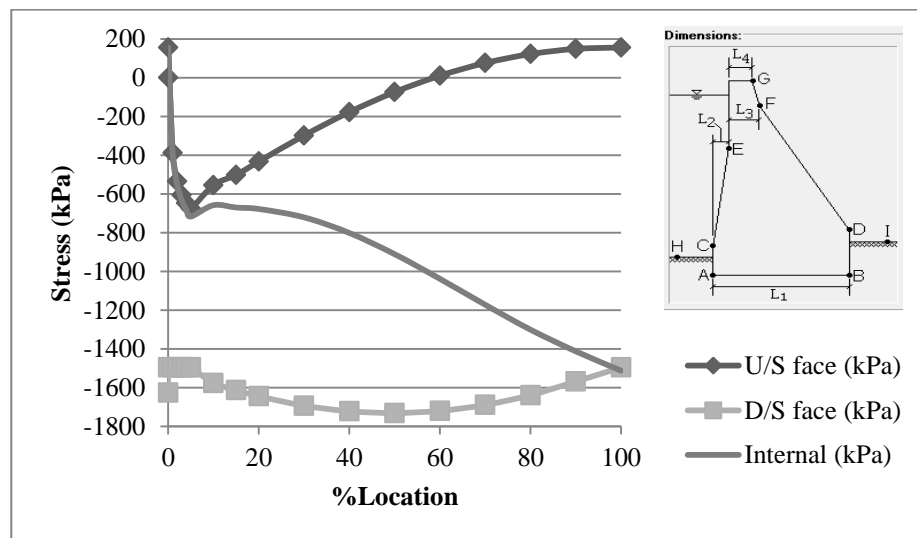


Figure 4-51 Stresses for X variations for Dam 3

The following discussions can be made for this case:

- The stresses at the downstream side are higher than the stresses developing at the upstream side for the unusual loading case. However, all stresses remain within the acceptable range.
- The stress on the upstream side starts at zero since the base is cracked when there is no gallery.
- For the H_4 variation case (Figure 4-50), the stresses upstream become positive (tension) when the gallery is located at 90% of the dam height and above since the base begins to crack at that point. The stresses downstream increase after the base cracks.
- For the X variation case (Figure 4-51), the stresses upstream increase till the gallery is at 4% of base width away from dam heel as before and then decreases to reach positive values (tension) at 60% indicating that the base is beginning to crack. Again, the internal stresses vary from the stress upstream to the stress downstream indicating the location of the gallery.

Figures 4-52 and 4-53 correspond to the stresses upstream and downstream, respectively for H_4 variations, 5 m spacing, and all diameters case. Moreover, Figures 4-54 and 4-55 correspond to the stresses upstream and downstream, respectively for X variations, 5 m spacing, and all diameters.

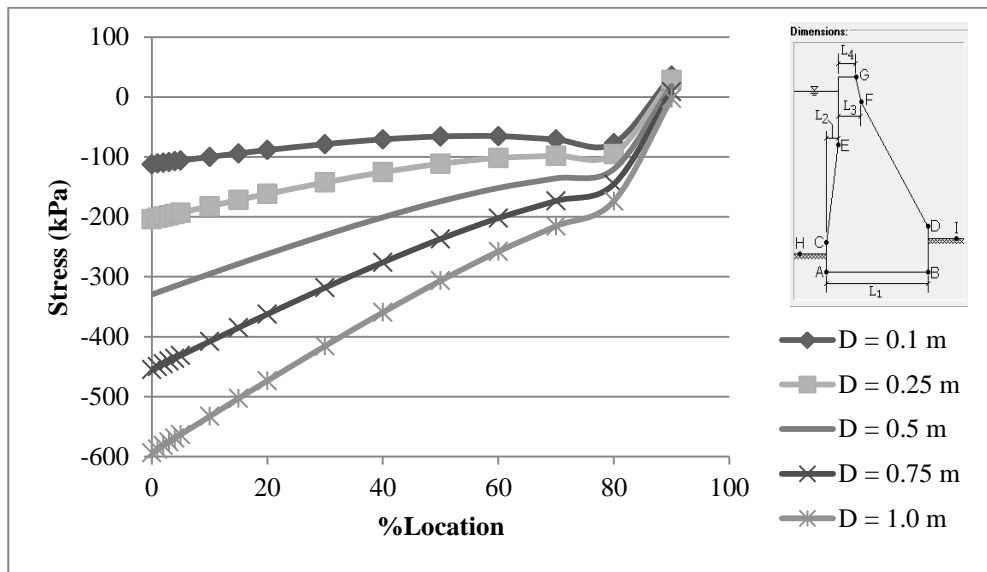


Figure 4-52 Stresses upstream, H_4 variations, $S = 5$ m, all D

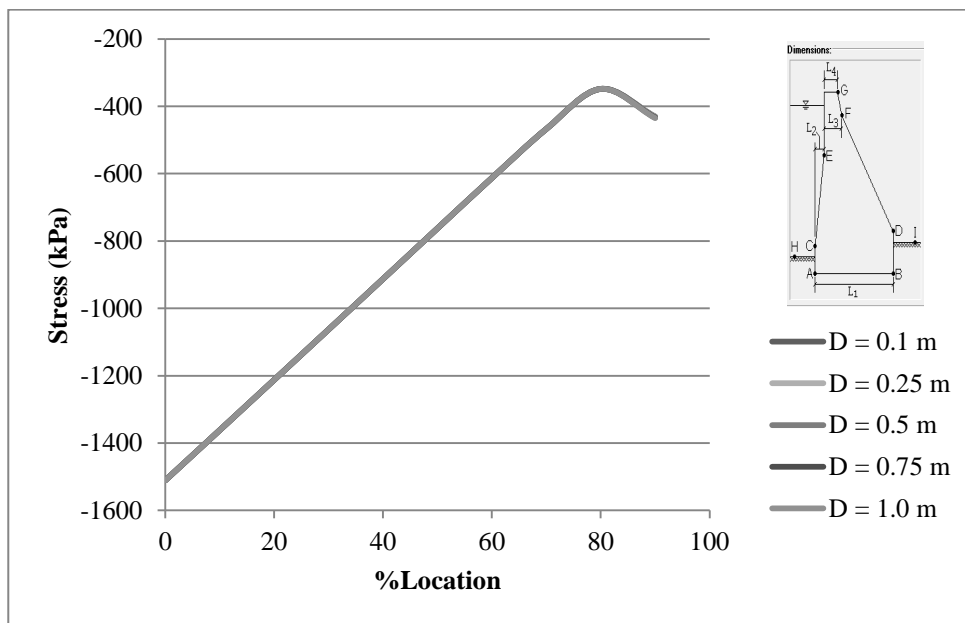


Figure 4-53 Stresses downstream, H_4 variations, $S = 5$ m, all D

As the diameter increases the stresses at the upstream also increase, due to increased hollow spaces leading to lower concrete area. However, the stresses downstream are not affected by the drain diameter size for H_4 variations, leading

to identical stress readings for all diameters (similar to Figure 4-31). For all cases, the stresses upstream reach a tension state and the stresses downstream increase after the gallery reaches 90% vertical location i.e. the point where the base cracks.

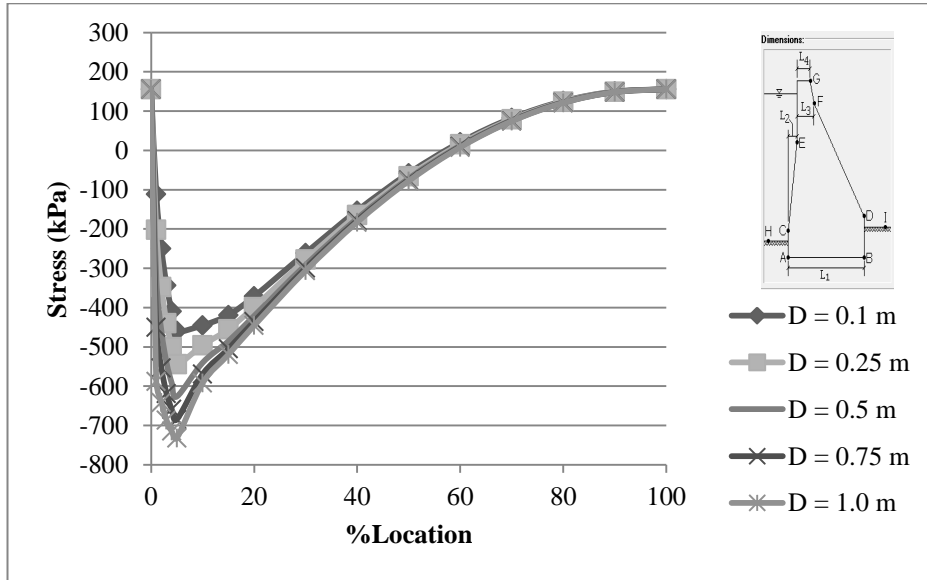


Figure 4-54 Stresses upstream, X variations, S = 5 m, all D

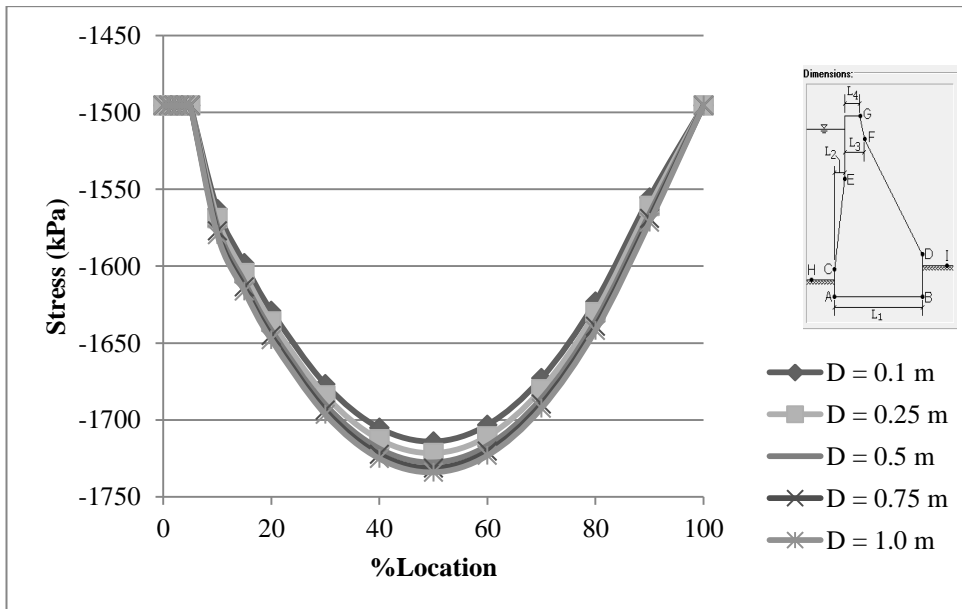


Figure 4-55 Stresses downstream, X variations, S = 5 m, all D

Again, the larger diameters generate more stresses both upstream and downstream due to reduced concrete area.

The internal stresses exhibit very similar results to those of the stresses upstream since the gallery is very close to the upstream face.

Figures 4-56 and 4-57 correspond to the stresses upstream and downstream, respectively, for H_4 variations, 0.25 m diameter, and all spacing case. Again, Figure 4-57 is similar to Figure 4-35 in the sense that the curves are stacked one on top of the other since the stresses downstream are not affected by drain spacing variation for various H_4 positions considered. Furthermore, Figures 4-58 and 4-59 correspond to the stresses upstream and downstream, respectively, for X variations, 0.25 m diameter, and all spacing.

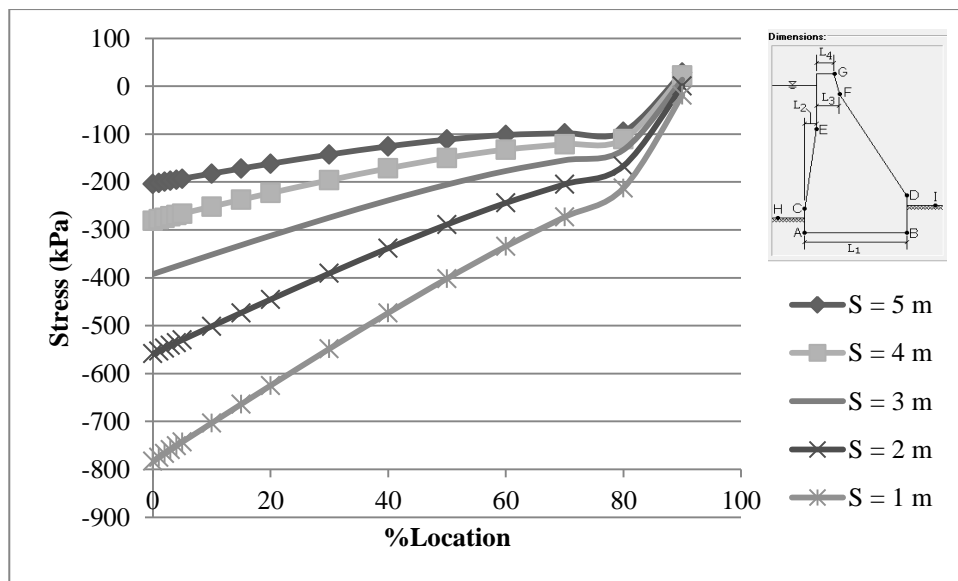


Figure 4-56 Stresses upstream, H_4 variations, $D = 0.25$ m, all S

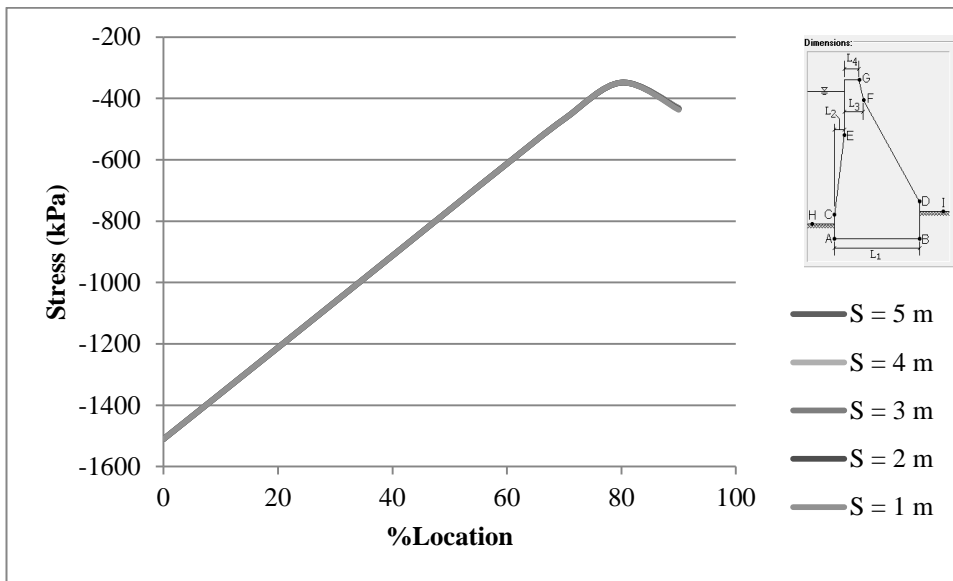


Figure 4-57 Stresses downstream, H_4 variations, $D = 0.25$ m, all S

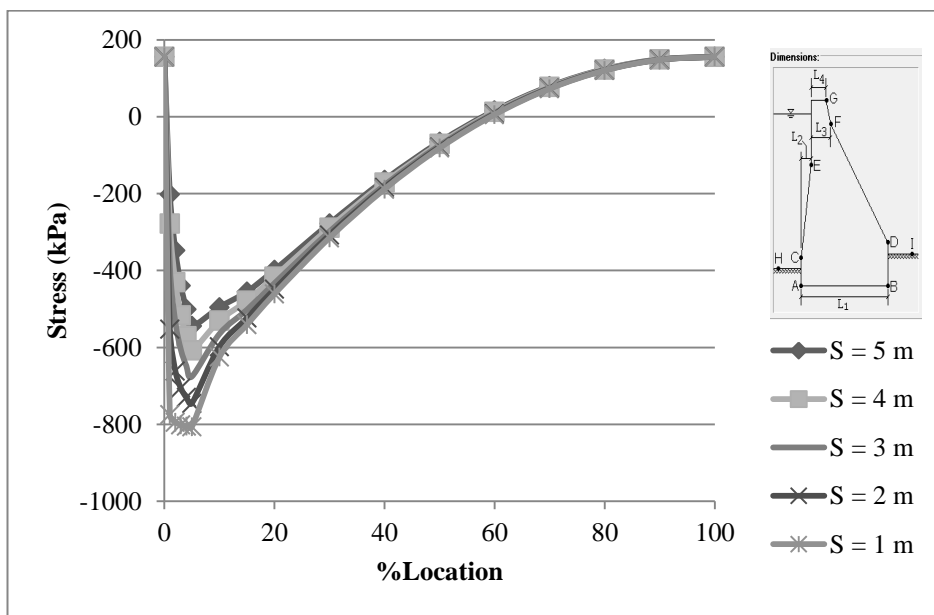


Figure 4-58 Stresses upstream, X variations, $D = 0.25$ m, all S

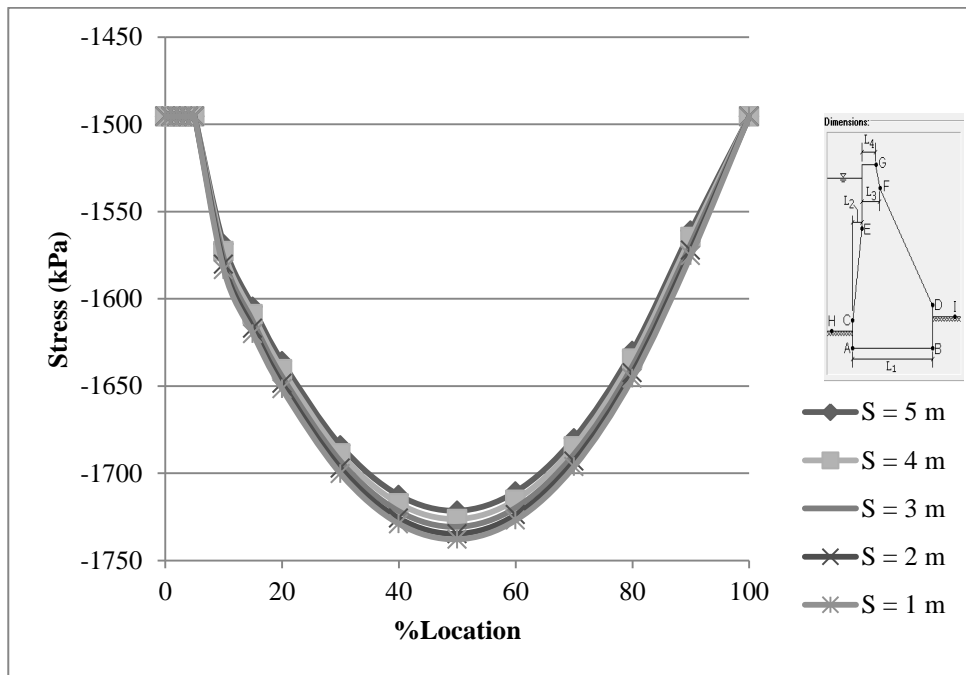


Figure 4-59 Stresses downstream, X variations, D = 0.25 m, all S

Both H_4 and X variations show that the stresses at both upstream and downstream increase as the spacing between the drains decrease, due to more drains per unit area decreasing the area of concrete. Comparing the stresses generated on the upstream and downstream sides for the usual loading combination for various drain diameter and spacing (Figures 4-30 through 4-37) with their counterparts for the unusual loading combination (Figures 4-52 through 4-59) provide similar conclusions i.e. larger diameter and smaller spacing generate more stresses. Moreover, the presence of cracks on the upstream side at the base level for the unusual loading case tends to relieve the stresses at the upstream side. Consequently, the figures representing the stresses on the upstream side for the unusual loading condition demonstrate lower stresses compared to their counterparts for the usual loading condition.

4.1.3.3 Extreme Loading Case

The uplift results are the same as those calculated for the usual loading case. Figure 4-60 shows the stress distribution at the upstream face for peak accelerations for H_4 variations. While Figure 4-61 shows the stress distribution at the upstream face for the sustained accelerations for X variations.

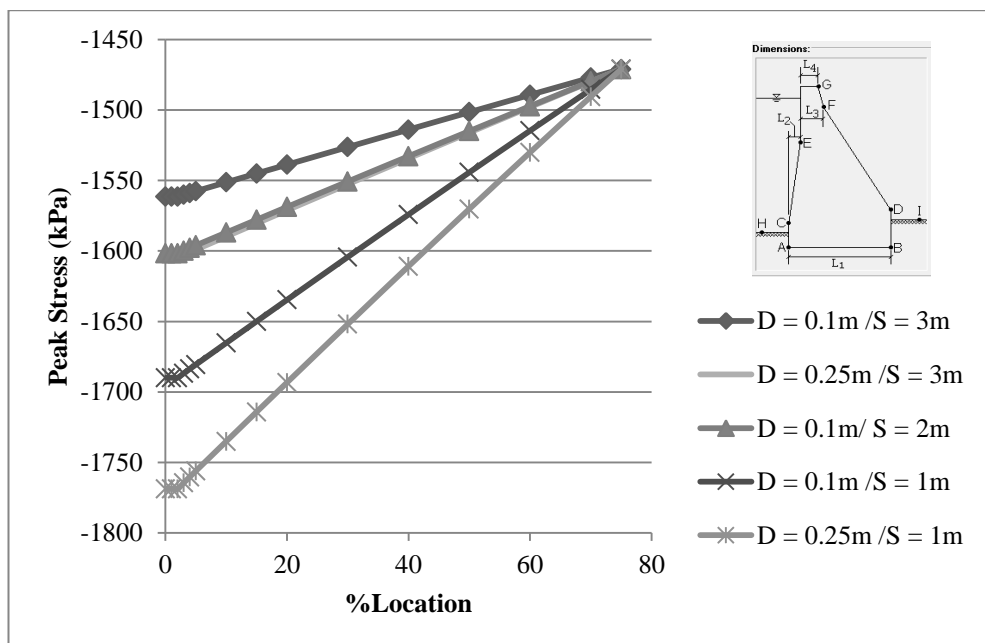


Figure 4-60 Peak stresses for H_4 variations

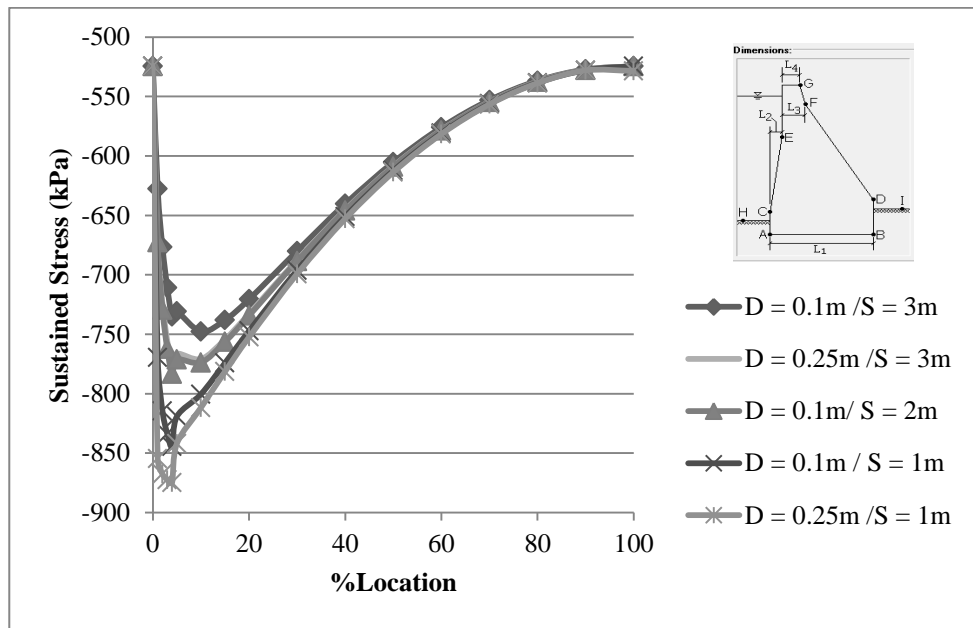


Figure 4-61 Sustained stresses for X variations

The stresses generated by the sustained accelerations are smaller than those generated by the peak accelerations. However, they follow the same pattern, meaning that the sustained stresses versus percent location resembles Figure 4-60 but with smaller stresses. The peak stresses versus percent location resembles Figure 4-61 but with larger stresses.

Similar to the previous results, higher stresses are generated for smaller spacing between the drains or larger drains, due to the presence of less solid material (concrete) to support the stress. Nonetheless, all stresses remain within the allowable compressive stress range. Figure 4-62 shows the crack generation recorded for each of those cases at the base level from the downstream face.

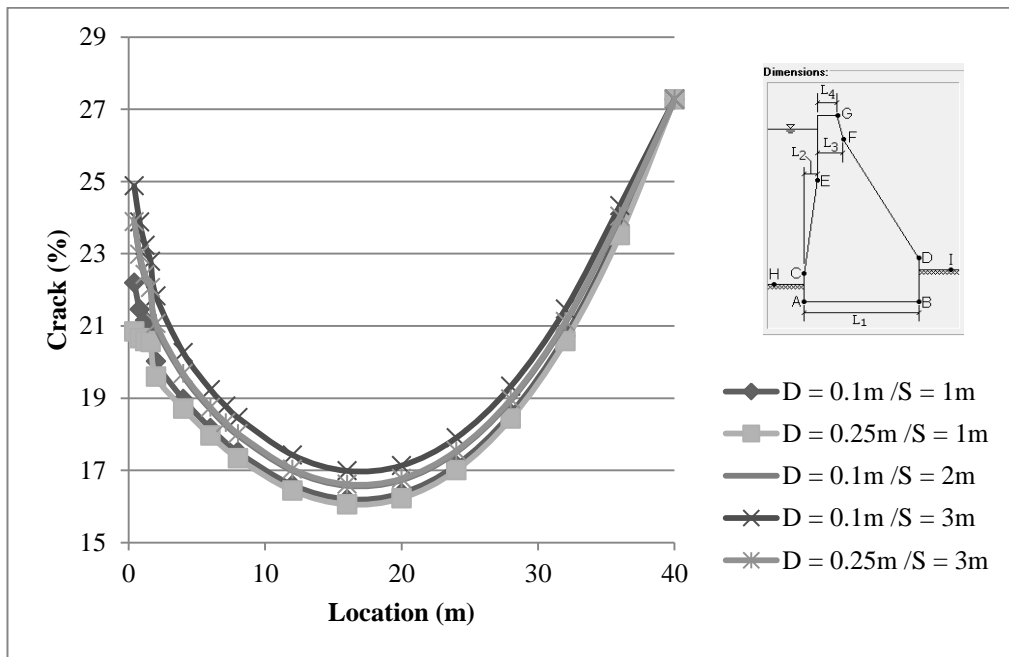


Figure 4-62 Crack length, extreme loading case

The crack length generated at the base decreases as the diameter increases and the spacing decreases. Maximum reduction in cracks occurs at a distance around 20% of the total base width from the upstream. However, at this level the uplift pressure will be much higher compared to a location closer to the upstream face. Thus, placing the drainage gallery at this location is not a feasible option. A location between maximum uplift reduction and maximum crack reduction could be selected as a compromise between both reduction factors.

4.1.3.4 Post Tension Cables

Figure 4-63 shows the amount of reduction of the crack generated at the downstream side due to earthquake load. These values are computed based on the reduction between the case without cables and each vertical position as stated earlier. The results show that the largest amount of reduction is achieved when the cables are closest to the downstream face (1 m vertical distance) and are vertically placed (90° angle).

It is also seen that the post tension cables are capable of reducing the crack generated at the downstream side by about 6% between the cases of no gallery and without cables (27.3% crack) and no gallery with cables (25.7% crack).

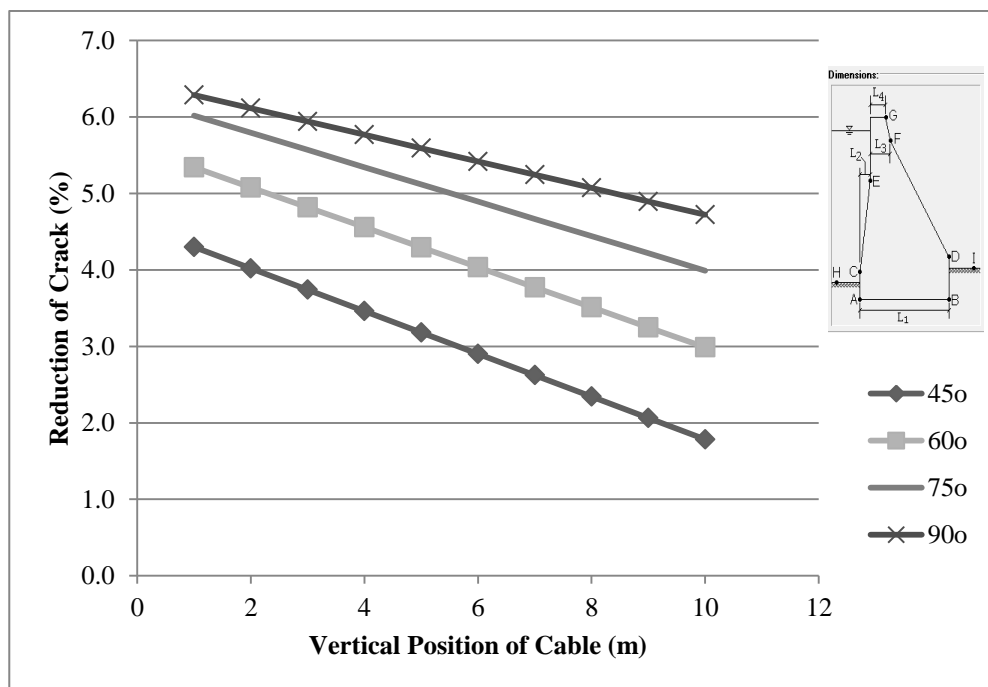


Figure 4-63 %Reduction of cracks vs vertical position of cables

4.2 The Analysis of Seepage Beneath the Dam

The dam used for the analysis (Dam 7) is shown in Figure 4-64.

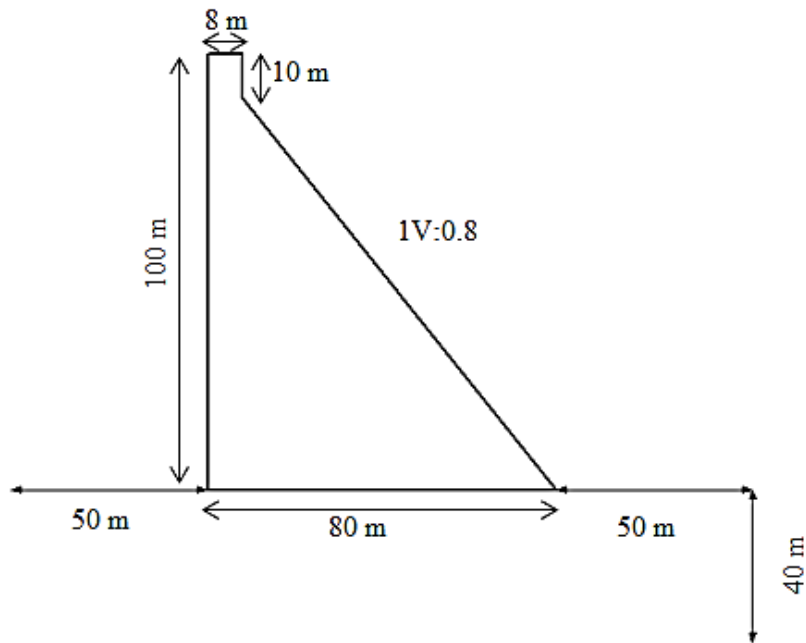


Figure 4-64 Cross sectional view of Dam 7

The material used for the foundation is fully saturated and has a hydraulic conductivity of 10^{-5} m/s and a saturated volumetric water content of $0.4 \text{ m}^3/\text{m}^3$ (Carsel and Parrish, 1988). To prevent seepage into the dam body, the edges of the dam in contact with the water or the foundation are defined as an interface layer.

The boundary conditions of the dam are as follows:

- Head (H): Water Level Upstream (115 m = 75 m from dam's heel).
- Total Flux (Q): Potential Seepage Face (Total Flux = $0 \text{ m}^3/\text{sec}$) defined at the downstream section.
- Pressure Head (P): Zero Pressure (Pressure = 0) at the gallery opening.

The points where the seepage rate and the pore water pressure were obtained are shown in Table 4-17.

Table 4-17 Location of points considered for the analysis

Name	% location with respect to base width	
Point 1	0	Below heel
Point 2	50	Center of dam
Point 3	100	Below toe
Point 4	G-0.125%	From left hand side end of the drain (0.1 m away)
Point 5	G+0.125%	From right hand side end the of drain (0.1 m away)

Points 1, 2, and 3 can be seen in Figure 4-66. Points 1, 4, and 5 are shown in Figure 4-67. The global mesh size was taken as 1 m to provide more accurate results. Figure 4-65 shows a comparison of the seepage rate readings measured at two locations showing variations for 1 m and 3 m mesh sizes. The results indicate that the 1 m mesh size provides consistent and less varied results. The governing equations are applied to each element in the analysis. Therefore, as the mesh size decreases and the number of elements increase, the equations will be applied to a larger number of nodes making the computed results closer to the true solution of the problem. The pore water pressure was measured 0.5 m below surface since closer locations may lead to an unstable solution due to the fact that the spacing becomes much smaller than the selected mesh size. Smaller mesh size could be selected but this will significantly increase the computation time with a minor impact on the accuracy of the results.

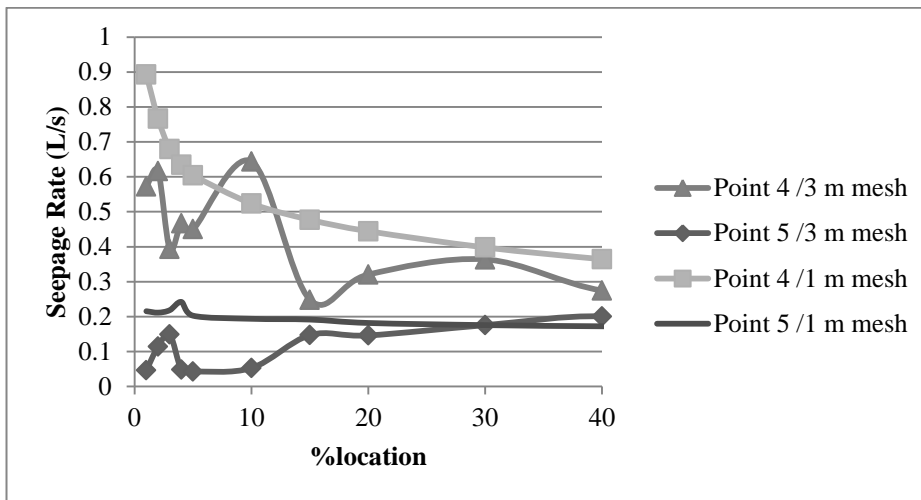


Figure 4-65 Comparison of 1 m and 3 m mesh size readings

The drain diameters considered are 0.2 m and 1 m as Case 1 and Case 2, respectively, to test the impact of the gallery's location at this step. Figure 4-66 shows the dam as defined on SEEP/W with all the materials and the boundary conditions and the flux sections. Figure 4-67 shows a closer look at the location of the gallery for Case 2.

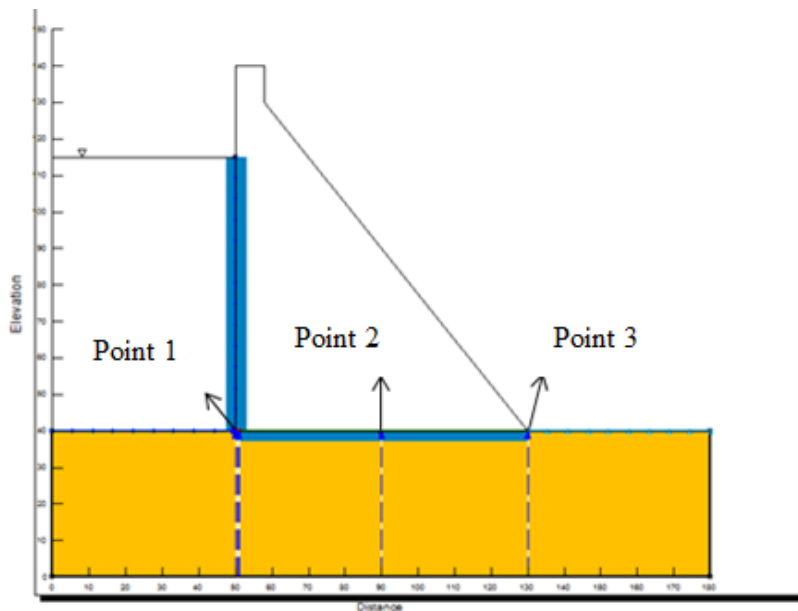


Figure 4-66 Definition of the Dam on SEEP/W

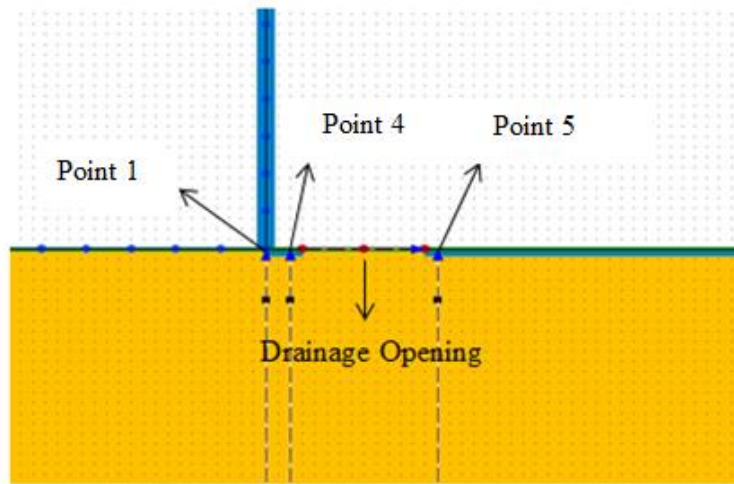


Figure 4-67 Drainage details for Case 2 on SEEP/W

4.2.1 Results and Discussion

Figures 4-68 and 4-69 show seepage analysis results for the case without drains and a 1 m diameter drain (Case 2) located at a distance of 1% of the base width away from the upstream face, respectively.

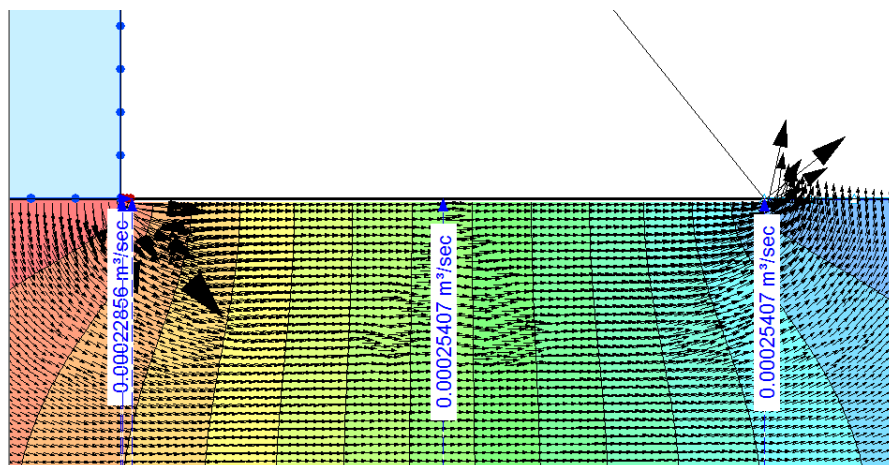


Figure 4-68 Seepage rates and the velocity field beneath the dam without drains

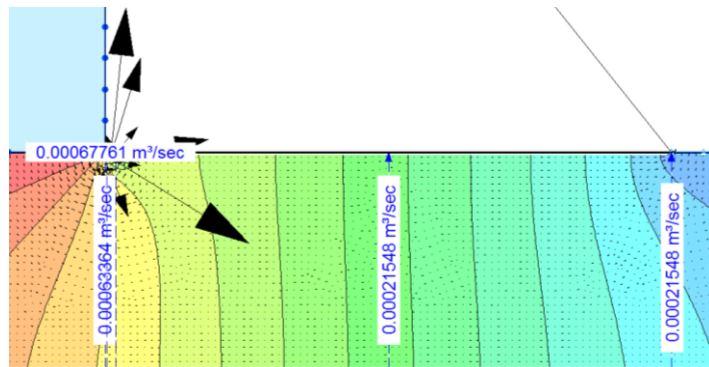


Figure 4-69 Seepage rates and the velocity field beneath the dam for Case 2

The location of the gallery horizontally is taken as those used previously in CADAM. The seepage rate and the pore water pressure calculated at each location are presented in Tables 4-18 and 4-19, respectively, for 1 m drain diameter, X variations.

Table 4-18 Seepage rate for Case 2

%Location (X)	Location (m)	At Gallery (G)	Seepage Rate (L/s)				
			Point 1	Point 4	Point 5	Point 2	Point 3
0	-		0.222			0.258	0.258
1	50.8	0.678	0.634	0.893	0.215	0.215	0.215
2	51.6	0.556	0.557	0.767	0.211	0.211	0.211
3	52.4	0.472	0.526	0.680	0.218	0.208	0.208
4	53.2	0.430	0.508	0.634	0.242	0.204	0.204
5	54	0.402	0.492	0.604	0.203	0.202	0.202
10	58	0.331	0.442	0.524	0.194	0.192	0.192
15	62	0.291	0.409	0.477	0.192	0.186	0.186
20	66	0.263	0.384	0.444	0.182	0.182	0.182
30	74	0.223	0.346	0.398	0.176	0.176	0.176
40	82	0.192	0.318	0.364	0.172	0.172	0.172
50	90	0.165	0.295	0.337	0.172	0.255	0.172
60	98	0.144	0.276	0.316	0.172	0.316	0.172
70	106	0.122	0.261	0.298	0.176	0.298	0.176
80	114	0.101	0.247	0.282	0.182	0.282	0.182
90	122	0.076	0.236	0.269	0.192	0.269	0.192

Table 4-19 Pore water pressure for Case 2

%location (X)	Location (m)	Pore Water Pressure (kPa)				
		Point 1	Point 4	Point 5	Point 2	Point 3
0	-	720.669			372.643	25.186
1	50.8	490.349	397.062	232.896	313.859	21.569
2	51.6	614.414	311.995	218.438	307.590	21.232
3	52.4	643.093	249.701	199.531	301.996	20.592
4	53.2	659.001	222.007	188.346	296.961	20.383
5	54	666.287	206.347	177.988	292.968	20.263
10	58	688.657	166.994	150.926	277.117	19.598
15	62	697.478	146.564	133.841	265.960	19.281
20	66	702.460	131.419	122.474	256.533	18.570
30	74	708.113	111.581	104.503	237.852	18.421
40	82	711.525	97.409	90.845	210.611	18.186
50	90	713.950	90.009	89.392	77.316	18.028
60	98	715.676	74.593	68.764	251.300	17.813
70	106	717.780	64.653	58.837	298.385	17.820
80	114	718.943	54.787	48.618	328.049	17.767
90	122	720.015	44.108	36.852	350.522	17.388

Figures 4-70 and 4-71 show the variation of seepage rate and pore water pressure with respect to the various horizontal positions of the gallery considered.

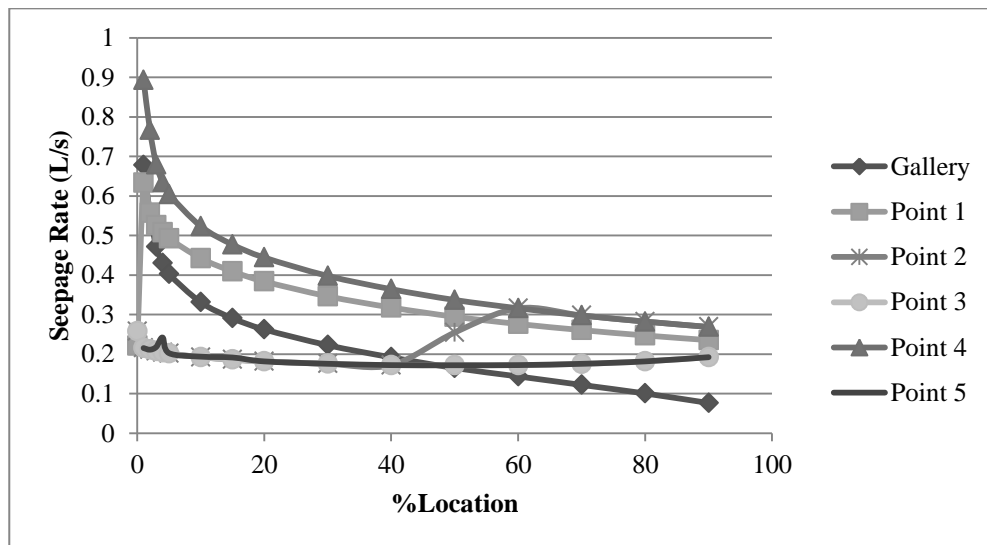


Figure 4-70 Seepage rate for X variations for Case 2

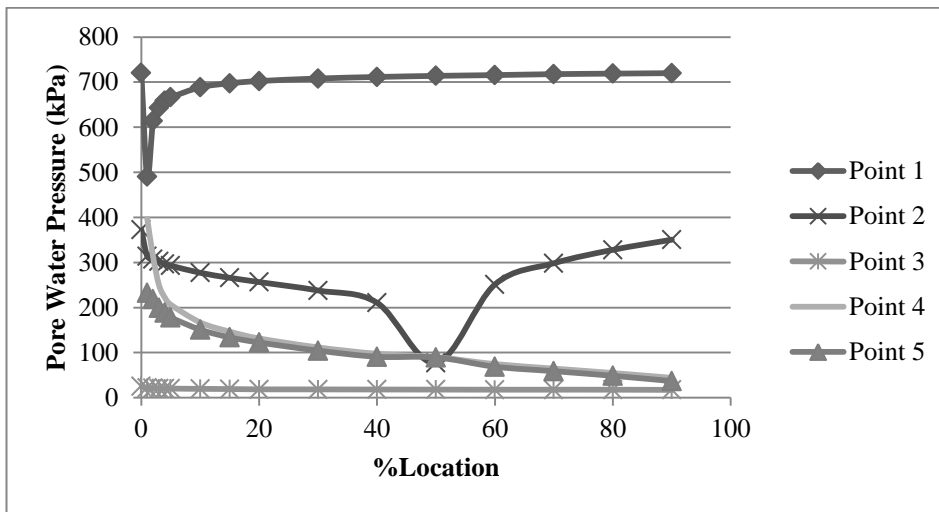


Figure 4-71 Pore water pressure for X variations for Case 2

Results show that seepage rate decreases as the gallery is moved downstream. The pore water pressure decreases as the gallery is moved downstream except at the 0% location (below the heel) where it increases. The introduction of the gallery (at 1% location) reduces the uplift pressure at Point 1 showing an increase in the seepage rate in Table 4-18 and Figure 4-70 and a decrease in the pore water pressure in Table 4-19 and Figure 4-71. However, as the gallery moves more towards the downstream side, its impact on reducing the pressure at Point 1 decreases. The jumps of Point 2 at 50% location are due to the presence of the gallery at that point leading to a pressure difference at that point allowing water to enter the gallery thus increasing the seepage rate and decreasing the pore water pressure at that particular point. Figures 4-72 and 4-73 show a closer look at the left section of Figure 4-70 and 4-71.

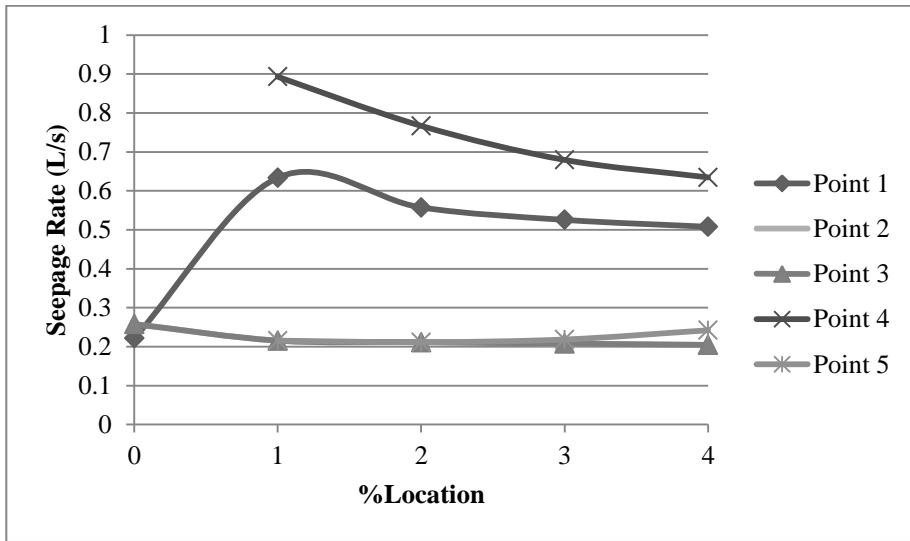


Figure 4-72 Seepage rate for X variations for Case 2 at 0-4%location

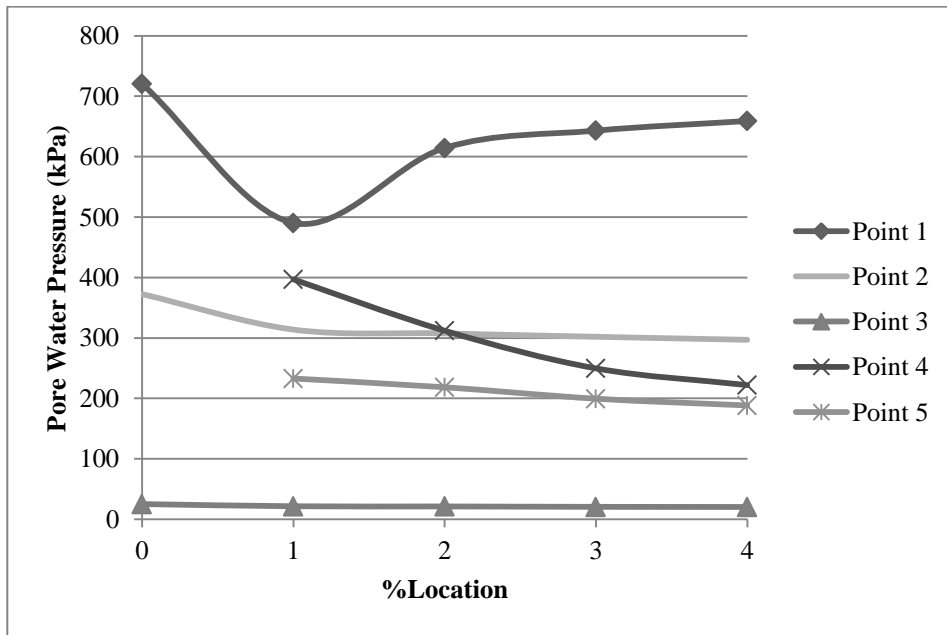


Figure 4-73 Pore water pressure for X variations for Case 2 at 0-4%location

These seepage rate graphs indicate that the maximum seepage rate occurs when the gallery is at a 1% location from the upstream. Due to continuity, the locations beyond the gallery i.e. Points 2, 3, and 5 have the same seepage rate,

until the gallery goes beyond Point 2. A closer look at Figure 4-73 shows that the lowest pore water pressure recorded at Point 1 occurs when the gallery is placed at a distance of 1% of the base width away from the upstream face.

Figure 4-74 is a comparison between the seepage rates for certain flux rate locations for Cases 1 and 2 for H_4 variations. Results show that varying the vertical position of the gallery has no effect on the seepage rate and the pore water pressure. Furthermore, the impact of the shape and size of the gallery within the dam did not lead to any variation in the seepage rate and the pore water pressure, only the opening through the foundation (drain diameter) had an impact on the results. Therefore, only the drain diameter is taken into consideration here.

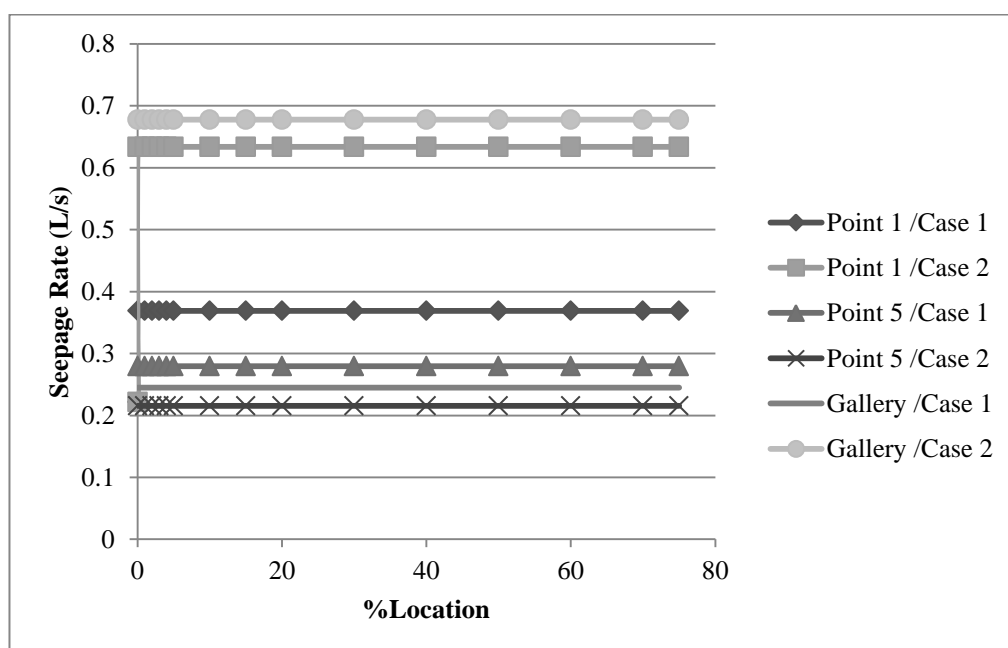


Figure 4-74 Seepage rate comparison for H_4 variations

The seepage rate at Point 1 and gallery location (G) flux rate for Case 2 are higher than those for Case 1. However, the seepage rates recorded at Point 5 for Case 1 are higher than those for Case 2 because the use of a smaller drain diameter allowed more water to seep to the downstream side.

Figures 4-75 and 4-76 show a similar comparison for Cases 1 and 2 for the seepage rate and pore water pressure for X variations, respectively. The conclusions that can be drawn from Figure 4-75 are the same as those drawn from Figure 4-74. The pore water pressure displays results opposite to those of the seepage rate. As expected, lower pressures are expected from larger diameter compared to smaller ones. The slight irregularity in the results of Case 1 could be due the mesh size being taken as 1 m in the simulations.

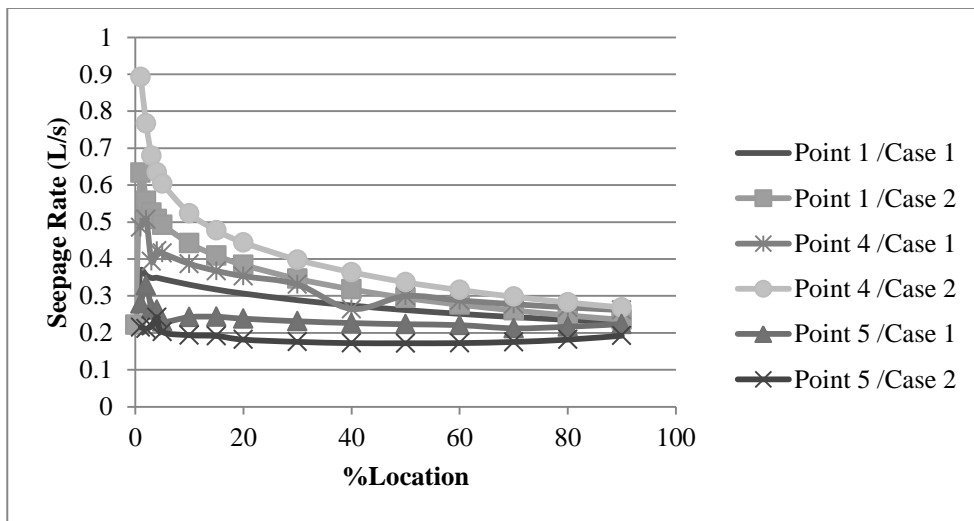


Figure 4-75 Seepage rate comparison for X variations

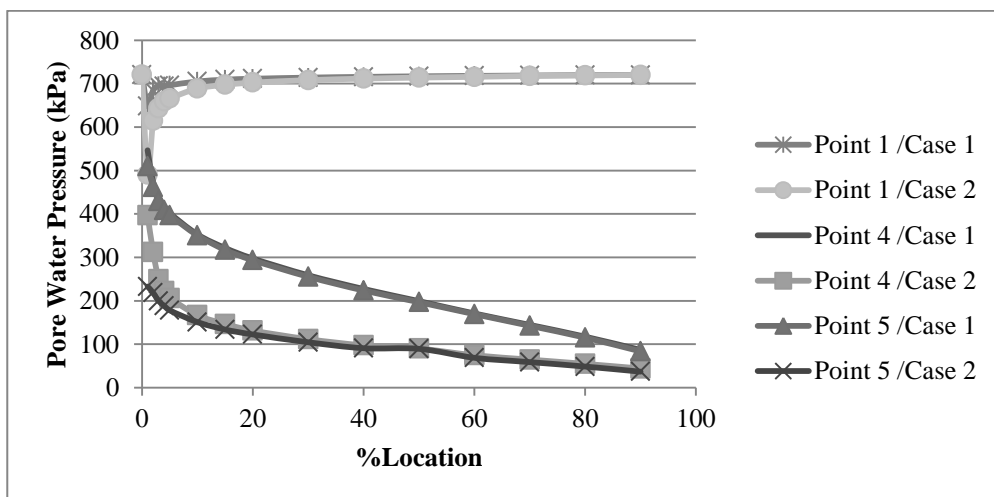


Figure 4-76 Pore water pressure for X variations

4.2.2 Sensitivity Analysis

The seepage rate through the upstream face is required in the computational part of the case study (Chapter 5). However, only a seepage rate for a case with a different hydraulic conductivity was found. Therefore, the impact of the hydraulic conductivity on seepage rate is needed to establish a relation between the available seepage rate and the case study to provide an estimation within a reasonable range of the desired seepage rate through the upstream face for the case study. Figure 4-77 shows a comparison between the seepage rate calculated at 0% and at the gallery locations for three different hydraulic conductivity values. On the left is the hydraulic conductivity used for the analysis $K = 10^{-5}$ m/s (Case 1) and in the middle is $K = 10^{-4}$ m/s (Case 2) and on the right is $K = 2 \times 10^{-6}$ m/s (Case 3). Comparing Cases 1 and 2, the seepage rates increased by a factor of 10 as the hydraulic conductivity was increased by a factor of 10. The same relation can be seen between Cases 1 and 3 for the same changes in the hydraulic conductivity rate. Nonetheless, the pore water pressure at all points did not change between any of the cases. Although the seepage rate is usually calculated using partial differential equations, and there is no direct relationship between the hydraulic conductivity value and the seepage rate. Based on these results a relationship might be assumed as long as the necessary modifications are made to the assumption as applied in the case study (Chapter 5).

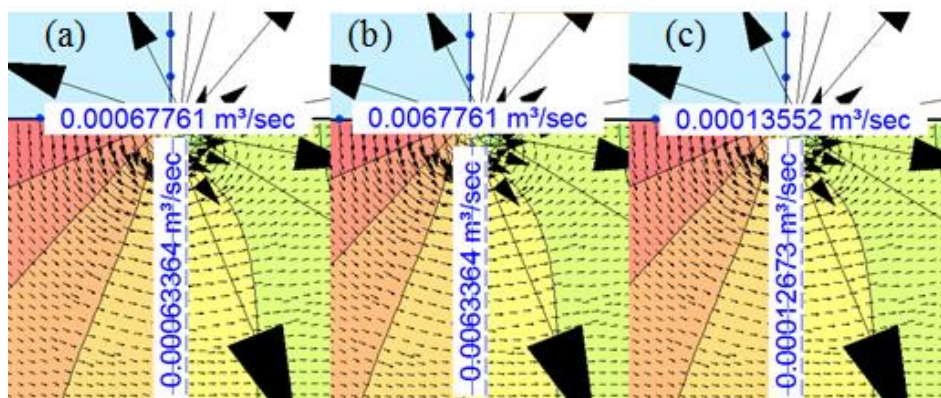


Figure 4-77 Seepage rates of (a) Case 1; (b) Case 2; (c) Case 3

CHAPTER 5

CASE STUDY

5.1 Introduction

Porsuk Dam, a concrete gravity dam type, is used as the case study in this model. It is located 25 km southwest of Eskişehir (Turkey), and on the Porsuk Stream, a tributary of Sakarya River (see Figure 5-1). The construction was conducted by the General Directorate of State Hydraulics Works (DSİ) between 1966 and 1972. The main purposes of the dam are flood control, irrigation, and industrial water supply. The geographic location of the dam is shown in Figure 5-2 and Table 5-1 presents some general information about the dam.



Figure 5-1 Porsuk Dam (DSI, 2012)



Figure 5-2 Porsuk Dam map (Courtesy of Google Maps)

Table 5-1 Porsuk Dam general information (DSİ) and (“Porsuk Dam (Eskisehir, 1972) | Structurae,” n.d.)

Height	49.7 m
Body Volume	224 dam ³
Retained Water Volume	431 hm ³
Water Surface Area	23 km ²
Irrigation Area	41 020 ha
Annual Drinking Water Supplied	31.54 hm ³ /year

5.2 The input Data and the computer model

The input data used to create Porsuk Dam on CADAM and SEEP/W are presented in this section.

Table 5-2 presents the detailed information and the input data required for the modeling of the dam.

Table 5-2 Porsuk Dam data Beşer, M. R. (2005)

Dam Height	49.70 m
Elevation	844.65 m
Crest Elevation	894.35 m
Crest Thickness (t_c)	4.50 m
H*	8.64 m (estimated)
Bottom Width (B)	39.4 m
Upstream Face Slope, m	0
Downstream Face Slope, n	0.85
Normal Reservoir Water Depth	45.60 m
Maximum Reservoir Water Depth	48.20 m
Tail Water Depth	6 m
Geological Composition of Foundation	Peridotite
Hydraulic Conductivity of Peridotite	$3-6 \times 10^{-7}$ m/s
Specific Weight of Concrete	24 kN/m^3
Effective Unit Weight of Silt Deposit	11 kN/m^3
Height of Silt Deposit	3 m
Internal Friction Angle	31°
Ice Thickness	0.52 m
Ice Load / Unit Length	100 kN/m
Compressive Strength of Concrete	30 000 kPa
Tensile Strength of Concrete	3 000 kPa
Internal Friction Angle	55° (peak), 45° (residual)
Cohesion of lift joint	931 kPa
Allowable Compressive Stress in Concrete	3750 kN/m^2
Allowable Compressive Stress at Foundation	4000 kN/m^2
Allowable Shear Stress at Foundation	1500 kN/m^2
Horizontal Peak Ground Acceleration	0.30g
Vertical Peak Ground Acceleration	0.20g

Based on the data presented in Beşer, M. R. (2005), Porsuk Dam is located in the second seismic zone of Turkey. The Vertical Peak Ground Acceleration was calculated with respect to the determined Horizontal Peak Ground Acceleration based on the Newmark relation. According to the relation, the Vertical to Horizontal Peak Ground Acceleration ratio is 2/3.

Figures 5-3 and 5-4 present the cross sectional view of the dam, and were used to estimate the values presented in Table 5-3.

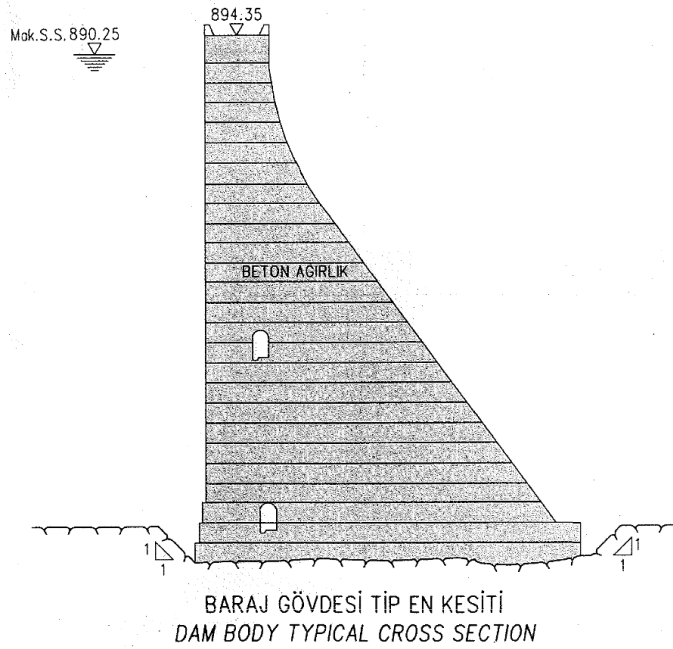


Figure 5-3 Porsuk Dam cross section (DSI)

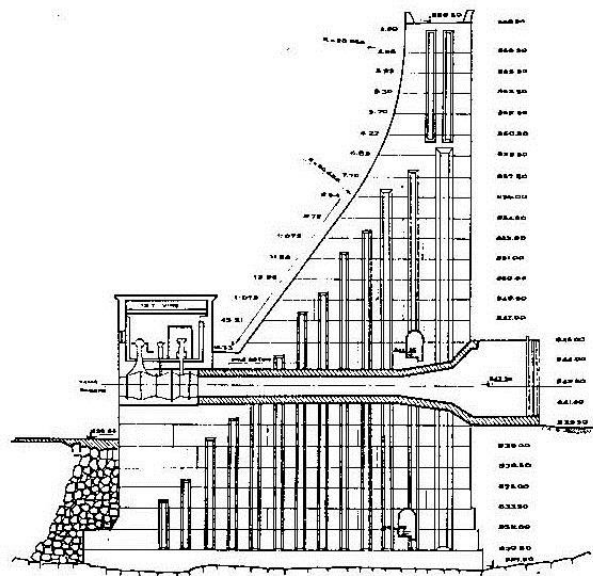


Figure 5-4 Porsuk Dam cross section (Ural and Ungan 1967)

Table 5-3 Porsuk Dam estimated data

Outlet Elevation	16.194 m
Foundation Gallery Elevation (H_4)	3.068 m
Foundation Gallery distance from heel (X)	7.012 m
Drain Diameter	0.12 m (Ural and Ungan 1967)
Drain Spacing (c/c)	2 m (Ural and Ungan 1967)

Figures 5-5 and 5-6 show the CADAM and SEEP/W models, respectively, for the aforementioned data. Figure 5-7 shows seepage passing under the dam, and Figure 5-8 gives a closer look at the flux rate calculated at the gallery.

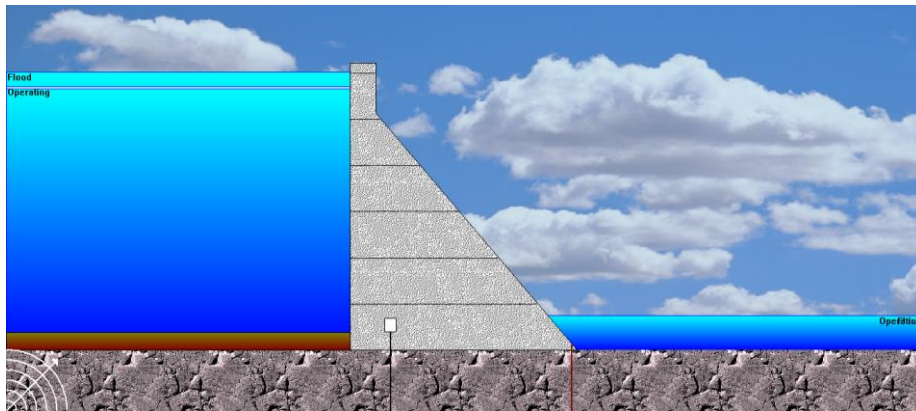


Figure 5-5 Porsuk Dam on CADAM

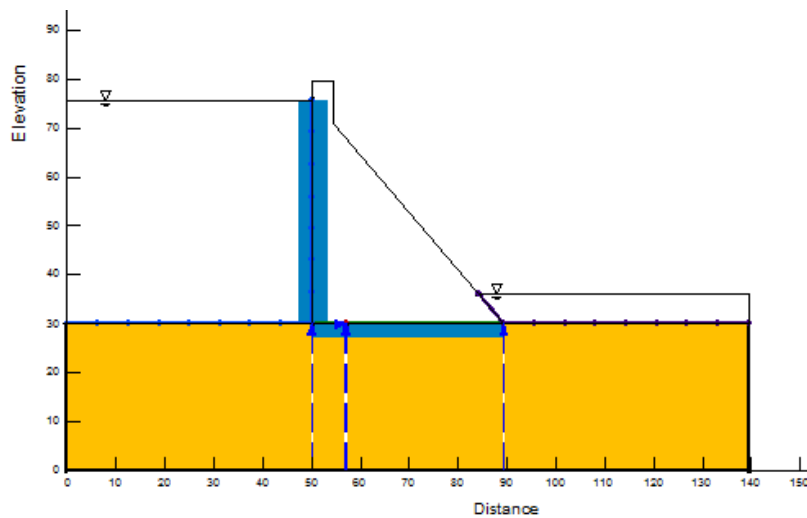


Figure 5-6 Porsuk Dam on SEEP/W

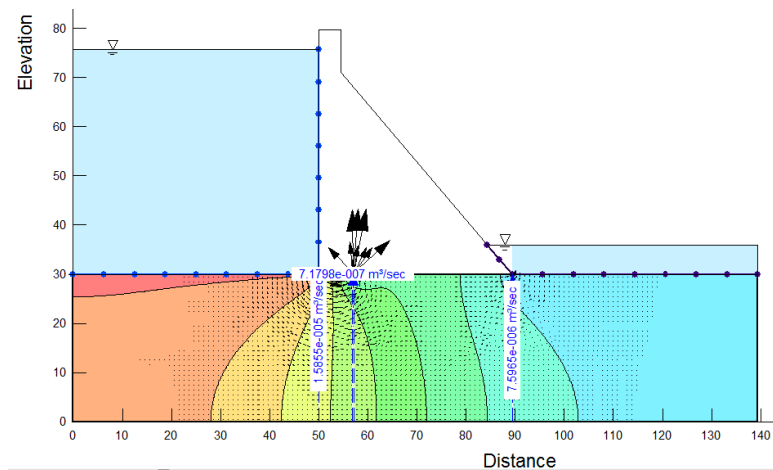


Figure 5-7 Seepage beneath Porsuk Dam

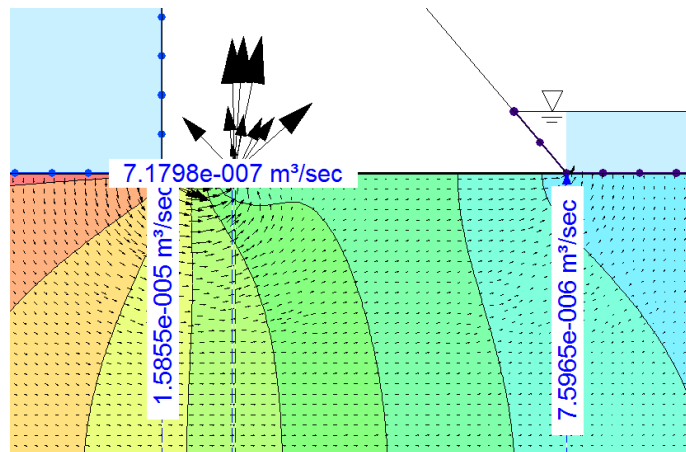


Figure 5-8 The seepage rates passing beneath, and through the drainage gallery of Porsuk Dam

5.3 The Location of the Drainage Gallery

Table 5-4 shows the comparison of six different scenarios, the horizontal position where the drainage gallery is located in Porsuk dam as mentioned earlier is 7.012 m from the upstream face (17.8%). The location suggested in this study based on the average location of maximum reduction of uplift for the given diameter and spacing of the drains is 3.94 m from the upstream face (10%) and the same location with added post-tension cables (indicated by asterisk) is also shown.

Table 5-4 Comparison between different X locations

%location	X	Uplift (kN/m)	Uplift Reduction (%)	Flood Uplift (kN/m)	Uplift Reduction (%)	Crack (%)	Crack Reduction (%)
17.80	7.012	4211.45		4335.69		-5.077	
10	3.94	3980.99	5.47	4090.11	5.66	-6.896	-35.83
10	3.94*	3980.99	5.47	4090.11	5.66	-5.529	-8.90
12.69	5*	4014.5	4.68	4125.82	4.84	-4.852	4.43
11.93	4.7*	3997.92	5.07	4108.15	5.25	-5.038	0.77
11.8	4.65*	3995.63	5.12	4105.7	5.30	-5.069	0.16
Factor of Safety (SSF Peak)	Stress (U/S) (Normal) (kPa)	Stress (D/S) (Normal) (kPa)	Stress (U/S) (Flood) (kPa)	Stress (D/S) (Flood) (kPa)	Stress Earthquake (Peak) (kPa)	Stress (U/S) (Residual) (kPa)	Stress (D/S) (Residual) (kPa)
2.544	-320.427	-596.983	-219.778	-691.325	-1205.469	-320.427	-596.983
2.576	-353.755	-575.353	-255.294	-668.275	-1241.596	-353.755	-575.353
2.598	-346.329	-590.719	-247.868	-683.642	-1232.031	-346.329	-590.719
2.594	-336.662	-598.685	-237.566	-692.130	-1221.473	-336.662	-598.685
2.596	-339.706	-596.483	-240.81	-689.784	-1224.75	-339.706	-596.483
2.596	-340.193	-596.112	-241.33	-689.388	-1225.277	-340.193	-596.112

The other three locations (further downstream) were considered to see at what point a compromise between the maximum uplift reduction and crack reduction could be achieved. Placing the gallery at a distance of 4.65 m away from the upstream face (11.8%) provides maximum uplift reduction while maintaining a positive crack reduction (lower than the original location) on the downstream side due to post-tension cables. Therefore, the optimal location depends on what is seen as more important: uplift reduction, or crack reduction, or a compromise between both.

The vertical position of the gallery was not considered since the original location (3.068 m) is below the downstream water level (6 m) and any variation in the vertical location as long as the gallery remains below the downstream water level will not lead to any change in the uplift, crack propagation, stresses, etc. Furthermore, any elevation above the downstream water level will lead to an increase in uplift and crack propagation, and should therefore be avoided.

5.4 Water Collection and Removal through Pumping

The water entering the drainage gallery from the foundation due to uplift will flow through the side channel of the drainage gallery until it is collected in a well called a sump. Furthermore, water seeping through the cracks in the concrete on the upstream face will also be collected in vertical drains inside the dam and will be transported to the drains.

The water collected in the sump well will then be pumped out of the dam. A common method is to pump the water to an elevation that is higher than the dam's outlet, thus allowing gravity to transport the water out of the dam through the outlet. Figure 5-9 shows the location and details of a typical sump well in a gravity dam.

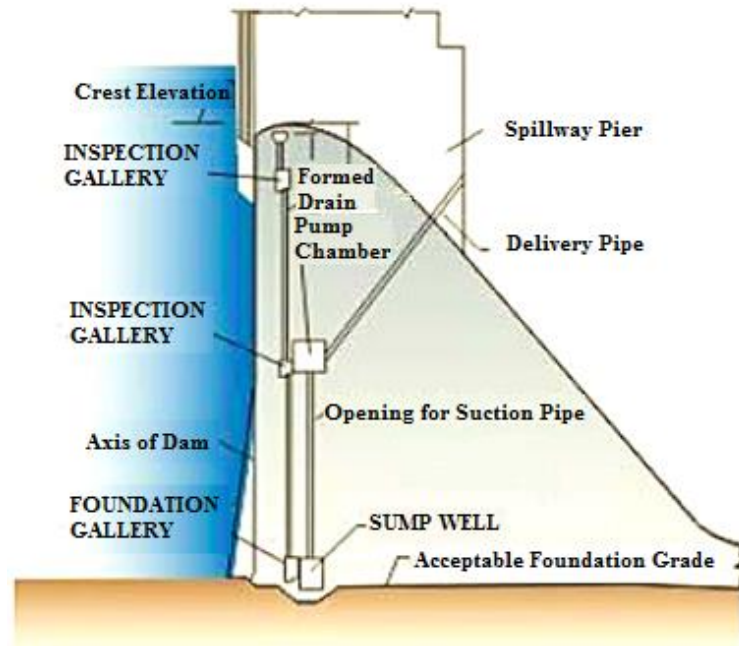


Figure 5-9 Sump well details (Kharagpur, 2012)

5.5 Pumping Schedule

In the scope of the study, a similar pump application is considered for Porsuk Dam. Some assumptions were made prior to the computation step. These are provided below:

- The very low hydraulic conductivity of the foundation material (6×10^{-7} m/s) taken from Priscu et al. (1998) results in a very low seepage rate (7.1798×10^{-7} m³/s) as can be seen in Figure 5-8. Therefore, a more reasonable seepage rate had to be estimated from the literature to account for seepage from under the dam and leakage through the upstream face and abutments. According to Scuero et al. (2015) the average seepage rate for the drainage system is around 2 l/s. However, this is the leakage through Geo-Membrane, an insulating material covering the upstream face to reduce leakage. Since Porsuk Dam does not have such a protective material, the average seepage rate had to be adjusted.

Weber and Zornberg (2007) state that the hydraulic conductivity of geo-membrane is around 10^{-15} m/s, while the hydraulic conductivity of concrete is 1.5×10^{-12} m/s (Zee et al., 2011). Based on the SEEP/W results, it is plausible to assume that there is a relation between the hydraulic conductivity and seepage rate for the sole purpose of adjusting the seepage rate to a reasonable value. By removing the geo-membrane and leaving plain concrete, the hydraulic conductivity would increase by 1500. The leakage rate is assumed to increase by the same amount (1500 m^3/s) i.e. 1.5 l/s added to the current leakage rate of 2 l/s leading to 3.5 l/s. A more conservative value of 4 l/s was taken as the leakage rate to account for further leakage and to create a safer design and to account for the fact that there is no actual relation between the hydraulic conductivity and the seepage rate.

- 3 m x 3 m x 2.5 m was taken as the size of the sump well. The top elevation of the well was placed at the same level as the bottom elevation of the drainage gallery to facilitate seepage from the gallery into the well and to prevent flooding of the gallery in case the well is full. The size of the sump well and the corresponding computations were based on Chauhan et al. (2008).
- The horizontal location of the gallery and the sump well were not considered in the calculations since the obtained seepage rates are very small and would not contribute significantly to the 4 l/s rate considered.
- The lowest vertical position of the gallery was taken as 4 m to leave 1.5 m thick layer of concrete between the bottom of the sump well and the foundation. CADAM results show that as long as the gallery is located below or at the level of the downstream water level, the uplift pressure and the downstream crack propagation will not change regardless of the

position. Thus, the alternate elevation of the gallery is taken as 6 m (downstream water level elevation). No higher elevations were considered since they would lead to more uplift pressure and higher crack propagation.

- Using online shopping sites, such as Amazon, the cost of pumps for various horse powers were estimated and are presented in Table 5-5.
- Pump efficiency is taken as 80%.
- The water will be pumped to an elevation that is higher than the outlet elevation (16.194 m) to allow gravity to transport the water out of the dam.
- The unit cost was estimated at 25.2 kurus/kWh Turkish Statistical Institute (2017). An exchange rate of 1 \$ = 3.53 TL (July 2017) was used to convert the unit cost to cent/kWh.

Table 5-5 Pump cost

HP	\$	Watt	\$/kW
1	49.99	0.7457	67.038
1.5	77.99	1.1186	69.724
2	169.99	1.4914	113.980
2.4	300.28	1.7897	167.784
3	399.99	2.237	178.798
3.5	525.42	2.6099	201.314
4	573.57	2.9828	192.293
5	669.93	3.7285	179.678
5.5	914.15	4.1014	222.890

The following Equations (5.1) through (5.8) were used for the computations of the terms shown in Table 5-6 for a gallery located at a vertical position of 4 m.

$$\text{Inflow Volume} = 4 \times 10^{-3} \times 24 \times 60 \times 60 = 345.6 \frac{\text{m}^3}{\text{day}} = 0.24 \frac{\text{m}^3}{\text{min}} \quad (5.1)$$

$$\text{Volume of sump well} = 3 \times 3 \times 2.5 = 22.5 \text{ m}^3 \quad (5.2)$$

Time to fully fill the well

$$\frac{x}{1440} \times 345.6 = 22.5 \rightarrow x = 93.75 \text{ min} \quad (5.3)$$

$$\text{Power} = \frac{\gamma Q H_p}{\mu} \quad (5.4)$$

where H_p is the head consisting of the height the water has to be pumped to (Pump H₄-Sump Well H₄) and the head losses.

Head losses are estimated using Darcy Welsbach equation

$$h_f = f \frac{L V^2}{D 2g} = \frac{8fLQ^2}{g\pi^2 D^5} \quad (5.5)$$

where

$f = 0.02$ (average value of the friction factor)

$L = \text{Pump H}_4 - \text{Sump Well H}_4$

$D =$ the same diameter as the pipes used to transport the water leaking through the upstream to the gallery, taken as 0.2 m (Kharagpur, 2012).

$$\text{Duration of pumping} = \frac{22.5 \text{ m}^3 (\text{Volume of sump well})}{Q - 0.24 \text{ m}^3 (\text{inflow rate/min})} \quad (5.6)$$

$$\text{Cost} = \text{Power} \times \text{unit cost} \times \frac{\text{duration of pumping}}{60} \quad (5.7)$$

$$\text{Annual Cost} = (\text{Daily cost} \times 365) + (\text{CRF} \times \text{Cost of Pump}) \quad (5.8)$$

where

CRF (Capital Recovery Factor) is taken as 0.1 based on Yanmaz (2013).

The Daily cost is estimated by multiplying the cost of each pumping session by the number of pumping sessions in a day (emptying time). The number of sessions (operations) is calculated by assuming that the sump well is filled completely and then emptied at the specified rate. This is repeated until 24 hours are achieved as shown in Table 5-7. The numbers below filling and emptying time indicate the number of operations in a day.

Table 5-6 Pump calculations

				efficiency	0.8		
Gallery X	3.94	m	γ	9.81	kN/m^3		
Gallery H ₄	4	m	cost	7.1388	cent/kwh		
Sump X	4.94	m	Outlet H ₄	16.194	m		
Sump H ₄	1.5	m	CRF	0.1			
Pump X	4.94	m					

Pump H ₄	Q (m ³ /s)	Head Loss	Power (kW)	Power (hp)	Cost (\$)	Daily Cost (\$)	Annual Cost (\$)	Q
16.5	0.00833	0.0054	1.5334	2.0563	0.158	1.105	433.412	0.5 Duration 86.538 min
17		0.0056	1.5845	2.1248	0.163	1.142	446.858	
17.5		0.0057	1.6356	2.1934	0.168	1.179	460.304	
18		0.0059	1.6867	2.619	0.174	1.216	473.751	
18.5		0.0061	1.7378	2.3304	0.179	1.253	487.197	
19		0.0063	1.7889	2.3990	0.184	1.289	510.614	
16.5	0.00667	0.0034	1.2265	1.6448	0.205	1.231	466.426	Q 0.4 m ³ /min
17		0.0036	1.2674	1.6996	0.212	1.272	481.407	Duration 140.625 min
17.5		0.0037	1.3083	1.7545	0.219	1.313	496.388	
18		0.0038	1.3492	1.8093	0.226	1.354	511.369	
18.5		0.0039	1.3901	1.8641	0.233	1.395	526.350	
19		0.0040	1.4310	1.9189	0.239	1.437	541.331	
16.5	0.0050	0.0019	0.9198	1.2335	0.410	1.231	457.181	Q 0.3 m ³ /min
17		0.0020	0.9505	1.2746	0.424	1.272	472.160	Duration 375 min
17.5		0.0021	0.9811	1.3157	0.438	1.313	487.140	
18		0.0021	1.0118	1.3568	0.451	1.354	502.119	
18.5		0.0022	1.0424	1.3979	0.465	1.395	517.099	
19		0.0023	1.0731	1.4391	0.479	1.436	532.078	

Table 5-7 Pumping sessions in a day

	Discharge rate	0.5 m ³ /min	Total duration for all sessions (hr)
	Pumping duration	86.538 min	
Operation	Filling	Emptying	
Number of operations in a day	8	7	
Total duration (min)	750	605.77	22.60

	Discharge rate	0.4 m ³ /min	Total duration for all sessions (hr)
	Pumping duration	140.625 min	
Operation	Filling	Emptying	
Number of operations in a day	6	6	
Total duration (min)	562.5	843.75	23.44

	Discharge rate	0.3 m ³ /min	Total duration for all sessions (hr)
	Pumping duration	375 min	
Operation	Filling	Emptying	
Number of operations in a day	3	3	
Total duration (min)	281.25	1125	23.44

Figures 5-10 and 5-11 show the daily cost and annual cost versus pump head for each pump rate case, respectively.

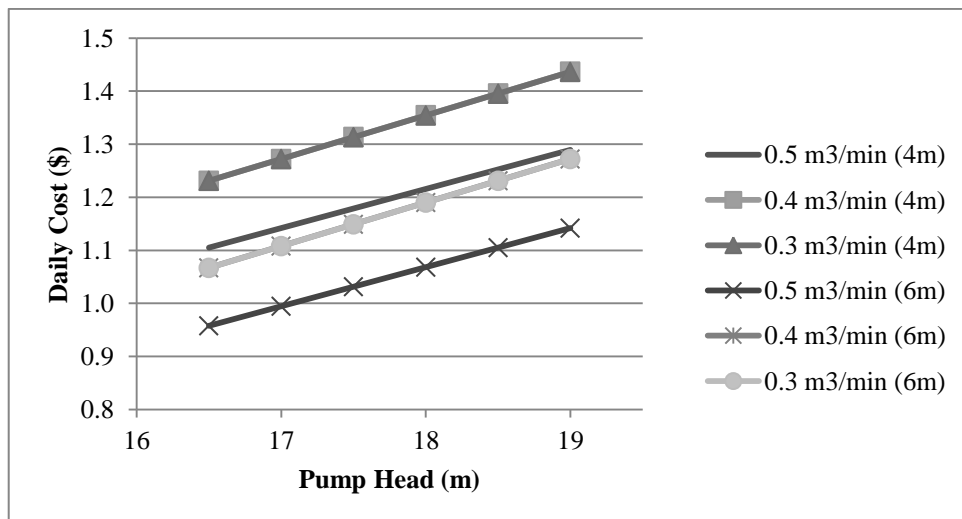


Figure 5-10 Daily cost for each pumping rate

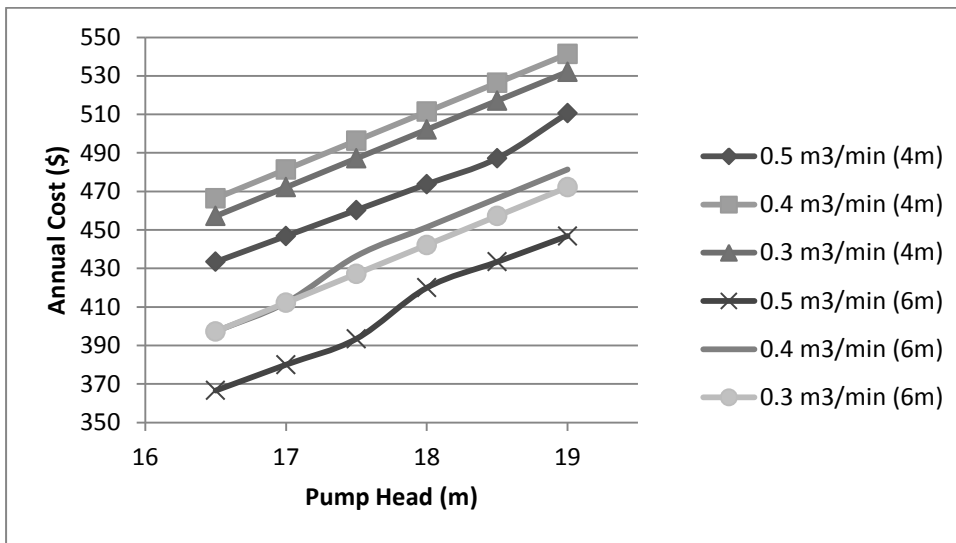


Figure 5-11 Annual cost for each pumping rate

Even though pumping at a higher discharge rate needs a more expensive, more powerful pump, it costs less on a daily run bases, since the duration of pumping decreases. While, pumping at a rate of 0.3 m³/min costs more per operation, the daily cost between 0.3 m³/min and 0.4 m³/min is identical for both elevations, since less pumping operations occur for the 0.3 m³/min discharge rate. However, when the price of the pump is included, the optimum pumping rate changes, the cheapest option becomes a variable depending on the required pump head.

Again, in the annual cost case for all pump head cases, the cheapest option is to pump water from the highest gallery elevation (6 m) at the highest rate (0.5 m³/min). There is a small intersection between the 0.3 m³/min and 0.4 m³/min discharge rates at the first few points for the 6 m elevation, indicating that either discharge rate could be used for these pumping elevations.

If more accurate pump costs were obtained, the gap between the potential cases might decrease, leading to a case where multiple options could lead to the optimal pump rate. Overall, placing the gallery (and the sump well) at a higher elevation decreases the pump head leading to lower power consumption and thus lower cost overall.

CHAPTER 6

CONCLUSIONS

In this study, the impact of the location of the gallery within the dam (both horizontally and vertically) on uplift pressure development, stresses within the dam, and crack generation and propagation was studied. The impact of the properties of the drainage system, such as drain diameter and spacing and location, and the impact of the dam geometry on the drainage system effectiveness were also considered. While previous studies considered the impacts of these variables for normal loading conditions, in this study these various scenarios and combinations were tested for usual, unusual, and extreme loading conditions, providing a more comprehensive investigation of the effects of these variables on the effectiveness of the drainage system. The investigations were conducted using two programs: CADAM and SEEP/W providing quick and accurate results. The conclusions based on these investigations were implemented on a case study to compare the actual drainage system in the dam and that proposed based on the results to find the optimum location for the drainage gallery such that minimum uplift pressure is achieved. Finally, various pumping options were considered to pump the water accumulated in the sump well out of the dam at the optimal pumping rate.

The main results and findings of this study are as follows:

- The presence of a gallery can reduce the uplift by over 60%, increasing the safety and the stability of the dam.

- The uplift pressure applied increases as the height of the dam and the base width of the dam increase due to the dam's ability to retain more water.
- The lowest uplift pressure is generated when the gallery is placed vertically close to the foundation. According to the construction manuals provided in the literature review section, there should be a minimum distance of 1.5 m clearance between the floor of the gallery and the foundation level.
- The uplift pressure, crack propagation, and stress developed will remain the same for any vertical position as long as the bottom elevation of the gallery (H_4) remains below or on the same level as the downstream water level.
- The position where the lowest uplift pressure is generated shifts more towards the upstream face as the height of the dam increases.
- The position where the lowest uplift pressure is generated shifts more towards the upstream face as the diameter of the drains increases and/or the spacing between the drain centerlines decreases.
- Larger drain diameters and smaller spacing between drain centerlines increase stresses, since more hollow spaces will reduce the effective area of concrete.
- Some combinations (small spacing and large diameters) lead to undesired and uneconomical results and should be avoided.
- The findings of the unusual loading combination follow the same pattern as those of the usual loading combination mentioned above.
- Due to the presence of more water on the upstream side (flooding), the uplift force and percent reduction for the unusual loading combination are higher than those for the usual combination for any dam configuration, drain diameter, or spacing considered.
- The stresses on the upstream side for the unusual case are lower than those for the usual case since the cracks generated at the base tend to relieve the stresses.

- The stresses for the extreme loading condition are consistent with the results presented above for usual and unusual combinations for various drain diameter and spacing. However, this loading condition leads to the generation of cracks on the downstream side.
- The generation and propagation of these cracks can be reduced by using larger drain diameter, smaller spacing between drains, or by moving the gallery to about 20% of the base width away from the upstream face. However, this last option tends to increase uplift pressure, since the gallery moves farther away from the upstream face.
- Post-tension cables can also be added along the downstream face to reduce cracking. The greatest reduction came from vertically placed cables and as close to the toe of the dam as feasibly possible.
- Placing the gallery at a distance of 10% of the base width from the upstream face generates the lowest uplift pressure on average. Moving in the downstream direction generates lower crack lengths compared to a location closer to the upstream face. However, with the addition of post tensioning cables along the downstream face, the crack length can be reduced while maintaining a high uplift pressure reduction.
- The optimal location depends on what is considered as more important: uplift reduction (more upstream), crack reduction (more downstream), or a compromise between both (in between both locations).
- Placing the gallery at a higher elevation reduces pump head and thus cost of pumping. Higher discharges require a shorter pumping duration and are therefore cheaper.
- The cheapest pump plan depends on the desired pump head.
- In this study, the cheapest pump schedule for Porsuk Dam was determined to be the case when the water was pumped out at a rate of $0.5 \text{ m}^3/\text{min}$ for a gallery located at an elevation of 6 m.

REFERENCES

- Amadei, B., & Illangasekare, T. (1992). Stability of Concrete Gravity Dams with Drained and Finite Cracks. *Journal of Energy Engineering*, 118(3), 149–163. [https://doi.org/10.1061/\(ASCE\)0733-9402\(1992\)118:3\(149\)](https://doi.org/10.1061/(ASCE)0733-9402(1992)118:3(149))
- Amadei, B., Illangasekare, T., Morris, D. I., & Boggs, H. (1989). Estimation of Uplift in Cracks in Older Concrete Gravity Dams: Analytical Solution and Parametric Study. *Journal of Energy Engineering*, 115(1), 19–38. [https://doi.org/10.1061/\(ASCE\)0733-9402\(1989\)115:1\(19\)](https://doi.org/10.1061/(ASCE)0733-9402(1989)115:1(19))
- ArcelorMittal. (2010). *Prestressed concrete Wire and strands*.
- ASDSO. (n.d.). ASDSO Lessons Learned from Dam Incidents and Failures. Retrieved October 29, 2017, from <http://damfailures.org/>
- Beşer, M. R. (2005). *A Study on the Reliability-Based Safety Analysis of Concrete Gravity Dams (master's thesis)*. Middle East Technical University (METU), Civil Engineering Department.
- Carsel, R. F., & Parrish, R. S. (1988). Developing joint probability distributions of soil water retention characteristics. *Water Resources Research*, 24(5), 755–769. <https://doi.org/10.1029/WR024i005p00755>
- Chauhan, R. S., Tulsianey, S. S. H., Aumta, K. L., Mahajan, J. P., & Gupta, S. (2008). Design aspect of Nathpa Dam.pdf. *Water & Energy International*, 65(Special Issue on 1500 MW Nathpa Jhakri Hydroelectric Project), 13.
- Chawla, A. S., Thakur, R. K., & Kumar, A. (1990). Discussion of “ Optimum Location of Drains in Concrete Dams .” *Journal of Hydraulic Engineering*, 116(7), 930–943. [https://doi.org/10.1061/\(ASCE\)0733-9429\(1992\)118:4\(644.2\)](https://doi.org/10.1061/(ASCE)0733-9429(1992)118:4(644.2))
- Concrete Society. (n.d.). Basic properties. Retrieved October 24, 2017, from <http://www.concrete.org.uk/fingertips-nuggets.asp?cmd=display&id=525>
- DSI. (2012). Dams- General Directorate Of State Hydraulic Works. Retrieved October 24, 2017, from <http://en.dsi.gov.tr/photo-gallery/dams>
- Duffaut, P. (2013). The traps behind the failure of Malpasset arch dam, France, in 1959. *Journal of Rock Mechanics and Geotechnical Engineering*, 5(5), 335–341. <https://doi.org/10.1016/j.jrmge.2013.07.004>

- El-razek, M. A., & Elela, M. M. A. (2001). Optimal Position of Drainage Gallery underneath Gravity Dam. *Sixth International Water Technology Conference, IWTC 2001, Alexandria Egypt*, 181–192.
- GEO-SLOPE > About. (2017). Retrieved October 24, 2017, from <https://www.geoslope.com/about>
- GEO-SLOPE International. (2010). *Seepage Modeling with SEEP / W 2007*. Geo-Slope International Ltd. Calgary, Alberta, Canada.
- Goodman, R. E., Amadei, B., & Sitar, N. (1983). Uplift Pressure in Crack Below Dam. *Journal of Energy Engineering*, 109(4), 207–221. [https://doi.org/10.1061/\(ASCE\)0733-9402\(1983\)109:4\(207\)](https://doi.org/10.1061/(ASCE)0733-9402(1983)109:4(207))
- Hannah, F. W. & Kennedy, R. C. (1938). *The Design of Dams* (2d ed.). New York, London: McGraw-Hill book company, inc., 1938.
- Hu, J., & Ma, F. (2016). Comprehensive Investigation Method for Sudden Increases of Uplift Pressures beneath Gravity Dams: Case Study. *Journal of Performance of Constructed Facilities*, 30(5), 4016023. [https://doi.org/10.1061/\(ASCE\)CF.1943-5509.0000874](https://doi.org/10.1061/(ASCE)CF.1943-5509.0000874)
- Jansen, R. B. (1988). *Advanced Dam Engineering for Design, Construction, and Rehabilitation*. (R. B. Jansen, Ed.). New York: Van Nostrand Reinhold. <https://doi.org/10.1007/978-1-4613-0857-7>
- Kharagpur. (2012). Design and Construction of Concrete Gravity Dams. In *Hydraulic Structures for Flow Diversion and Storage* (2012th ed., p. 69). Indian Institute of Technology Kharagpur.
- Kline, R. A., & Fleming, G. (2013). The Bayless Dam Failure : Separating Fact From Folklore The Early Days of Gravity Dams in the U . S . In *ASDSO Annual Conference* (p. 21). Retrieved from <http://damfailures.org/wp-content/uploads/2015/07/The-Bayless-Dam-Failure.pdf>
- Leclerc, M., Léger, P., & Tinawi, R. (2001). *CADAM user's manual*.
- Leclerc, M., Léger, P., & Tinawi, R. (2002). Computer aided stability analysis of gravity dams - CADAM. In *4th Structural Specialty Conference of the Canadian Society for Civil Engineering* (p. 10).
- Leclerc, M., Léger, P., & Tinawi, R. (2003). Computer aided stability analysis of gravity dams - CADAM. *Advances in Engineering Software*, 34(7), 403–420. [https://doi.org/10.1016/S0965-9978\(03\)00040-1](https://doi.org/10.1016/S0965-9978(03)00040-1)
- Porsuk Dam (Eskisehir, 1972) | Structurae. (n.d.). Retrieved October 24, 2017, from <https://structurae.net/structures/porsuk-dam-1972>
- Prestressing Manual. (2011). Retrieved October 25, 2017, from https://freyssinet-india.com/pdf/prestressing_manual.pdf

- Priscu, D. M., Mitri, H. S., & Beauchamp, Y. (1998). Mine Planning and Equipment Selection-Modelling of Groundwater Flow Through Rock and Soil Masses. In R. K. Singhal (Ed.) (p. 830). CRC Press.
- Rogers, J. D. (2006). Lessons Learned from the St. Francis Dam Failure. *Geo-Strata*, 6(2), 14–17.
- Rogers, J. D., & McMahon, D. J. (1993). Reassessment of the St . Francis Dam. In *ASDSO Annual Conference* (pp. 333–339). Retrieved from http://damfailures.org/wp-content/uploads/2015/07/120_Reassessment-of-the-St.-Francis-Dam-Failure.pdf
- Rose, A. T. (2013). The Influence of Dam Failures on Dam Safety Laws in Pennsylvania 1889 Failure of South Fork Dam. In *ASDSO Annual Conference* (p. 19). Retrieved from <http://damfailures.org/wp-content/uploads/2015/07/The-Influence-of-Dam-Failures-on-Dam-Safety-Laws-in-Pennsylvania.pdf>
- Scuero, A., Vaschetti, G. Jiménez, M. J., & Cowland, J. (2015). Geomembranes on RCC Dams : A Case History After 13 Years of Service. *The 7th International Symposium on Roller Compacted Concrete (RCC) Dams*, 10.
- Turkish Statistical Institute. (2017). Turkish Statistical Institute Electricity and Natural Gas Prices I. Period: January-June, 2016. Retrieved October 25, 2017, from <http://www.turkstat.gov.tr/PreHaberBultenleri.do?id=21586>
- URAL, O.M., & UNGAN, Ü. (1967). *Large Dams in Turkey*. Ankara: The General Directorate of State Hydraulic Works Ministry of Power and Natural Resources,.
- US Army Corps of Engineers. (1995). *Gravity Dam Design. USACE Engineer Manual*. Washington, DC.
- US Army Corps of Engineers. (2000). *Evaluation and Comparison of Stability Analysis and Uplift Criteria for Concrete Gravity Dams by Three Federal Agencies*. Washington, DC.
- USBR. (1976). Galleries and Adits. In *Design of gravity dams* (p. 586). Denver, Colorado: United States Government Printing Office.
- Weber, C. T., & Zornberg, J. G. (2007). Leakage through geosynthetic dam lining systems. *Association of State Dam Safety Officials - Dam Safety 2007*, 9, 1–9.
- Yanmaz, A. M. (2013). *Applied Water Resources Engineering* (3rd Edit.). Ankara: METU Press.
- Zee, C.-H., Zee, R., & Zee, R. (2011). Pore Pressures in Concrete Dams. *Journal of Geotechnical and Geoenvironmental Engineering*, 137(12), 1254–1264. [https://doi.org/10.1061/\(ASCE\)GT.1943-5606.0000536](https://doi.org/10.1061/(ASCE)GT.1943-5606.0000536)